

hep-ph/0005196

ANL-HEP-PR-00-045

DESY 00-069

Next-to-Leading Order SUSY-QCD Predictions for Associated Production of Gauginos and Gluinos

Edmond L. Berger^a, Michael Klasen^b, and Tim M. P. Tait^a

^a*High Energy Physics Division, Argonne National Laboratory*

Argonne, Illinois 60439

^b*II. Institut für Theoretische Physik, Universität Hamburg*

Hamburg, Germany

(November 1, 2018)

Abstract

We present complete results of a next-to-leading order calculation of the production of gaugino-like charginos ($\tilde{\chi}^\pm$) and neutralinos ($\tilde{\chi}^0$) in association with gluinos (\tilde{g}) at hadron colliders, including the strong corrections from the exchange of colored particles and sparticles. Adopting a variety of models for the sparticle mass spectrum, including typical supergravity (SUGRA) models and a light gluino model, we provide predictions for total and differential cross sections at the energies of the Fermilab Tevatron and CERN Large Hadron Collider (LHC).

12.38.Bx, 12.60.Jv, 13.85.Fb

Typeset using REVTeX

I. INTRODUCTION

Weak scale supersymmetry (SUSY) [1] is a theoretically attractive extension of the Standard Model of particle physics. Supersymmetric theories can solve the Higgs hierarchy puzzle [2], break electroweak symmetry radiatively at low energies [3], and explain the unification of the gauge couplings at a high energy scale [4]. SUSY introduces a superpartner for each Standard Model particle with the same quantum numbers, but for a difference in spin of $1/2$. If supersymmetry were exact, these superparticles would be degenerate in mass with their Standard Model partners. However, SUSY can be broken softly in such a way that its attractive features survive, while the superpartners become heavy enough to evade current limits from collider searches [5]. A powerful and general parametrization for the soft SUSY-breaking terms is provided by the Minimal Supersymmetric Standard Model (MSSM) [6]. Soft breaking mechanisms require that the superpartners remain lighter than a few TeV, and thus there is reason to expect that high energy investigations, such as those at LEP II, Run II of the Fermilab Tevatron, and the CERN Large Hadron Collider (LHC) will discover supersymmetric particles or place strong constraints on supersymmetric models.

The search for direct experimental evidence of supersymmetry at colliders requires a good understanding of theoretical predictions of the cross sections for production of the superparticles. In the case of hadron colliders, where collisions of strongly interacting hadrons are studied, the large strong coupling strength (α_S) leads to potentially large contributions beyond the leading order (LO) in a perturbation series expansion of the cross section. To have accurate theoretical estimates of production rates and differential cross sections, it is necessary to include corrections at next-to-leading order (NLO) or beyond. Next-to-leading order calculations of the hadroproduction of gluinos and squarks [7], top squarks [8], sleptons [9,10], and gauginos [10] have been published, including our brief report on associated production of gauginos and gluinos [11]. In this paper, we provide a detailed exposition of our calculation of associated production, and we present new predictions of total and differential cross sections for a variety of assumptions about the superpartner mass spectrum.

Associated production of a gaugino ($\tilde{\chi}$) with a gluino (\tilde{g}) or with a squark (\tilde{q}) is potentially a very important production mechanism. Associated production processes are semi-weak in that they involve one somewhat smaller coupling constant than the production of a pair of colored sparticles. However, in popular models of SUSY breaking [12,13], the mass spectrum favors much lighter masses for the color-neutral, low-lying neutralinos and charginos than for the colored squarks and gluinos. Their lighter mass means that the phase space for production of neutralinos and charginos, and the relevant partonic luminosities, will be greater than that for gluinos and squarks. This effect is potentially decisive at a collider with limited energy, such as the Tevatron. Indeed, as our numerical results show, the extra phase space may more than offset the smaller coupling, and gauginos may be produced more copiously than squarks at the Tevatron. Another point in favor of associated production is the relative simplicity of the final state. For example, the lowest lying neutralino is the (stable) lightest supersymmetric particle (LSP) in supergravity (SUGRA) models [12], manifest only as missing energy in the events, and it is the second lightest in gauge-mediated models [13]. The charginos and higher mass neutralinos may decay leptonically leaving a lepton signature plus missing transverse energy; relatively clean events ensue. Furthermore, associated production may be the best channel for measurement of the gluino mass [14].

In this paper we present our complete NLO calculation in SUSY-QCD of the hadroproduction of a gluino in association with a gaugino, including contributions from virtual loops of colored sparticles and particles, and three-particle final states in which light quarks or gluons are emitted. We extract the ultraviolet, infrared, and collinear divergences by use of dimensional regularization and illustrate how they may be absorbed by the usual renormalization and mass factorization procedures. In computing the virtual contributions, we encountered divergent four-point functions that had not been evaluated previously. We use a combined analytic and numerical phase space slicing method to treat the contributions from real emission of light particles. Associated production was calculated at LO some years ago [14,15]. Our reason to focus first on the $\tilde{\chi}$ plus \tilde{g} final state, rather than the $\tilde{\chi}$ plus \tilde{q}

final state, is that the LO cross sections for $\tilde{\chi} + \tilde{g}$ are 3 to 6 times greater than those for $\tilde{\chi} + \tilde{q}$ at the energy of the Tevatron when the mass $m_{\tilde{g}} = m_{\tilde{q}} = 300$ GeV, and 6 to 15 times greater when $m_{\tilde{g}} = m_{\tilde{q}} = 600$ GeV. These comparisons are pertinent for the lighter mass neutralinos $\tilde{\chi}_{1,2}^0$ and chargino $\tilde{\chi}_1^\pm$. In obtaining the \tilde{q} cross sections, we sum over five flavors of degenerate squarks and antisquarks.

Our analysis is general in that it is not tied to a particular SUSY breaking model. We can provide cross sections for arbitrary gluino and gaugino masses, and, indeed, the values of the cross sections at Tevatron and LHC energies depend crucially on the sparticle masses. Mass generation in supersymmetry is accomplished in a hidden sector and transmitted to the MSSM fields. In SUGRA models [12], transmission is through gravitational interactions, while in gauge-mediated [13] and gaugino-mediated [16–18] models, it occurs through gauge interactions. Anomaly mediated SUSY breaking, also gravitational in origin, is a fourth possibility [19]. In the presentation of predictions for cross sections, we consider illustrative mass spectra typical of each scenario and consistent with bounds established from current data [20,21]. We also examine the phenomenologically open case of a gluino with mass light compared to the SUSY scale, $m_{\tilde{g}} \simeq 30$ GeV. This possibility arises in some models of gauge-mediated SUSY breaking [22,23].

As is shown in detail below, the NLO corrections to associated production are generally positive, but they can be modest in size, ranging in the SUGRA model from a few percent at the energy of the Fermilab Tevatron to 100% at the energy of the LHC, depending on the sparticle masses. In the light-gluino case, NLO contributions increase the cross section by factors of 1.3 to 1.4 at the energy of the Tevatron and by factors of 2 to 3.5 at the energy of the LHC. Owing to these enhancements, collider searches for signatures of associated production will generally discover or exclude sparticles with masses larger than one would estimate based on LO production rates alone. More significant from the viewpoint of reliability, the renormalization and factorization scale dependence of the cross sections is reduced by a factor of more than two when NLO contributions are included.

At Run II of the Fermilab Tevatron, for an integrated luminosity of 2 fb^{-1} , we expect

that 10 or more events could be produced in each of the lighter gaugino channels of the SUGRA model, $\tilde{g}\tilde{\chi}_1^0$, $\tilde{g}\tilde{\chi}_2^0$, and $\tilde{g}\tilde{\chi}_1^\pm$, provided that the gluino mass $m_{\tilde{g}}$ is less than 450 GeV. The cross sections for the three heavier gaugino channels, $\tilde{g}\tilde{\chi}_3^0$, $\tilde{g}\tilde{\chi}_4^0$, and $\tilde{g}\tilde{\chi}_2^\pm$, are smaller by an order of magnitude or more than those of the lighter gaugino channels. In the light gluino model that we consider, more than 100 events could be produced in the three lighter gaugino channels provided that the common GUT-scale fermion mass $m_{1/2}$ is less than 400 GeV, and as many as 10 events in the three heavier gaugino channels as long as $m_{1/2}$ is less than 200 GeV. At the higher energy and luminosity of the LHC, at least a few events should be produced in every channel in the SUGRA model and many more in the light gluino model.

The shapes of the rapidity distributions of the gauginos are not altered appreciably by NLO contributions, but the locations of the maximum cross section in transverse momentum (p_T) are shifted to smaller values by NLO contributions. At LHC energies where the contribution of the $q\bar{q}$ initial state is important, modifications of the p_T spectra can be pronounced.

We begin in Sec. II with a brief review of the LO calculation in order to introduce our notation. In this section, we also introduce the SUSY breaking models we adopt and summarize salient aspects of their predicted mass spectra. This discussion is followed in Sec. III by a detailed presentation of our NLO $\mathcal{O}(\alpha\alpha_s^2)$ calculation. We present partonic scaling functions in Sec. IV as well as predictions for inclusive and differential cross sections at Tevatron and LHC energies. Our conclusions may be found in Sec. V. In Appendices A – E, we present detailed analytic results related to the NLO calculation.

II. LEADING ORDER PRODUCTION OF GAUGINOS AND GLUINOS

We begin with the Born level cross sections for the partonic processes

$$q\bar{q} \rightarrow \tilde{g}\tilde{\chi}_k^0, q\bar{q} \rightarrow \tilde{g}\tilde{\chi}_k^\pm, \quad (1)$$

derived first in [14,15]. In anticipation of the renormalization and mass factorization of the NLO contributions, we proceed in the $n = 4 - 2\epsilon$ dimensions of standard dimensional regularization. We assume that there is no mixing between squarks of different generations and that the squark mass eigenstates are aligned with the squark chirality states, equivalent to the assumption that the two squarks of a given flavor are degenerate in mass. We ignore the $n_f = 5$ light quark masses in all of the kinematics and couplings, and thus study the production of gaugino-like charginos and neutralinos, but not the production of Higgsino-like ones [24]. We assume further that the entries in the chargino and neutralino mass matrices are real, and thus that the unitary transformations from the $(\tilde{B}, \tilde{W}_3, \tilde{H}_1, \tilde{H}_2)$ and $(\tilde{W}^+, \tilde{H}^+)$ bases to the $(\tilde{\chi}_1^0, \tilde{\chi}_2^0, \tilde{\chi}_3^0, \tilde{\chi}_4^0)$ and $(\tilde{\chi}_1^\pm, \tilde{\chi}_2^\pm)$ bases are given by orthogonal matrices. A result of this convention is that it is possible for the mass of one or more neutralinos to be negative inside a polarization sum. The chargino masses are chosen to be positive as may be done for Dirac fermions.

The Dirac matrix γ_5 (or equivalently the projectors $P_{L(R)} = (1 \pm \gamma_5)/2$) appearing in the gaugino and gluino couplings is treated in the ‘naive’ scheme in which it anti-commutes with all of the other γ_μ matrices. This scheme is acceptable at the one loop level for calculations free from anomaly. In evaluating the Feynman diagrams involving Majorana and explicitly charge-conjugated fermions, we have followed the approach described in Ref. [25].

We express our leading order results in terms of the Mandelstam variables

$$\begin{aligned} s &= (p_a + p_b)^2 \\ t &= (p_b - p_2)^2 & t_1 &= (p_b - p_2)^2 - m_1^2 & t_2 &= (p_b - p_2)^2 - m_2^2 \\ u &= (p_a - p_2)^2 & u_1 &= (p_a - p_2)^2 - m_1^2 & u_2 &= (p_a - p_2)^2 - m_2^2, \end{aligned} \tag{2}$$

where p_a, p_b, p_1 , and p_2 refer to the four-momenta of the incoming quark, the incoming anti-quark, the produced gluino, and the produced gaugino, respectively. Variable m_1 denotes the mass of the gluino and m_2 that of the gaugino. The incoming partons are treated as massless. The momenta are on mass-shell, $p_a^2 = p_b^2 = 0$, $p_1^2 = m_1^2$, and $p_2^2 = m_2^2$. The invariants obey the relation $s + t + u = m_1^2 + m_2^2$.

After the n -dimensional phase space integration we obtain the lowest order partonic differential cross section,

$$\begin{aligned} \frac{d^2 \hat{\sigma}_{ij}^B}{dt_2 du_2} &= \frac{\pi S_\epsilon}{s^2 \Gamma(1-\epsilon)} \left[\frac{t_2 u_2 - m_2^2 s}{\mu^2 s} \right]^{-\epsilon} \Theta(t_2 u_2 - m_2^2 s) \\ &\quad \times \Theta(s - (m_1 + m_2)^2) \delta(s + t + u - m_1^2 - m_2^2) \overline{|\mathcal{M}_{ij}^B|^2}, \end{aligned} \quad (3)$$

where $S_\epsilon = (4\pi)^{-2+\epsilon}$. The arbitrary scale μ is introduced, as usual, to provide the correct mass dimension for the coupling in n dimensions; $\overline{|\mathcal{M}_{ij}^B|^2}$ is the leading order matrix element summed over the colors and helicities of all of the outgoing particles, and averaged over the colors and helicities of the incoming ones. The indices (i, j) label the incident partons. For neutralino production at leading order, the partons are quarks and antiquarks of the same flavor. For chargino production, the incident quarks and antiquarks have different flavor. At next-to-leading order, quark gluon initial states contribute also.

As is shown in Fig. 1, the Born matrix element for associated production of gluinos and gauginos proceeds via t - or u - channel exchange of a squark. In the case of charged gauginos, only the left-handed chiral squarks participate, whereas neutral gauginos receive contributions from both left- and right-handed chiral squarks. Furthermore, in the case of charged gaugino production, the squarks exchanged in the t - and u - channels correspond to different flavors, while in the neutral case the t - and u - channel squarks have the same flavor. Under our assumption that the squark mass eigenstates correspond to squarks of definite chirality, the (massless) incoming quark and anti-quark are forced to have a particular helicity, and thus the sets of graphs in which a right-handed chiral squark is exchanged cannot interfere with those mediated by a left-handed chiral squark. The matrix element has the analytic form [14]

$$\overline{|\mathcal{M}^B|^2} = \frac{8\pi \hat{\alpha}_S}{9} \left[\frac{X_t t_1 t_2}{(t - m_{\tilde{q}_t}^2)^2} - \frac{2 X_{tu} s m_1 m_2}{(t - m_{\tilde{q}_t}^2)(u - m_{\tilde{q}_u}^2)} + \frac{X_u u_1 u_2}{(u - m_{\tilde{q}_u}^2)^2} \right], \quad (4)$$

where $\hat{\alpha}_S = \hat{g}_s^2/4\pi$ is the coupling between gluinos, squarks, and quarks; $m_{\tilde{q}_{t(u)}}$ is the mass of the squark exchanged in the t - (u -) channel graph; and the X represent the gaugino interactions with quark and squark.

For production of a neutralino of type $\tilde{\chi}_k^0$, the X are [26]

$$X_t = X_{tu} = X_u = 2 \left| e e_q N'_{k1} + \frac{e}{\sin \theta_W \cos \theta_W} (T_q - e_q \sin^2 \theta_W) N'_{k2} \right|^2. \quad (5)$$

In the expressions above, e is the electron charge, θ_W the weak mixing angle, T_q the third component of the weak isospin for the squark, and e_q is the charge of the quark in units of e . For up-type quarks $e_q = 2/3$ and for down-type quarks $e_q = -1/3$. The matrix N' is the transformation from the interaction to mass eigenbasis defined in Ref. [26]. The expressions for production of a positive chargino of type $\tilde{\chi}_k^+$ are

$$X_t = \frac{e^2}{\sin^2 \theta_W} |V_{k1}|^2, \quad X_{tu} = \frac{e^2}{\sin^2 \theta_W} \text{Re} (V_{k1} U_{k1}^*), \quad X_u = \frac{e^2}{\sin^2 \theta_W} |U_{k1}|^2. \quad (6)$$

For the negative chargino $\tilde{\chi}_k^-$ they have the form,

$$X_t = \frac{e^2}{\sin^2 \theta_W} |U_{k1}|^2, \quad X_{tu} = \frac{-e^2}{\sin^2 \theta_W} \text{Re} (V_{k1}^* U_{k1}), \quad X_u = \frac{e^2}{\sin^2 \theta_W} |V_{k1}|^2. \quad (7)$$

Matrices U and V are the chargino transformation matrices from interaction to mass eigenstates defined in Ref. [26].

To compute cross sections for hadroproduction,

$$h_a h_b \rightarrow \tilde{g} \tilde{\chi}_k^0 X, \quad h_a h_b \rightarrow \tilde{g} \tilde{\chi}_k^\pm X, \quad (8)$$

where h_a and h_b label the incoming hadrons, one must convolve the partonic cross section with the parton distribution functions. In the high energy scattering limit, one may neglect the mass of the incoming hadrons compared with their momenta, and obtain

$$S = (P_a + P_b)^2 \quad (9)$$

$$T = (P_b - p_2)^2 \quad T_1 = (P_b - p_2)^2 - m_1^2 \quad T_2 = (P_b - p_2)^2 - m_2^2$$

$$U = (P_a - p_2)^2 \quad U_1 = (P_a - p_2)^2 - m_1^2 \quad U_2 = (P_a - p_2)^2 - m_2^2,$$

in which P_i indicates the momentum of hadron h_i . We define x_i by the relations

$$s = x_a x_b S, \quad t_2 = x_b T_2, \quad u_2 = x_a U_2. \quad (10)$$

The convolution with the parton distribution functions may be written [7] as

$$\frac{d^2\sigma}{dT_2 dU_2}(S, T, U, \mu_F^2) = \sum_{i,j=q,\bar{q}} \int_{x_a^-}^1 dx_a \int_{x_b^-}^1 dx_b x_a f_i^{h_a}(x_a, \mu_F^2) x_b f_j^{h_b}(x_b, \mu_F^2) \frac{d^2\hat{\sigma}_{ij}(s, t, u, \mu_F^2)}{dt_2 du_2}. \quad (11)$$

In this equation μ_F refers to the factorization scale, and $d^2\hat{\sigma}_{ij}/dt_2 du_2$ is the hard cross section, equal to the Born cross section at leading order. The lower limits of integration on the convolution are

$$x_a^- = \frac{-T_1}{S + U_2}, \quad (12)$$

$$x_b^- = \frac{-x_a U_2 - m_2^2 + m_1^2}{x_a S + T_2}. \quad (13)$$

The differential cross section in the transverse momentum (p_T) and rapidity (y) of the gaugino is related to the differential cross section in U_2 and T_2 by

$$\frac{d^2\sigma(S, p_T, y, \mu_F^2)}{dp_T dy} = 2 p_T S \frac{d^2\sigma(S, T, U, \mu_F^2)}{dT_2 dU_2}, \quad (14)$$

with

$$p_T^2 = \frac{T_2 U_2}{S} - m_2^2 = \frac{t_2 u_2}{s} - m_2^2, \quad (15)$$

$$y = \frac{1}{2} \log \left(\frac{T_2}{U_2} \right). \quad (16)$$

The total cross section is obtained by integrating over the full range of transverse momentum and rapidity,

$$\sigma(S, \mu_F^2) = \int_0^{p_T^{max}(0)} dp_T \int_{-y^{max}(p_T)}^{y^{max}(p_T)} dy \frac{d^2\sigma(S, p_T, y, \mu_F^2)}{dp_T dy} \quad (17)$$

$$= \int_{-y^{max}(0)}^{y^{max}(0)} dy \int_0^{p_T^{max}(y)} dp_T \frac{d^2\sigma(S, p_T, y, \mu_F^2)}{dp_T dy}. \quad (18)$$

The limits of integration are

$$p_T^{max}(y) = \frac{1}{2\sqrt{S} \cosh(y)} \sqrt{(S + m_2^2 - m_1^2)^2 - 4 m_2^2 S \cosh^2(y)}, \quad (19)$$

and

$$y^{max}(p_T) = \text{ArcCosh} \left(\frac{S + m_2^2 - m_1^2}{2\sqrt{S(p_T^2 + m_2^2)}} \right). \quad (20)$$

A. Supersymmetry Breaking Models

The physical gluino and gaugino masses that we use, as well as the gaugino mixing matrices, are based on four popular SUSY breaking models plus a fifth scenario in which the gluino mass is relatively light.

For our *default* minimal SUGRA scenario [12], we select the common scalar and fermion masses at the GUT scale to be $m_0 = 100$ GeV and $m_{1/2} = 150$ GeV. The trilinear coupling $A_0 = 300$ GeV, and the ratio of the Higgs vacuum expectation values, $\tan\beta = 4$. The absolute value of the Higgs mass parameter μ is fixed by electroweak symmetry breaking, and we choose $\mu > 0$. (Our sign convention for A_0 is opposite to that in the ISASUGRA code [27].) For this scenario, the neutralino masses $m_{\tilde{\chi}_{1-4}^0}$ are 55, 104, 283, and 309 GeV with $m_{\tilde{\chi}_3^0} < 0$ inside a polarization sum. The chargino masses $m_{\tilde{\chi}_{1,2}^\pm}$ are 101 and 308 GeV and therefore almost degenerate with the masses of $\tilde{\chi}_{2,4}^0$. The gluino mass $m_{\tilde{g}}$ is 410 GeV, and the squark mass is 359 GeV. All of these masses are above the exclusion limits established from LEP and Tevatron collider data [20,21]. Since the gluino and gaugino masses vary principally with $m_{1/2}$, we freeze the values of the other four parameters, and we vary $m_{1/2}$ over the range 100 to 400 GeV. The squark, gluino, and gaugino masses all increase as $m_{1/2}$ increases.

In considering gauge-mediated SUSY breaking (GMSB), we adopt the parameters of model I studied for the SUSY/Higgs Run II workshop [28], with $\tan\beta = 2.5$, $\mu > 0$, one messenger SU(5) generation, and a messenger scale $M = 2\Lambda$. Parameter Λ is the scale of SUSY breaking. We examine six cases in which Λ varies from 40 to 150 TeV. GMSB does not favor associated production at Tevatron energies because it results in a pattern of gaugino masses in which $M_3(M)/M_2(M) = \alpha_3(M)/\alpha_2(M)$, where M_3 and M_2 are the masses of the gluino and weak gaugino, and α_3 and α_2 are the SU(3) and SU(2) gauge couplings. Since M is a low scale, α_3 is still quite strong. The gluino is generally heavy compared to the other gauginos. Selecting $\Lambda = 40$ TeV, M_1 , M_2 , $\mu = 56.47, 112.8, 241.7$ GeV, and we obtain neutralino masses $m_{\tilde{\chi}_{1-4}^0} = 45, 88, 245, \text{ and } 281$ GeV with $m_{\tilde{\chi}_3^0} < 0$ inside a polarization

sum. The chargino masses $m_{\tilde{\chi}_{1,2}^\pm}$ are 82 and 277 GeV and again almost degenerate with the masses of $\tilde{\chi}_{2,4}^0$. The gluino mass $m_{\tilde{g}} = 367$ GeV, and the squark mass is 471 GeV. The spectrum of masses is similar to that of our default SUGRA scenario, and the masses grow as we increase Λ . For comparable gluino and gaugino masses, we find that LO cross sections are roughly a factor of 5 (3) smaller at Tevatron (LHC) energies than in the SUGRA model, related to the larger squark mass.

Our anomaly mediated (AMSB) scenario is based on the work in Ref. [19]. It is less well-defined in the sense that scalar masses are not understood, and thus the value of μ is not determined through radiative electroweak symmetry breaking. However, M_1, M_2 , and M_3 are well specified. We fix the squark masses to be 350 GeV and choose $\tan\beta = 2$. The gaugino masses are controlled by the gravitino mass. The gluino tends to be heavy in this scenario, disfavoring associated production. However, the gluino mass has phase π relative to M_1 and M_2 , resulting in constructive interference at LO in the production of $\tilde{\chi}_1^0, \tilde{\chi}_2^0$, and $\tilde{\chi}_4^0$, and negative interference in production of $\tilde{\chi}_3^0$, in contrast to the SUGRA scenario. In AMSB the lightest neutralino is always a \tilde{W} and has a large coupling to (s)quarks, in contrast to the \tilde{B} -like lightest neutralino of the SUGRA model. We vary the gravitino mass parameter $m_{3/2}$ from 30 to 60 TeV. For M_1, M_2 , and $\mu = 272, 80$, and -300 GeV, we obtain neutralino masses $m_{\tilde{\chi}_{1-4}^0} = 91, 269, 309$, and 371 GeV with $m_{\tilde{\chi}_4^0} < 0$ inside a polarization sum. The chargino masses are $m_{\tilde{\chi}_{1,2}^\pm} = 91$ and 318 GeV. The gluino mass $m_{\tilde{g}} = -672$ GeV. The masses grow as we increase $m_{3/2}$. For the $\tilde{g}\tilde{\chi}_1^0$ channel the LO cross section is roughly a factor of 15 larger at Tevatron energies than in the SUGRA model, for comparable masses. However, the fact that the combination of the gluino and neutralino masses exceeds 750 GeV makes this model an unlikely candidate for discovery at the Tevatron.

Gaugino dominated boundary conditions [16] offer another interesting possibility, exemplified by gaugino-mediated SUSY breaking (\tilde{g} MSB) [17,18]. In this class of models, gauge fields propagate freely in the five-dimensional bulk, whereas fermions are confined to one or more four-dimensional hyper-surfaces. Supersymmetry is broken at a distant point in the extra dimension, giving mass to the gauginos, and the gauge interactions communicate this

breaking to the scalar fermions as well. We present results based on the model of Ref. [18], which combines this simple mechanism of SUSY breaking with a model of quark masses and mixings. This model has two input parameters, $m_{1/2}$ and the mass of the down-type Higgs at the GUT scale, m_{H_d} . Fixing, for example, $m_{H_d} = 200$ GeV and $m_{1/2} = 150$ GeV (which determines $\tan\beta \sim 15$ [18]), we find a spectrum with gluino mass 379 GeV, neutralino masses 57, 103, -224, and 249 GeV, chargino masses 101 and 251 GeV, and squark masses of about 330 GeV. This spectrum is similar to the default SUGRA scenario, with the principal differences that the Higgsino masses are somewhat lighter because the non-universal boundary conditions at the GUT scale result (through the requirement of radiative EWSB) in a non-SUGRA μ -term at the weak scale. For the light gaugino-like states the cross sections are virtually unchanged with respect to the SUGRA scenario, whereas the LO cross sections for $\tilde{\chi}_3^0$, $\tilde{\chi}_4^0$, and $\tilde{\chi}_2^\pm$ are 7, 5, and 5 times larger than those in the default SUGRA scenario, because of the increased phase space for these states.

An intriguing scenario is that of a light gluino LSP [22]. Gluino masses in the range of 25 to 35 GeV may still be allowed [23]. Since the work of Ref. [23] treats only the strong SUSY sector, we make some assumptions about the weak parameters, respecting LEP limits [21] on neutralino and chargino masses. We choose $m_{\tilde{g}} = 30$ GeV and $m_{\tilde{q}} = 450$ GeV. For the weak sector, we adopt masses typical of SUGRA models, discussed above. Since the gluino mass is light, there is much more phase space available, and cross sections for associated production are substantial at Tevatron energies, reaching $\sim 1\text{pb}^{-1}$ for a wide range of values of $m_{1/2}$.

Because the GMSB, \tilde{g} MSB and AMSB cross sections at LO are not too dissimilar from those of the SUGRA case at Tevatron energies, we focus our NLO work on the SUGRA and light gluino models.

III. NEXT-TO-LEADING ORDER CONTRIBUTIONS

The next-to-leading order contributions to the associated production of gluinos and gauginos can be separated into virtual corrections that contain internal loops of colored particles, and 2-to-3 parton real emission contributions in which a light gluon or quark is emitted. The kinematics of the virtual contributions are identical to the Born case described in Sec. II whereas the presence of an additional out-going particle in the emission contributions requires integration over a three-body (rather than two-body) phase space. It is useful to separate the real emission contributions into parts in which the additional parton's energy approaches zero (and thus the three body final state effectively becomes a two-body one) and parts in which the additional parton is hard (energetic). We refer to these two parts as soft emission and hard emission contributions, respectively.

All of these NLO contributions contain singularities. The virtual corrections contain ultraviolet (UV) singularities that may be absorbed into the definitions of the couplings and operators in the usual renormalization procedure. Both virtual and emission contributions contain infrared (IR) singularities when the energy of the produced or exchanged particle approaches zero. These singularities cancel when the virtual and emission contributions are combined. Finally, there are collinear singularities when the produced particle is emitted collinearly with another massless colored object. These singularities are absorbed into the (universal) NLO definition of the parton distribution functions.

A. Virtual Corrections

In this subsection we present the virtual corrections to the associated production of gauginos and gluinos in hadron collisions. They arise from the interference of the Born matrix elements presented in Sec. II with the one-loop amplitudes shown generically in Fig. 2. In these diagrams, the crossed regions indicate contributions from self-energy corrections (Fig. 3) and vertex corrections (Fig. 4) that are present one at a time at next-to-leading

order. Additional contributions arise from the box diagrams in Fig. 5. We include the full supersymmetric spectrum of strongly interacting particles in the virtual loops, i.e. squarks and gluinos as well as quarks and gluons.

Since these virtual loop contributions contain ultraviolet and infrared singularities, we regularize the cross sections by computing the phase space and matrix elements in $n = 4 - 2\epsilon$ dimensions. We then obtain the virtual differential cross section from

$$\begin{aligned} \frac{d^2 \hat{\sigma}_{ij}^V}{dt_2 du_2} = & \frac{\pi S_\epsilon}{s^2 \Gamma(1 - \epsilon)} \left[\frac{t_2 u_2 - m_2^2 s}{\mu^2 s} \right]^{-\epsilon} \Theta(t_2 u_2 - m_2^2 s) \Theta(s - (m_1 + m_2)^2) \\ & \times \delta(s + t + u - m_1^2 - m_2^2) \overline{(\mathcal{M}^B \mathcal{M}^{V*} + \mathcal{M}^V \mathcal{M}^{B*})}. \end{aligned} \quad (21)$$

As in the Born case, the matrix elements are summed (averaged) over the colors and spins of the outgoing (incoming) particles.

We calculate the traces of Dirac matrices with the help of the computer algebra program FORM [29] using the so-called “naive” γ_5 scheme. In this scheme, γ_5 anticommutes with all other γ_μ matrices, which is justified for anomaly-free one-loop amplitudes [30]. The γ_5 matrix enters the calculation through both the quark-squark-gluino and quark-squark-gaugino Yukawa couplings. The integration over the internal loop momenta is simplified by reducing all tensorial integration kernels to expressions that are only scalar functions of the loop momentum [31]. The resulting one-, two-, three-, and some four-point functions were computed in the context of other physical processes [7]. However, two previously unknown divergent four-point functions are computed here for the first time due to the fact that the final state particles, i.e. the gluino and the gaugino, have different masses in general. The absorptive parts are obtained with Cutkosky cutting rules and the real parts with dispersion techniques. The results are collected in Appendix B.

The virtual one-loop corrections contain ultraviolet divergences that appear as poles in $1/\epsilon$ in the one- and two-point functions. They are removed by renormalization of the coupling constants in the modified-minimal-subtraction scheme ($\overline{\text{MS}}$) scheme at the renormalization scale μ [32], and of the masses of the heavy particles (squarks and gluinos) in the on-shell scheme. A difficulty arises from the fact that gluons have $n - 2$ possible polarizations,

whereas gluinos have 2, leading to violation of supersymmetry in the $\overline{\text{MS}}$ scheme. The simplest procedure to restore supersymmetry, which we adopt here, is through a finite shift in the quark-squark-gluino Yukawa coupling:

$$\hat{g}_s = g_s \left[1 + \frac{\alpha_s}{4\pi} \left(\frac{2}{3}N - \frac{1}{2}C_F \right) \right] = g_s \left[1 + \frac{\alpha_s}{3\pi} \right]. \quad (22)$$

This shift was discussed first in Ref. [33].

The virtual corrections can be classified into a C_F and a N_C color class depending on the color flow or the Abelian or non-Abelian nature of the correction vertices. In addition to UV singularities they have collinear and infrared singularities that appear as $1/\epsilon$ or $1/\epsilon^2$ poles in the derivatives of the two-point- and in the three- and four-point functions. The generally divergent scalar integrals are always multiplied by finite coefficient functions proportional to parts of the Born matrix elements. The full result is given in Appendix A.

B. Real Emission Contributions

At NLO, the production of gluinos and gauginos receives contributions from real emission of gluons or massless quarks and anti-quarks. In the following sub-sections both of these types of two-to-three partonic contributions are dealt with separately.

Following the notation developed in Ref. [34], we express our results in terms of the following sets of invariants,

$$\begin{aligned} s &= (p_a + p_b)^2 & s_5 &= (p_1 + p_2)^2 \\ s_3 &= (p_3 + p_2)^2 - m_1^2 & s_4 &= (p_3 + p_1)^2 - m_1^2 \\ t &= (p_b - p_2)^2 & t' &= (p_b - p_3)^2 \\ u &= (p_a - p_2)^2 & u' &= (p_a - p_3)^2 \\ u_6 &= (p_b - p_1)^2 - m_1^2 & u_7 &= (p_a - p_1)^2 - m_1^2, \end{aligned} \quad (23)$$

where p_a and p_b are the four-momenta of the incoming (massless) partons, p_1 and p_2 are the \tilde{g} and $\tilde{\chi}$ momenta, and p_3 is the momentum of the additional massless parton. We also find

it useful to define the following derived quantities:

$$\begin{aligned}
t_1 &= t - m_1^2 & t_2 &= t - m_2^2 \\
u_1 &= u - m_1^2 & u_2 &= u - m_2^2 \\
\Delta_u &= m_1^2 - m_{\tilde{q}_u}^2 & \Delta_t &= m_1^2 - m_{\tilde{q}_t}^2 \\
u_{6\Delta} &= u_6 + \Delta_u & u_{7\Delta} &= u_7 + \Delta_t \\
s_{4\Delta} &= s_4 + \Delta_u & s_{3\Delta} &= s_3 + \Delta_t .
\end{aligned} \tag{24}$$

Energy and momentum conservation provide relations among these quantities:

$$\begin{aligned}
s_4 &= s + t_2 + u_1 & s_3 &= s + u_6 + u_7 \\
s_5 &= s + t' + u' & u_6 &= -s - t_2 - t' \\
u_7 &= -s - u_2 - u' .
\end{aligned} \tag{25}$$

The n -dimensional three-body phase space may be derived conveniently if we integrate the general fully differential cross section in the 1-3 rest frame [34]. In this frame the 4-dimensional components of the n -dimensional momenta are expressed as:

$$\begin{aligned}
p_a &= (\omega_a, 0, \omega_a \sin \psi, \omega_a \cos \psi) \\
p_b &= (\omega_b, 0, 0, \omega_b) \\
p_1 &= (E_1, -\omega_3 \sin \theta_1 \sin \theta_2, -\omega_3 \sin \theta_1 \cos \theta_2, -\omega_3 \cos \theta_1) \\
p_2 &= (E_2, \omega_a \sin \psi, \omega_a \cos \psi + \omega_b) \\
p_3 &= (\omega_3, \omega_3 \sin \theta_1 \sin \theta_2, \omega_3 \sin \theta_1 \cos \theta_2, \omega_3 \cos \theta_1),
\end{aligned} \tag{26}$$

with

$$\begin{aligned}
\omega_a &= \frac{s + u_2}{2\sqrt{s_4 + m_1^2}} & \omega_b &= \frac{s + t_2}{2\sqrt{s_4 + m_1^2}} \\
\omega_3 &= \frac{s_4}{2\sqrt{s_4 + m_1^2}} & E_1 &= \frac{s_4 + 2m_1^2}{2\sqrt{s_4 + m_1^2}} \\
E_2 &= -\frac{t_2 + u_2 + 2m_1^2}{2\sqrt{s_4 + m_1^2}} & \cos \psi &= \frac{-s(s_4 + m_1^2 + m_2^2) + t_2 u_2}{(s + t_2)(s + u_2)} .
\end{aligned} \tag{27}$$

Using this parameterization, we may express the invariants defined in Eq. (23) in terms of θ_1 , θ_2 , and the θ -independent variables $\omega_{(a,b,3)}$, $E_{(1,2)}$, and ψ . For the real emission contributions, it is sometimes convenient to parameterize these momenta with the \hat{z} axis aligned along p_a or p_2 . As these alternate frames are related by a simple spatial rotation, the expressions for $E_{(1,2)}$, and $\omega_{(a,b,3)}$ remain unchanged. The general three-body cross section may be expressed in this frame as

$$\begin{aligned} \frac{d^3 \hat{\sigma}_{ij}^R}{ds_4 du_2 dt_2} &= \frac{S_\epsilon^2 \mu^{2\epsilon}}{2 s^2 \Gamma(1-2\epsilon)} \left[\frac{t_2 u_2 - s m_2^2}{s \mu^2} \right]^{-\epsilon} \Theta(t_2 u_2 - s m_2^2) \Theta(s_4) \\ &\times \Theta(s - (m_1 + m_2)^2) \frac{s_4^{1-2\epsilon}}{(s_4 + m_1^2)^{1-\epsilon}} \delta(s + t_2 + u_1 - s_4) \int d\Omega_n |\overline{\mathcal{M}}^R|^2, \end{aligned} \quad (28)$$

in which $|\overline{\mathcal{M}}^R|^2$ is the real emission matrix element squared, summed over final spins and colors and averaged over initial spins and colors, and the n -dimensional angular integration is $d\Omega_n = \sin^{1-2\epsilon}(\theta_1) d\theta_1 \sin^{-2\epsilon}(\theta_2) d\theta_2$.

In evaluating the integration over the angular variables in Eq. (28), we follow the procedure outlined in Ref. [34], in which we use the relations among the invariants, Eq. (25), to reduce all of the angular integrals to the form,

$$\begin{aligned} I_n^{(k,l)} &= \int_0^\pi \sin^{1-2\epsilon}(\theta_1) d\theta_1 \int_0^\pi \sin^{-2\epsilon}(\theta_2) d\theta_2 \\ &\times (a + b \cos \theta_1)^{-k} (A + B \cos \theta_1 + C \sin \theta_1 \cos \theta_2)^{-l}, \end{aligned} \quad (29)$$

the necessary expressions for which may be found in Ref. [34]. The angular integrations involving negative powers of t' and u' produce poles in ϵ which correspond to collinear singularities in which particle 3 is collinear with particle a or b (c.f. Figs. (6) and (7)). Because these singularities follow a universal structure, they may be removed from the cross section and absorbed into the parton distribution functions according to the usual mass factorization procedure [35]. The non-zero mass of the gluino kinematically forbids collinear emission, and thus the gluino has no associated collinear singularities.

The collinear singular pieces have the factorized form

$$\begin{aligned} \frac{d^2 \hat{\sigma}_{ij}^R(s, t_2, u_2, \mu^2)}{dt_2 du_2} &= \int_0^1 dx_1 x_1 \int_0^1 dx_2 x_2 \sum_{k,l} \Gamma_{ki}(x_1, \mu_F^2, \mu^2, \epsilon) \\ &\times \Gamma_{lj}(x_2, \mu_F^2, \mu^2, \epsilon) \frac{d^2 \hat{\sigma}_{kl}^R(\hat{s}, \hat{t}_2, \hat{u}_2, \mu_F^2)}{d\hat{t}_2 d\hat{u}_2}, \end{aligned} \quad (30)$$

in which $\hat{s} = x_1 x_2 s$, $\hat{u}_2 = x_1 u_2$, $\hat{t}_2 = x_2 t_2$. The universal splitting functions Γ_{ij} contain the collinear divergences associated with incoming parton j splitting into parton i , and the hard scattering cross section, $d^2 \hat{\sigma}_{kl}^R / d\hat{t}_2 d\hat{u}_2$, is free from singularities. The splitting functions may be redefined by an arbitrary finite term, and thus one must choose a factorization scheme. In order to use recent sets of parton distributions extracted from data we adopt the $\overline{\text{MS}}$ scheme, in which the splitting functions at $\mathcal{O}(\alpha_S)$ are

$$\Gamma_{ij}(x, \mu_F^2, \mu^2, \epsilon) = \delta_{ij} \delta(x-1) + \frac{\alpha_S}{2\pi} \left[-\frac{1}{\epsilon} + \gamma_E - \log(4\pi) + \log\left(\frac{\mu_F^2}{\mu^2}\right) \right] P_{ij}(x). \quad (31)$$

In the above expression, the $P_{ij}(x)$ are the Altarelli-Parisi evolution kernels [36],

$$\begin{aligned} P_{qq}(x_i) &= P_{q\bar{q}}(x_i) = C_F \left[\frac{1+x_i^2}{1-x_i} \Theta(1-\delta_i-x_i) + \left(2\log\delta_i + \frac{3}{2} \right) \delta(1-x_i) \right], \\ P_{gq}(x_i) &= P_{g\bar{q}}(x_i) = C_F \frac{1+(1-x_i)^2}{x_i}, \\ P_{qg}(x_i) &= P_{\bar{q}g}(x_i) = T_F [x_i^2 + (1-x_i)^2], \\ P_{gg}(x_i) &= 2N_C \left[\frac{1}{x_i(1-x_i)} + x_i(1-x_i) - 2 \right] \Theta(1-x_i-\delta_i) \\ &\quad + \left[2N_C \log\delta_i + \frac{1}{2}\beta_0^L \right] \delta(1-x_i), \end{aligned} \quad (32)$$

with $C_F = 4/3$ and $T_F = 1/2$ for $N_C = 3$ colors of quarks; $\beta_0^L = 11N_C/6 - 2n_F T_F/3$. The quantities δ_i express the slicing of s_4 into hard and soft regimes in terms of the x_a and x_b variables. They can be related to the Δ of Section III B 1 by $\delta_a = \Delta/(s+u_2)$ and $\delta_b = \Delta/(s+t_2)$.

We set the renormalization and factorization scales equal to each other, $\mu_F = \mu$, and expand Eq. (30) to $\mathcal{O}(\alpha_S)$ to derive the expression for the reduced cross section,

$$\begin{aligned}
\frac{d^2 \hat{\sigma}_{ij}^R(s, t_2, u_2, \mu^2)}{dt_2 du_2} &= \frac{d^2 \hat{\sigma}_{ij}^R(s, t_2, u_2, \mu^2)}{dt_2 du_2} \\
&+ \frac{\alpha_S}{2\pi} \frac{1}{\bar{\epsilon}} \int_0^1 dx_1 x_1 P_{li}(x_1) \frac{d^2 \hat{\sigma}_{lj}^0(x_1 s, t_2, x_1 u_2, \mu^2)}{dt_2 d\hat{u}_2} \\
&+ \frac{\alpha_S}{2\pi} \frac{1}{\bar{\epsilon}} \int_0^1 dx_2 x_2 P_{kj}(x_2) \frac{d^2 \hat{\sigma}_{ik}^0(x_2 s, x_2 t_2, u_2, \mu^2)}{dt_2 du_2}.
\end{aligned} \tag{33}$$

We employ the compact notation $\bar{\epsilon}^{-1} = \epsilon^{-1} - \gamma_E + \log(4\pi)$; $d^2 \hat{\sigma}_{ik}^0/dt_2 du_2$ is the leading order cross section for $i k \rightarrow \tilde{g} \tilde{\chi}$. The resulting hard scattering cross section is free from collinear singularities, as the implicit ϵ -dependence of $d^2 \hat{\sigma}_{ij}/dt_2 du_2$ cancels with the explicit ϵ -dependence of the second and third terms.

1. Gluon Emission

The NLO real contributions with an additional gluon in the final state,

$$q \bar{q} \rightarrow g \tilde{g} \tilde{\chi}, \tag{34}$$

proceed from the Feynman diagrams shown in Fig. 6. As was the case for the leading order cross section for production of neutralinos with gluinos, the set of graphs in which a right-handed squark is exchanged cannot interfere with the graphs in which a left-handed squark is exchanged because the incoming quark and anti-quark must have definite helicity. Production of charginos in association with gluinos involves only left-handed squarks.

In addition to the collinear singularities described above, this set of corrections also has infrared singularities that arise when the energy of the emitted gluon approaches zero. These singularities appear as poles in s_4 in the reduced cross section, and must also be extracted so that they can be combined with corresponding terms in the virtual corrections and shown to cancel.

To make this cancellation conveniently, we slice the gluon emission corrections into hard and soft pieces,

$$\frac{d^2 \hat{\sigma}_{ij}^R}{dt_2 du_2} = \int_0^\Delta ds_4 \frac{d^3 \hat{\sigma}_{ij}^S}{dt_2 du_2 ds_4} + \int_\Delta^{s_4^{max}} ds_4 \frac{d^3 \hat{\sigma}_{ij}^H}{dt_2 du_2 ds_4}, \tag{35}$$

where Δ is an arbitrary cut-off between what we call soft gluon radiation and hard gluon radiation. When the cut-off is much smaller than the other invariants, $\Delta \ll s, t, u, m_i^2$, the s_4 integration for the soft term becomes very simple and can be evaluated analytically. This operation results in singular terms

$$\begin{aligned} \frac{d^2 \hat{\sigma}_{ij}^B}{dt_2 du_2} & \left[\left(\frac{C_F \alpha_S}{\pi} \right) \left\{ \frac{1}{\epsilon^2} + \left(\frac{3}{2} + \log \frac{\mu^2}{s} \right) \frac{1}{\epsilon} \right\} \right. \\ & \left. - \left(\frac{N_C \alpha_S}{2\pi} \right) \left\{ \log \left(\frac{(s+t_2)(s+u_2)}{s m_1^2} \right) - 1 \right\} \frac{1}{\epsilon} \right]. \end{aligned} \quad (36)$$

In Eq. (36) we distinguish the contributions from the N_C and C_F color classes.

The singular expression may then be combined with the virtual corrections discussed in Sec. III A to yield the combined “soft and virtual” contribution free from infrared singularities. The residual finite soft contributions are presented in Appendix C.

In the hard gluon regime, there are collinear singularities, but no IR singularities, and thus the most singular terms are proportional to ϵ^{-1} . After the mass subtraction described above is performed, the results are singularity-free, and they can be presented as minimally subtracted, singularity-free integrals,

$$\begin{aligned} \hat{I}(f(\theta_1, \theta_2)) &= \int_0^\pi d\theta_1 \int_0^\pi d\theta_2 \sin^{1-2\epsilon}(\theta_1) \sin^{-2\epsilon}(\theta_2) f(\theta_1, \theta_2) \\ &- \frac{1}{\epsilon} \lim_{\epsilon \rightarrow 0} \left(\epsilon \int_0^\pi d\theta_1 \int_0^\pi d\theta_2 \sin^{1-2\epsilon}(\theta_1) \sin^{-2\epsilon}(\theta_2) f(\theta_1, \theta_2) \right), \end{aligned} \quad (37)$$

which contain only the finite terms with the ϵ^{-1} poles subtracted. The resulting expression consists of a simple power series in ϵ , which may then be evaluated in 4 dimensions by setting $\epsilon \rightarrow 0$. Note that the function $f(\theta_1, \theta_2)$ can involve coefficients for angular expressions that have mass dimension, and thus the mass dimension of $\hat{I}(f(\theta_1, \theta_2))$ will depend on $f(\theta_1, \theta_2)$. The gluon emission matrix elements are presented in Appendix D.

The cutoff on the s_4 integration introduces an implicit logarithmic dependence on Δ that is matched by the explicit logarithms of Δ which appear in the combined soft and virtual term. The total correction is independent of the value of Δ . Choosing for illustration $m_{1/2} = 400$ GeV, we display in Fig. 8 the dependence of various contributions on our

cutoff δ . The Born contribution is obviously independent of δ , but its contribution helps to show the relative magnitude of different terms. The combined soft and virtual contribution is positive but falls as an explicit analytic function of $\log\delta$. The hard part of the gluon emission contribution is negative, but its numerical value grows more positive as a implicit function of $\log\delta$. The figure shows that two contributions balance each other well, and the combined soft/virtual plus hard contribution is independent of the cutoff for $\delta < 2 \cdot 10^{-3}$. The figure also shows that the net small next-to-leading order contribution is obtained after large cancellations take place. The case chosen for display in Fig. 8 is a worst case. With $m_{1/2} = 400$ GeV, $m_{\tilde{\chi}_4^0} = 679$ GeV, and $m_{\tilde{g}} = 1012$ GeV. The energy chosen is that of the Tevatron, $\sqrt{S} = 2$ TeV, so phase space limitations are relatively severe for this set of masses. For all other cases, the cross sections are independent of δ for a larger range of δ .

2. Light Quark (Anti-Quark) Emission

A second set of real emission corrections involves an additional light quark (or anti-quark) in the final state, through the partonic reactions,

$$q g \rightarrow q \tilde{g} \tilde{\chi}, \bar{q} g \rightarrow \bar{q} \tilde{g} \tilde{\chi}. \quad (38)$$

The set of Feynman diagrams contributing to emission of a quark is shown in Fig. 7. They include diagrams in which an incoming gluon splits into a $q\bar{q}$ pair as well as diagrams in which an intermediate squark splits into a quark and either a gluino or gaugino. This set of corrections does not have an IR divergence, and thus it is not necessary to slice it into hard and soft regimes. However, after all of the initial state collinear singularities are removed by the mass factorization procedure described above, the matrix elements may still contain integrable singularities if the mass of the squark is larger than the mass of the gluino or gaugino. In these cases, the intermediate squark state can be on its mass-shell, and the variables $s_{4\Delta}$ and $s_{3\Delta}$ go to zero inside the region of integration. This problem was encountered previously [7], and we follow the same procedure. These singularities represent

the LO production of a squark and a gluino or gaugino, followed by the LO decay of the squark. They may be removed if one includes the full Breit-Wigner form for the squark propagator, which regulates the squark resonance by the squark width. This procedure amounts to the replacements,

$$\begin{aligned}\frac{1}{s_{4\Delta}} &\rightarrow \frac{1}{s_{4\Delta} + i m_{\tilde{q}_u} \Gamma_{\tilde{q}_u}} \rightarrow \mathcal{P}\left(\frac{1}{s_{4\Delta}}\right) - i \pi \delta(s_{4\Delta}) \\ \frac{1}{s_{3\Delta}} &\rightarrow \frac{1}{s_{3\Delta} + i m_{\tilde{q}_t} \Gamma_{\tilde{q}_t}} \rightarrow \mathcal{P}\left(\frac{1}{s_{3\Delta}}\right) - i \pi \delta(s_{3\Delta}),\end{aligned}\tag{39}$$

where \mathcal{P} indicates the principal value function, and the final distribution identity holds in the limit of small squark widths, $\Gamma_{\tilde{q}} \ll m_{\tilde{q}}$. The replacement removes the singularities, and when both $s_{4\Delta}$ and $s_{3\Delta}$ are zero it generates an additional real term from the product of δ functions.

There is a further subtlety associated with the requirement that we not double-count the region of phase space in which the squark is on-shell. Properly, the kinematic configuration with an on-shell squark is included in the LO production of a squark and a gluino or a squark and a gaugino, and thus should not be considered as a genuine higher order correction to the production of gluinos with gauginos. To avoid double counting, we thus subtract the on-shell squark contribution by defining the total cross section (for illustration, we deal with the $s_{4\Delta}$ singular case),

$$\hat{\sigma} = \int_0^{s_4^{max}} ds_4 \int_{t_2^-(s_4)}^{t_2^+(s_4)} dt_2 \frac{d^2 \hat{\sigma}}{dt_2 ds_4} = \int_0^{s_4^{max}} ds_4 \frac{f(s_{4\Delta})}{s_{4\Delta}^2 + m_{\tilde{q}}^2 \Gamma_{\tilde{q}}^2}.\tag{40}$$

The on-shell contribution then corresponds to $f(0) / (s_{4\Delta}^2 + m_{\tilde{q}}^2 \Gamma_{\tilde{q}}^2)$, with

$$f(0) = \hat{\sigma}_{\tilde{\chi}\tilde{q}}^B \frac{m_{\tilde{q}} \Gamma_{\tilde{q}}}{\pi} \frac{\Gamma_{\tilde{q} \rightarrow q \tilde{g}}^B}{\Gamma_{\tilde{q}}} \rightarrow \hat{\sigma}_{\tilde{\chi}\tilde{q}}^B BR(\tilde{q} \rightarrow q \tilde{g}) (s_{4\Delta}^2 + m_{\tilde{q}}^2 \Gamma_{\tilde{q}}^2) \delta(s_{4\Delta}).\tag{41}$$

It can be subtracted leaving a genuine NLO contribution

$$\hat{\sigma}^{\text{NLO}} = \int_0^{s_4^{max}} ds_4 \frac{f(s_{4\Delta}) - f(0)}{s_{4\Delta}^2 + m_{\tilde{q}}^2 \Gamma_{\tilde{q}}^2}\tag{42}$$

which may once again be expressed as a principal value function, since $s_{4\Delta} / (s_{4\Delta} + m_{\tilde{q}}^2 \Gamma_{\tilde{q}}^2) \rightarrow \mathcal{P}(1/s_{4\Delta})$ in the limit of small squark width. The $s_{3\Delta}$ singular terms may be treated in a

similar way, with the added complication that the integration over $s_{3\Delta}$ is hidden in the angular integrations [7].

The quark emission matrix elements are presented in Appendix E.

For the parameters of the SUGRA model that we adopt, the gluino mass remains greater than the squark mass for all values of $m_{1/2}$, and there is never an intermediate squark-to-gluino-plus-quark final state singularity. However, the two chargino masses and all four neutralino masses are always less than the squark mass, and the final-state on-shell squark-to-gaugino-plus-quark singularity comes into play in all cases. In the light gluino model, with $m_{\tilde{q}} = 450$ GeV, the gluino mass of 30 GeV is light enough that on-shell intermediate squark decay into a gluino is always active. In this light gluino model, as $m_{1/2}$ is varied from 100 to 400 GeV, the masses of the lighter gauginos ($\tilde{\chi}_1^0$, $\tilde{\chi}_2^0$, and $\tilde{\chi}_1^\pm$) remain less than the squark mass so that the on-shell intermediate squark decay into a gaugino is active over the whole range of $m_{1/2}$ for these light channels. The situation changes for the heavier gauginos ($\tilde{\chi}_3^0$, $\tilde{\chi}_4^0$, and $\tilde{\chi}_2^\pm$). For small $m_{1/2}$ their masses are below the squark mass, and the on-shell decay is active. However, above roughly $m_{1/2} = 250$ GeV, the masses of the heavier gauginos exceed the squark mass and the on-shell possibility closes.

IV. QUANTITATIVE RESULTS

In this section we collect our main results on total and differential cross sections for the associated production of gauginos and gluinos at Tevatron and LHC energies.

A. Scaling Functions

We begin with the cross section at the parton level expressed as

$$\hat{\sigma}_{ij} = \frac{\alpha\alpha_S(\mu)}{m^2} \left\{ f_{ij}^B(\eta) + 4\pi\alpha_S(\mu) \left[f_{ij}^{V+S}(\eta, \mu) + f_{ij}^H(\eta, \mu) \right] \right\}. \quad (43)$$

It has been integrated over the Mandelstam invariants t and s_4 and depends on the partonic center-of-mass energy s through the scaling variable

$$\eta = \frac{s}{4m^2} - 1, \quad (44)$$

where m is the average mass of the produced sparticles,

$$m = \frac{m_1 + m_2}{2}. \quad (45)$$

It also depends on the produced masses m_1 and m_2 and on the squark mass $m_{\tilde{q}}$ (through the internal squark propagator). The common renormalization and factorization scale is denoted by μ . The partonic initial state is labeled $i, j = g, q, \bar{q}$.

Equation (43) defines the dimensionless scaling functions f_{ij} , studied in Ref. [37]. These functions are independent of the coupling constants α and α_S , of parton densities, and of the collider type and energy. They permit precise checks of individual contributions and of the threshold, resonance, and high energy behaviors of the production process.

The Born f_{ij}^B and the summed virtual and soft scaling functions f_{ij}^{V+S} receive contributions only from $q\bar{q}$ initial states, where $q = u$ or d , with the possible emission of a soft and/or collinear gluon. The hard scaling function f_{ij}^H has contributions from qg initial states when an additional quark or antiquark is emitted together with the gluino and the gaugino. We eliminate the explicit dependence of the soft contributions on the technical cut-off $\delta = \Delta/m^2$ by subtracting the $\log^{(1,2)} \delta$ terms. These terms are then added to the hard contribution such that this contribution is also independent of δ . In Sec. III we show that our results are independent of δ at least in the range $\delta \in [10^{-5}; 10^{-3}]$, and we use the value $\delta = 10^{-4}$ in the following.

The scaling functions for the production of a \tilde{g} and a $\tilde{\chi}_2^0$ are presented in Fig. 9 and those for a \tilde{g} and a $\tilde{\chi}_1^\pm$ in Fig. 10. Here we set the scale μ equal to the average particle mass m . The masses are those of our default SUGRA scenario. As discussed in Sec. III B 2, the emission of an additional quark or antiquark can lead to intermediate on-shell squarks and therefore to a singular squark propagator in Feynman diagrams. After the LO two-body $q + g \rightarrow \tilde{g} + \tilde{q}$ contribution is removed, the remaining integrable singularities can be identified as spikes in the gu and gd scaling functions in the two figures. They yield finite contributions after

integration over the momentum fractions x_a and x_b of the incoming partons or, equivalently, over the partonic center-of-mass energy $s = x_a x_b S$.

Evident from Figs. 9 and 10 is that next-to-leading order contributions do not alter either the threshold or high energy asymptotic behaviors in η , unlike, e.g., the situation for pair production of heavy quarks [37,38]. The combined virtual and soft scaling functions f_{ij}^{V+S} contribute negatively but are small in magnitude when compared with the hard scaling functions f_{ij}^H . The figures show that one should expect only modest enhancements in predicted rates when the $u\bar{u}$, $d\bar{d}$, and $u\bar{d}$ production channels are dominant, as is true at Tevatron energies, for which the quark/antiquark parton luminosity is large and the range in η is limited ($\eta < 15$ for these two channels in our default scenario). The contribution of the qg channel can become important if phase space is open to large values of η . At LHC energies, η extends to nearly 800. This range in η , along with the large qg luminosity, suggests that the qg channel will supply significant enhancements in the predicted rates at LHC energies, as is demonstrated below.

Scaling functions for the $\tilde{g}\tilde{\chi}_1^0$, $\tilde{g}\tilde{\chi}_4^0$, and $\tilde{g}\tilde{\chi}_2^\pm$ channels show behavior similar to that seen in Figs. 9 and 10, with the notable exception that the positive excursion at large η in the qg channels is relatively more prominent for $\tilde{g}\tilde{\chi}_4^0$ and $\tilde{g}\tilde{\chi}_2^\pm$ than for $\tilde{g}\tilde{\chi}_2^0$ and $\tilde{g}\tilde{\chi}_1^\pm$. The $\tilde{g}\tilde{\chi}_3^0$ channel is distinguished primarily by the fact that the peak in the η distribution at the Born level occurs near $\eta = 0.4$ whereas the peaks occur at larger η , in the range of $\eta = 1$ to 2, in all other cases. There is also a noticeable difference in threshold behaviors of the Born and NLO hard-gluon emission contributions for this channel. We relate these differences to the fact that only the $\tilde{g}\tilde{\chi}_3^0$ channel exhibits positive interference at the Born level between the t- and u-channel contributions, c.f., Eq. (4). Because $m_{\tilde{\chi}_3^0}$ is negative in the SUGRA model, the term proportional to X_{tu} in Eq. (4) is positive for $\tilde{g}\tilde{\chi}_3^0$ production but negative in all other cases.

B. Hadronic Total Cross Sections

The hadronic total cross section is obtained from the partonic cross section through

$$\sigma^{h_1 h_2}(S, \mu) = \sum_{i,j=g,q,\bar{q}} \int_{\tau}^1 dx_a \int_{\tau/x_a}^1 dx_b f_i^{h_1}(x_a, \mu) f_j^{h_2}(x_b, \mu) \hat{\sigma}_{ij}(x_a x_b S, \mu), \quad (46)$$

where

$$\tau = \frac{4m^2}{S}, \quad (47)$$

and \sqrt{S} is the hadronic center-of-mass energy (2 TeV for Run II at the Fermilab $p\bar{p}$ collider Tevatron and 14 TeV at the CERN pp collider LHC). Our NLO predictions are calculated in the $\overline{\text{MS}}$ scheme with the CTEQ5M parametrization [39] for the parton densities $f(x, \mu)$ in the proton and antiproton and a two-loop approximation for the strong coupling constant α_S with $\Lambda^{(5)} = 226$ MeV. This value of $\Lambda^{(5)}$ is used also in the renormalization group evolution equations for our SUSY scenarios. In obtaining LO cross sections, we use the CTEQ5L LO parton densities and the one-loop approximation for α_S , with $\Lambda^{(5)} = 146$ MeV.

1. SUGRA model results

For the SUGRA scenario, we present the total hadronic cross sections for the associated production of gluinos and gauginos at Run II of the Tevatron in Fig. 11 and for the LHC in Fig. 12. We vary the SUGRA parameter $m_{1/2}$ from 100 to 400 GeV and keep the other SUGRA parameters fixed at the values described in Sec. II A. The squark mass runs from 250 GeV to 890 GeV in this region. The cross sections are presented as a function of the physical gluino mass $m_{\tilde{g}}$. The corresponding gaugino mass ranges are 31 to 163 GeV for $\tilde{\chi}_1^0$, 62 to 317 GeV for $\tilde{\chi}_2^0$ and $\tilde{\chi}_1^{\pm}$, 211 to 666 GeV for $\tilde{\chi}_3^0$, and 240 to 679 GeV for $\tilde{\chi}_4^0$ and $\tilde{\chi}_2^{\pm}$. The chargino cross sections are summed over positive and negative charges. The renormalization and factorization scale μ is set equal to the average particle mass m . We truncate Fig. 11 at a cross section of 10^{-5} pb since the anticipated integrated luminosity at Run II is at most

30 fb⁻¹. For the convenience of the reader, we provide numerical values of the cross sections in Table I for a few selected points.

For small $m_{\tilde{g}}$ one might expect the largest cross section for the lightest gaugino, $\tilde{\chi}_1^0$. However, its coupling is dominantly of type \tilde{B} and therefore smaller than the \tilde{W}_3 -type coupling of $\tilde{\chi}_2^0$ which, in turn, has a larger cross section despite its larger mass. The heavier gauginos $\tilde{\chi}_{3,4}^0$ and $\tilde{\chi}_2^\pm$ are dominantly Higgsino and are therefore suppressed by several orders of magnitude with respect to the lighter gauginos because of the light quark Yukawa couplings. At the LHC, the $\tilde{\chi}_1^\pm$ cross section is dominant. At small values of $m_{\tilde{g}}$, the LHC cross sections are a factor of about 30 greater than at the Tevatron, and at large $m_{\tilde{g}}$, the factor is about 10⁴.

Comparing the NLO predictions in Figs. 11 and 12 (solid curves) with the LO predictions (dashed curves) we observe that the NLO corrections are all positive and substantially larger at the LHC than at the Tevatron. At the Tevatron, some of the NLO predictions fall below the LO predictions at large mass, a point to which we return below. The NLO enhancements are more evident in the ratio of the NLO over the LO cross section (K factors) shown in Figs. 13 and 14. The K factors are computed at the scale $\mu = m$. At the Tevatron, the NLO corrections amount to at most a 10% increase in cross section. At the LHC, they appear generally in the range of 20 to 40% but can amount to a factor of 2 for $\tilde{\chi}_4^0$ and $\tilde{\chi}_2^\pm$.

The very modest size of the NLO enhancement at the Tevatron is somewhat expected from the behavior of the scaling functions, but it is also attributable partly to differences in the NLO and LO parton densities. Recalculating the K factors with the CTEQ4 parametrization [40], we find increases in K by as much as 0.1 at the Tevatron energy. The change from CTEQ4 to CTEQ5 is interesting. The u quark density at NLO decreased by 1 to 5% and the d quark density at NLO increased by up to 10% over the range $0.1 < x < 0.6$. On the other hand, the LO u quark density increased by about 1% and the LO d quark density by up to 20%. These purely parton density effects result in a net increase in the LO cross sections and decrease in the NLO cross sections, a drop in the calculated K factors

from CTEQ4 to CTEQ5.

The contribution from the qg initial state at the energy of the Tevatron is insignificant (less than 10^{-3} of the total) for all six gaugino channels, but it is considerable at the energy of the LHC. In Fig. 15 we show the fraction of the NLO cross section at the LHC attributed to the qg initial state. At the energy of the LHC, the contribution from the $q\bar{q}$ channel is less dominant, and the qg contribution becomes significant owing to the large gluon density. A similar effect is seen in single top quark production [41] for comparable values of the average produced mass m .

The large K factor for $\tilde{\chi}_4^0$ and $\tilde{\chi}_2^\pm$ production at the LHC is associated with a large contribution from the qg channel at this energy. For these two channels, there is strong interference at LO between the t- and u-channel exchange diagrams that does not occur in the NLO quark emission graphs.

The dependence of the predicted cross sections on the renormalization and factorization scale is reduced considerably at next-to-leading order. As an example, in Fig. 16 we show the scale dependences for the $\tilde{\chi}_2^0$ channel at the Tevatron. All six channels show similar behavior at the Tevatron. Cross sections vary by $\pm 23\%$ at LO but only by $\pm 8\%$ at NLO as the scale ratio μ/m is varied over the range 0.5 to 2.0, a substantial improvement in reliability. Here m is the average mass for the default scenario. At the Tevatron, the NLO and LO cross sections intersect at scale ratio near unity. In Fig. 17 we show the μ dependences for the $\tilde{\chi}_2^0$ channel at the LHC. Again, all six channels show similar behavior. Cross sections vary by $\pm 12\%$ at LO but only by $\pm 4.5\%$ at NLO in the region $0.5 < \mu/m < 2.0$. However, unlike the situation at the Tevatron, owing to the important contribution of the qg channel at the energy of the LHC, the NLO and LO cross sections do not intersect at scale ratio near unity. Instead, if they intersect at all, the crossing point is at a very low scale.

Uncertainties in the cross section from parton density variation may be estimated roughly if we compare NLO results obtained with CTEQ4M and CTEQ5M. For $\tilde{\chi}_2^0$ production at the Tevatron in our default SUGRA scenario, we compute cross sections of 0.0244 pb (CTEQ4M) and 0.0219 pb (CTEQ5M), a 12% difference. At the LHC, the cross sections are 1.138 pb

(CTEQ4M), and 1.095 pb (CTEQ5M), a 4% difference.

2. Light gluino model

For the light gluino model, we present the total hadronic cross sections for the associated production of gluinos and gauginos at Run II of the Tevatron in Fig. 18 and for the LHC in Fig. 19. As mentioned in Sec. II A, we fix $m_{\tilde{g}} = 30$ GeV and $m_{\tilde{q}} = 450$ GeV. We display the cross sections as functions of the mass of the common GUT-scale fermion mass $m_{1/2}$. As we vary $m_{1/2}$ from 100 to 400 GeV, the gaugino masses range from 31 to 163 GeV for $\tilde{\chi}_1^0$, 62 to 317 GeV for $\tilde{\chi}_2^0$ and $\tilde{\chi}_1^\pm$, 211 to 666 GeV for $\tilde{\chi}_3^0$, and 240 to 679 GeV for $\tilde{\chi}_4^0$ and $\tilde{\chi}_2^\pm$. It is worth noting that the coupling strengths also vary with $m_{1/2}$. The chargino cross sections are summed over positive and negative charges. The renormalization and factorization scale μ is set equal to the average of the masses of the gaugino and gluino in each of the channels.

Evident in Figs. 18 and 19 is that the cross sections do not depend strongly on the gaugino masses. The values of $m_{1/2}$ in these figures extend below the value $\simeq 150$ GeV believed excluded since LEP data [21] set a lower bound on the mass of $\tilde{\chi}_1^\pm$ of about 100 GeV. Nevertheless, even above $m_{1/2} = 150$ GeV, the Tevatron cross sections for the three lighter gluino channels are predicted to be in the range of 0.1 to 0.5 pb. The cross sections would be increased if $m_{\tilde{q}}$ were reduced from the value 450 GeV that we use.

The relatively large cross sections suggest that associated production is a good channel for discovery of a light gluino at the Tevatron, for closing the window on this possibility, and/or for setting limits on light gaugino masses. We remark in this connection that the usual searches for a light gluino LSP begin with the assumption of pair production of gluinos. In this situation, the dominant background is QCD pair production of hadronic jets. Hard cuts on transverse momentum must be made to reduce this background to tolerable levels. The cuts, in turn, mitigate against gluinos of modest mass. By contrast, if light gluinos are produced in association with gauginos, one can search for light gluino monojets accompanied by leptons and/or missing transverse energy from gaugino decays.

The K factors for the light gluino case are shown in Figs. 20 and 21. At the Tevatron, the NLO corrections amount to a 30% to 40% increase in cross section. At the LHC, they are generally in the range of a factor of 2 to 3.5. The large K factors owe their origins to the important role of the gq channel. The gluon parton density is very large at small values of x . Contributions from the gq production channel are more intense in the light gluino case than in the SUGRA case where average produced masses and, thus, typical values of x are larger. At the energy of the Tevatron, the gq channel accounts for more than 20% of the NLO cross section in the $\tilde{\chi}_1^0$ and $\tilde{\chi}_1^\pm$ channels at small values of $m_{1/2}$ and more than 10% at large $m_{1/2}$. At the energy of the LHC, the fraction exceeds 60% in the $\tilde{\chi}_1^0$, $\tilde{\chi}_2^0$, and $\tilde{\chi}_1^\pm$ channels for the entire range of $m_{1/2}$. It hovers above 50% in the $\tilde{\chi}_3^0$, $\tilde{\chi}_4^0$, and $\tilde{\chi}_2^\pm$ channels at small values of $m_{1/2}$ and near 20% at large $m_{1/2}$.

Motivated by the curious behavior of the K factors for the three heavier gaugino channels at the LHC energy, we examined the change in the scaling functions for the $\tilde{\chi}_4^0$ case as $m_{1/2}$ is varied. In the $q\bar{q}$ channel, the net (virtual plus soft plus hard) NLO contribution is positive for all η , and, relative to the Born contribution, its magnitude grows gradually with $m_{1/2}$. The $q\bar{q}$ channel accounts for a slightly increasing component of K , hovering about 1.5. On the other hand, the contribution from the gq channel changes markedly as $m_{1/2}$ increases. Below about $m_{1/2} = 200$ GeV, its scaling function is large, with significant support below $\eta = 1$, where the gluon parton density is large. As $m_{1/2}$ increases above 200 GeV, the gq scaling function decreases in magnitude. The gq channel supplies a component of K that increases slightly from about 2 to 2.5 as $m_{1/2}$ increases to 200 GeV and then falls gradually to below 0.5 at $m_{1/2} = 400$ GeV.

We attribute the sharp decrease of the K factor for the three heavier gaugino channels to the role of on-shell intermediate squark decay into a gaugino, discussed in Sec. III B 2. In the light gluino model, as $m_{1/2}$ is varied from 100 to 400 GeV, the masses of the lighter gauginos ($\tilde{\chi}_1^0$, $\tilde{\chi}_2^0$, and $\tilde{\chi}_1^\pm$) remain less than the squark mass so that the on-shell intermediate squark decay into a gaugino is active over the whole range of $m_{1/2}$ for these light channels. The situation changes for the heavier gauginos ($\tilde{\chi}_3^0$, $\tilde{\chi}_4^0$, and $\tilde{\chi}_2^\pm$). For small $m_{1/2}$ their

masses are below the squark mass, and the on-shell decay is active. However, above roughly $m_{1/2} = 250$ GeV, the masses of the heavier gauginos exceed the squark mass and the on-shell possibility closes.

C. Differential Cross Sections

In Figs. 22 and 23, we display the differential cross sections in the rapidity y and in the transverse momentum p_T of $\tilde{\chi}_1^\pm$ at the energy of the Tevatron collider. Here the $\tilde{\chi}_1^\pm$ and \tilde{g} masses are set at their default values in the SUGRA scenario, 101 and 410 GeV, respectively. The rapidity distribution is obtained after integration over all p_T , and the p_T distribution after integration over all y . More restrictive selections could be made, but until experimental conditions are better known, any such restrictions (cuts) would be unmotivated. The NLO (solid) curve in Fig. 22 shows a modest enhancement in the rapidity distribution in the central region with respect to the LO (dashed) curve, but the shape of the distribution is unchanged qualitatively. The p_T distributions in Fig. 23 show that the NLO contribution tends to shift the distribution to somewhat smaller values of p_T . Since the contribution of the gq initial state is very small at the energy of the Tevatron, the shift in the p_T distribution is associated with next-to-leading order corrections in the dominant $q\bar{q}$ initial state.

The features of the y distributions are qualitatively similar for all gauginos except for the expected and systematic narrowing of the y distribution with increasing gaugino mass. We show one example representative of the full set. The p_T distributions for the different gauginos are also qualitatively similar except that the maximum in the distribution moves to larger p_T as the gaugino mass is increased. The location of the peak is specified roughly by $m/2$, where m is the average mass of the produced sparticles. The one exception is $\tilde{\chi}_3^0$ production. In this case, the peak occurs at a smaller value (about 100 GeV for the default masses), an effect correlated with the fact that the location of the peak in the scaling function occurs at a smaller value of η . Interference effects enhance the cross section at small p_T for $\tilde{\chi}_3^0$ production.

We show differential cross sections in y and p_T for $\tilde{\chi}_1^\pm$ at the energy of the LHC collider in Figs. 24 and 25, and in Fig. 26 we present the p_T distribution for $\tilde{\chi}_4^0$. The rapidity and transverse momentum distributions are much broader than at the Tevatron. As at the energy of the Tevatron, the features of the y distributions are qualitatively similar for all gauginos except for the expected and systematic narrowing of the y distribution with increasing gaugino mass. The NLO contributions enhance the y distributions at all y .

At the energy of the LHC, the p_T spectra are qualitatively similar for the relatively light $\tilde{\chi}_1^0$, $\tilde{\chi}_2^0$, and $\tilde{\chi}_1^\pm$ states, illustrated by the $\tilde{\chi}_1^\pm$ case in Fig. 25. The enhancement factor K is near unity at small p_T but becomes sizeable at larger p_T . For $\tilde{\chi}_4^0$ and $\tilde{\chi}_2^\pm$, the p_T spectra are altered significantly by NLO contributions. As illustrated in Fig. 26, the NLO contribution associated with the important qg channel fills in the distribution at small p_T and softens the overall p_T distribution in these two cases. At LHC energies, it is therefore not a good approximation to assume that the enhancement factor K is roughly independent of p_T .

V. CONCLUSIONS

In this paper we report a complete next-to-leading order analysis of the associated production of gauginos and gluinos at hadron colliders. If supersymmetry exists at the electroweak scale, the cross section for this process is expected to be observable at the Fermilab Tevatron and/or the CERN LHC. It is enhanced by the large color charge of the gluino and the relatively small mass of the light gauginos in many SUSY models. Associated production represents a chance to study in detail the parameters of the soft SUSY-breaking Lagrangian. The rates are proportional to the phases of the gaugino and gluino masses, and to the mixings in the squark and chargino/neutralino sectors. Thus, in combination with other channels, associated production could allow one to measure some or all of these quantities.

The physical gluino and gaugino masses that we use, as well as the gaugino mixing matrices, are based on four popular SUSY breaking models plus a fifth scenario in which the

gluino mass is relatively light. Because the LO cross sections in gauge-mediated, gaugino-mediated, and anomaly-mediated supersymmetry breaking models are not too dissimilar from those of the SUGRA case at Tevatron energies, we focus our NLO work on the SUGRA model and on a model with a light gluino LSP, with $m_{\tilde{g}} = 30$ GeV.

In the SUGRA model, the largest cross sections at the Fermilab Tevatron energy are those for $\tilde{\chi}_2^0$, enhanced by its \tilde{W}_3 -like coupling with respect to the \tilde{B} -like $\tilde{\chi}_1^0$, and the $\tilde{\chi}_1^\pm$, which is about equal in mass with the $\tilde{\chi}_2^0$. The NLO corrections to associated production are generally positive, but they can be modest in size, ranging in the SUGRA model from a few percent at the energy of the Tevatron to 100% at the energy of the LHC, depending on the sparticle masses. In the light-gluino case, NLO contributions increase the cross section by factors of 1.3 to 1.4 at the energy of the Tevatron and by factors of 2 to 3.5 at the energy of the LHC. The large K factors owe their origins to the important role of the gq channel that enters first at NLO.

Owing to the NLO enhancements, collider searches for signatures of associated production will generally discover or exclude sparticles with masses larger than one would estimate based on LO production rates alone. More significant from the viewpoint of reliability, the renormalization and factorization scale dependence of the cross sections is reduced by a factor of more than two when NLO contributions are included.

At Run II of the Fermilab Tevatron, for an integrated luminosity of 2 fb^{-1} , we expect that 10 or more events could be produced in each of the lighter gaugino channels of the SUGRA model, $\tilde{g}\tilde{\chi}_1^0$, $\tilde{g}\tilde{\chi}_2^0$, and $\tilde{g}\tilde{\chi}_1^\pm$, provided that the gluino mass $m_{\tilde{g}}$ is less than 450 GeV. The cross sections for the three heavier gaugino channels, $\tilde{g}\tilde{\chi}_3^0$, $\tilde{g}\tilde{\chi}_4^0$, and $\tilde{g}\tilde{\chi}_2^\pm$, are smaller by an order of magnitude or more than those of the lighter gaugino channels. In the light gluino model, more than 100 events could be produced in the three lighter gaugino channels provided that the common GUT-scale fermion mass $m_{1/2}$ is less than 400 GeV, and as many as 10 events in the three heavier gaugino channels as long as $m_{1/2}$ is less than 200 GeV. At the higher energy and luminosity of the LHC, at least a few events should be produced in every channel in the SUGRA model and many more in the light gluino model.

The shapes of the rapidity distributions of the gauginos are not altered appreciably by NLO contributions, but the locations of the maximum cross section in transverse momentum (p_T) are shifted to smaller values by NLO contributions. At LHC energies where the contribution of the qg initial state is important, modifications of the p_T spectra can be pronounced.

The relatively large cross sections suggest that associated production is a good channel for discovery of a light gluino at the Tevatron, for closing the window on this possibility, and/or for setting limits on light gaugino masses. The usual searches for a light gluino LSP are based on the assumption that gluinos are produced in pairs. In this situation, the dominant background is QCD production of hadronic jets. Hard cuts on transverse momentum must be made to reduce this background to tolerable levels. The cuts, in turn, mitigate against gluinos of modest mass. By contrast, if light gluinos are produced in association with gauginos, one can search for light gluino monojets accompanied by leptons and/or missing transverse energy from gaugino decays.

ACKNOWLEDGMENTS

Work in the High Energy Physics Division at Argonne National Laboratory is supported by the U.S. Department of Energy, Division of High Energy Physics, under Contract W-31-109-ENG-38. M. Klasen is supported by the Bundesministerium für Bildung und Forschung under Contract 05 HT9GUA 3, by the Deutsche Forschungsgemeinschaft under Contract KL 1266/1-1, and by the European Commission under Contract ERBFMRXCT980194. The authors are grateful for correspondence with W. Beenakker and T. Plehn and conversations with S. Mrenna. T. Tait benefitted from discussions with D. Kaplan, G. Kribs, and C.–P. Yuan.

APPENDIX A: VIRTUAL LOOP CONTRIBUTIONS

At the one-loop level in SUSY-QCD, virtual corrections contribute to the hadroproduction of supersymmetric particles through the interference of self-energy corrections, vertex corrections, and box diagrams with the tree-level diagrams. For the associated production of gluinos and gauginos one has to calculate the self-energy corrections in Fig. 3, the vertex corrections in Fig. 4, and the box diagrams in Fig. 5.

The self-energy corrections for the external quark and antiquark factorize the complete Born matrix element and are independent of the underlying scattering process. Since the quark and antiquark are treated as massless, only the squark-gluino loop contributes to

$$|\overline{\mathcal{M}}^q|^2 = i[B_0(0; m_{\tilde{g}}, m_{\tilde{q}}) + B'_0(0; m_{\tilde{g}}, m_{\tilde{q}})(m_{\tilde{g}}^2 - m_{\tilde{q}}^2)]2C_F\hat{g}_s^2|\overline{\mathcal{M}}^B|^2, \quad (\text{A1})$$

where the factor of two accounts for the sum of the quark and antiquark contributions. Functions $B_0(p^2; m_1, m_2)$ and $B'_0(p^2; m_1, m_2)$ stand for the scalar two-point integral and its derivative. They are defined in Appendix B. The quark-gluon loop contains an infrared singularity

$$|\overline{\mathcal{M}}_{\text{IR}}^q|^2 = C_\epsilon \frac{1}{\epsilon} 2C_F g_s^2 |\overline{\mathcal{M}}^B|^2, \quad (\text{A2})$$

where $C_\epsilon = (4\pi)^\epsilon / (16\pi^2) e^{-\epsilon\gamma_E}$. This infrared singularity is not shown in the result above since it is canceled by an ultraviolet singularity when infrared and ultraviolet singularities are not distinguished in dimensional regularization.

The external gluino self-energy also factorizes the complete Born matrix element and is independent of the underlying scattering process:

$$\begin{aligned} |\overline{\mathcal{M}}^{\tilde{g}}|^2 = & i \left[\frac{A_0(m_{\tilde{g}})}{m_{\tilde{g}}^2} (1 - \epsilon) - 4B'_0(m_{\tilde{g}}^2; 0, m_{\tilde{g}}) m_{\tilde{g}}^2 \right] N_C g_s^2 |\overline{\mathcal{M}}^B|^2 \\ & + i \left[-\frac{A_0(m_{\tilde{q}})}{2m_{\tilde{g}}^2} + B_0(m_{\tilde{g}}^2; m_{\tilde{q}}, 0) \frac{m_{\tilde{g}}^2 + m_{\tilde{q}}^2}{2m_{\tilde{g}}^2} + B'_0(m_{\tilde{g}}^2; m_{\tilde{q}}, 0) (m_{\tilde{g}}^2 - m_{\tilde{q}}^2) \right] n_f 4 \frac{1}{2} \hat{g}_s^2 |\overline{\mathcal{M}}^B|^2 \\ & + i \left[\frac{A_0(m_t)}{2m_{\tilde{g}}^2} - \frac{A_0(m_{\tilde{q}})}{2m_{\tilde{g}}^2} + B_0(m_{\tilde{g}}^2; m_{\tilde{q}}, m_t) \frac{m_{\tilde{g}}^2 - m_t^2 + m_{\tilde{q}}^2}{2m_{\tilde{g}}^2} + B'_0(m_{\tilde{g}}^2; m_{\tilde{q}}, m_t) \right. \\ & \quad \left. \times (m_{\tilde{g}}^2 + m_t^2 - m_{\tilde{q}}^2) \right] 4 \frac{1}{2} \hat{g}_s^2 |\overline{\mathcal{M}}^B|^2. \end{aligned} \quad (\text{A3})$$

The scalar one-point integral $A_0(m)$ is defined in Appendix B. Except for the gluino mass and the N_C color factor, the gluon-gluino loop is identical to the heavy-quark self-energy. It contains an infrared singularity in the derivative of the scalar two-point integral:

$$\overline{|\mathcal{M}_{\text{IR}}^g|^2} = -C_\epsilon \frac{1}{\epsilon} 4 \frac{N_C}{2} g_s^2 \overline{|\mathcal{M}^B|^2}. \quad (\text{A4})$$

The quark-squark loop with a color factor of $1/2$ contributes through two different fermion number flows due to the Majorana nature of gluinos. We take into account $n_f = 5$ light (s)quark flavors and a heavy top (s)quark. We do not include mixing in the top squark sector and take the top squark mass equal to the light squark masses. We set $m_t = 175$ GeV.

The gaugino couples only electroweakly to the quarks and squarks and thus does not give rise to strong self-energy corrections. All external particle self-energies have been renormalized on-shell and multiplied by a factor of $1/2$ for proper wave function renormalization.

The self-energy correction of the internal squark propagator depends on the off-shell squark four-momentum squared. Therefore, it factorizes only the corresponding t - or u -channel interference piece of the Born matrix element:

$$\begin{aligned} \overline{|\mathcal{M}^{\tilde{q}i}|^2} = & i \left[B_0(t; m_{\tilde{g}}, 0) \frac{t - m_{\tilde{g}}^2}{t - m_{\tilde{q}}^2} - B_0(m_{\tilde{q}}^2; m_{\tilde{g}}, 0) \frac{m_{\tilde{q}}^2 - m_{\tilde{g}}^2}{t - m_{\tilde{q}}^2} \right] 4C_F \hat{g}_s^2 [\overline{|\mathcal{M}^t \mathcal{M}^{t*}|} + \overline{|\mathcal{M}^t \mathcal{M}^{u*}|}] \\ & - i \left[B_0(t; m_{\tilde{q}}, 0) \frac{t + m_{\tilde{q}}^2}{t - m_{\tilde{q}}^2} - B_0(m_{\tilde{q}}^2; m_{\tilde{q}}, 0) \frac{2m_{\tilde{q}}^2}{t - m_{\tilde{q}}^2} \right] 4C_F g_s^2 [\overline{|\mathcal{M}^t \mathcal{M}^{t*}|} + \overline{|\mathcal{M}^t \mathcal{M}^{u*}|}]. \quad (\text{A5}) \end{aligned}$$

The ultraviolet divergences cancel between the quark-gluino loop contribution and its supersymmetric counterpart, the squark-gluon loop contribution. Since the gluon tadpole contribution is quadratic in the loop momentum it vanishes in dimensional regularization. The squark tadpole contribution vanishes after renormalization. The u -channel result can be obtained from the t -channel result given above through the exchange $t \leftrightarrow u$.

Like the self-energy correction of the squark propagator, the corrections to the quark-squark-gluino and quark-squark-gaugino vertices depend on the four-momentum squared of the squark and factorize only the t - or u -channel interference pieces of the Born matrix element. The quark-squark-gaugino vertex receives corrections through a gluon and a gluino

exchange between the initial state quark or antiquark and the squark that are proportional to the gauge and Yukawa coupling, respectively. For the t -channel we find

$$\begin{aligned}
\overline{|\mathcal{M}^{q\bar{q}\tilde{\chi}}|^2} &= i \left[B_0(t; m_{\tilde{g}}, 0) - B_0(m_{\tilde{\chi}}^2; m_{\tilde{q}}, 0) + C_0(m_{\tilde{\chi}}^2, 0, t; 0, m_{\tilde{q}}, m_{\tilde{g}})(t + m_{\tilde{q}}^2 - m_{\tilde{g}}^2 - m_{\tilde{\chi}}^2) \right] \\
&\quad \times \frac{m_{\tilde{g}} m_{\tilde{\chi}}}{t - m_{\tilde{\chi}}^2} 4C_F \hat{g}_s^2 \frac{X_t^{q'\tilde{q}\tilde{\chi}*}}{X_t^{q\bar{q}'\tilde{\chi}}} [\overline{|\mathcal{M}^t \mathcal{M}^{t*}|} + \overline{|\mathcal{M}^t \mathcal{M}^{u*}|}] \\
&\quad + i \left[B_0(t; m_{\tilde{q}}, 0) \frac{t + m_{\tilde{\chi}}^2}{2(t - m_{\tilde{\chi}}^2)} - B_0(m_{\tilde{\chi}}^2; m_{\tilde{q}}, 0) \frac{m_{\tilde{\chi}}^2}{t - m_{\tilde{\chi}}^2} + C_0(m_{\tilde{\chi}}^2, 0, t; m_{\tilde{q}}, 0, 0) \right. \\
&\quad \left. \times (m_{\tilde{\chi}}^2 - m_{\tilde{q}}^2) \right] 4C_F g_s^2 [\overline{|\mathcal{M}^t \mathcal{M}^{t*}|} + \overline{|\mathcal{M}^t \mathcal{M}^{u*}|}]. \tag{A6}
\end{aligned}$$

Function $C_0(p_1^2, p_2^2, (p_1 + p_2)^2; m_1, m_2, m_3)$ stands for the scalar three-point integral defined in Appendix B. The ratio of quark-squark-gaugino couplings $X_t^{q'\tilde{q}\tilde{\chi}*}/X_t^{q\bar{q}'\tilde{\chi}}$ accounts for reversed flavor flow in the vertex correction with respect to the underlying Born matrix element in the case of the exchange of an additional gluino. For neutralinos with real couplings it reduces to unity, whereas for charginos with real couplings it is given by a ratio of chargino mixing matrix elements. The infrared singularities

$$\overline{|\mathcal{M}_{\text{IR}}^{q\bar{q}\tilde{\chi}}|^2} = -C_\epsilon \left[\frac{1}{\epsilon} + \frac{1}{\epsilon} \log \left(\frac{m_{\tilde{q}}^2 - t}{m_{\tilde{q}}^2 - m_{\tilde{\chi}}^2} \right) \frac{m_{\tilde{q}}^2 - m_{\tilde{\chi}}^2}{t - m_{\tilde{\chi}}^2} \right] 4C_F g_s^2 [\overline{|\mathcal{M}^t \mathcal{M}^{t*}|} + \overline{|\mathcal{M}^t \mathcal{M}^{u*}|}] \tag{A7}$$

arise from the gluon exchange correction. In dimensional regularization, the gauge bosons have $(n - 2)$ degrees of freedom whereas their supersymmetric counterparts, the gauginos, have two. This difference leads to a mismatch between the quark-quark-gauge boson gauge couplings and the quark-squark-gaugino Yukawa couplings through finite next-to-leading order terms. The (super-)symmetry between the gauge and Yukawa couplings can be restored through a finite renormalization contribution

$$\overline{|\mathcal{M}_{\text{finite}}^{q\bar{q}\tilde{\chi}}|^2} = -C_\epsilon C_F g_s^2 [\overline{|\mathcal{M}^t \mathcal{M}^{t*}|} + \overline{|\mathcal{M}^t \mathcal{M}^{u*}|}], \tag{A8}$$

that can be found by comparing the quark-squark-gaugino vertex correction given above with the corresponding quark-quark-gauge boson vertex correction in exact supersymmetry. All u -channel results can again be obtained through the exchange $t \leftrightarrow u$.

The quark-squark-gluino vertex correction can be obtained from the quark-squark-gaugino vertex correction if $m_{\tilde{\chi}}$ is replaced with $m_{\tilde{g}}$ and the color factor C_F with $C_F - N_C/2$.

There are, however, two additional contributions with a color factor of $N_C/2$, due to the non-Abelian gauge coupling of the gluino to the gluon, when a gluon is exchanged between the final state gluino and the initial state quark or antiquark and the squark. For the total quark-squark-gluino vertex correction in the t -channel we find

$$\begin{aligned}
\overline{|\mathcal{M}^{q\bar{q}\tilde{g}}|}^2 &= \overline{|\mathcal{M}^{q\bar{q}\tilde{\chi}}|}^2(m_{\tilde{\chi}} \rightarrow m_{\tilde{g}}, C_F \rightarrow C_F - N_C/2) \\
&+ i \left[B_0(t; m_{\tilde{g}}, 0) \left(\frac{m_{\tilde{g}}^2}{t - m_{\tilde{g}}^2} + \epsilon \right) - B_0(m_{\tilde{g}}^2; m_{\tilde{g}}, 0) \frac{t}{t - m_{\tilde{g}}^2} + C_0(m_{\tilde{g}}^2, 0, t; m_{\tilde{g}}, 0, 0)(t - m_{\tilde{g}}^2) \right. \\
&+ \left. B_0(t; 0, m_{\tilde{q}}) \frac{t + m_{\tilde{q}}^2}{2(t - m_{\tilde{q}}^2)} - B_0(m_{\tilde{q}}^2; 0, m_{\tilde{q}}) \frac{t}{t - m_{\tilde{q}}^2} + C_0(m_{\tilde{q}}^2, 0, t; 0, m_{\tilde{q}}, m_{\tilde{q}}) \frac{m_{\tilde{q}}^4 - tm_{\tilde{q}}^2}{t - m_{\tilde{q}}^2} \right] \\
&\times 4 \frac{N_C}{2} g_s^2 [\overline{|\mathcal{M}^t \mathcal{M}^{t*}|} + \overline{|\mathcal{M}^t \mathcal{M}^{u*}|}]. \tag{A9}
\end{aligned}$$

It contains the following infrared singularities:

$$\begin{aligned}
\overline{|\mathcal{M}_{\text{IR}}^{q\bar{q}\tilde{g}}|}^2 &= \overline{|\mathcal{M}_{\text{IR}}^{q\bar{q}\tilde{\chi}}|}^2(m_{\tilde{\chi}} \rightarrow m_{\tilde{g}}, C_F \rightarrow C_F - N_C/2) \\
&- C_\epsilon \left[\frac{1}{2\epsilon^2} + \frac{1}{\epsilon} + \frac{1}{2\epsilon} \log \left(\frac{Q^2}{m_{\tilde{g}}^2} \right) - \frac{1}{\epsilon} \log \left(\frac{m_{\tilde{g}}^2 - t}{m_{\tilde{g}}^2} \right) \right] \\
&\times 4 \frac{N_C}{2} g_s^2 [\overline{|\mathcal{M}^t \mathcal{M}^{t*}|} + \overline{|\mathcal{M}^t \mathcal{M}^{u*}|}]. \tag{A10}
\end{aligned}$$

The finite renormalization contribution for the gluino vertex correction is

$$\overline{|\mathcal{M}_{\text{finite}}^{q\bar{q}\tilde{g}}|}^2 = C_\epsilon \left(\frac{4}{3} N_C - C_F \right) g_s^2 [\overline{|\mathcal{M}^t \mathcal{M}^{t*}|} + \overline{|\mathcal{M}^t \mathcal{M}^{u*}|}]. \tag{A11}$$

For the u -channel contribution, t and u have to be exchanged as before.

Turning to the box diagrams that contribute to the associated production of gluinos and gauginos, we notice that they depend naturally on the four-momentum squared of the exchanged squark. Therefore, we do not expect the full Born matrix element to factorize. In addition, the traces of the Dirac matrices project out terms that depend on the final state masses separately from those that do not, so that the squared t -channel and u -channel diagrams and the interference term can only be factorized individually.

For the first box diagram in Fig. 5 we find

$$\begin{aligned}
|\overline{\mathcal{M}^{\text{BoxI}}}|^2 &= iB_0(t; m_{\bar{q}}, 0)(t - m_{\bar{q}}^2)g_s^2(C_F - N_C/2)4|\overline{\mathcal{M}^t\mathcal{M}^{u*}}|/s \\
&+ iB_0(t; m_{\bar{q}}, 0)(t - m_{\bar{q}}^2)g_s^2(C_F - N_C/2)2|\overline{\mathcal{M}^t\mathcal{M}^{t*}}| \\
&\quad (-2m_{\bar{g}}^2/(t - m_{\bar{\chi}}^2)/(t - m_{\bar{g}}^2) - 2/(t - m_{\bar{\chi}}^2)) \\
&+ iB_0(s; 0, 0)(t - m_{\bar{q}}^2)/K(s, m_{\bar{\chi}}^2, m_{\bar{g}}^2)g_s^2(C_F - N_C/2)2|\overline{\mathcal{M}^t\mathcal{M}^{u*}}| \\
&\quad (2s + 4(t - m_{\bar{g}}^2) - 2m_{\bar{\chi}}^2 + 2m_{\bar{g}}^2) \\
&+ iB_0(s; 0, 0)(t - m_{\bar{q}}^2)/K(s, m_{\bar{\chi}}^2, m_{\bar{g}}^2)g_s^2(C_F - N_C/2)2|\overline{\mathcal{M}^t\mathcal{M}^{t*}}| \\
&\quad (8sm_{\bar{g}}^4/(t - m_{\bar{\chi}}^2)/(t - m_{\bar{g}}^2) + 2sm_{\bar{\chi}}^2/(t - m_{\bar{\chi}}^2) + 8sm_{\bar{g}}^2/(t - m_{\bar{\chi}}^2) \\
&\quad - 6sm_{\bar{g}}^2/(t - m_{\bar{g}}^2) + 2m_{\bar{\chi}}^2m_{\bar{g}}^2/(t - m_{\bar{\chi}}^2) - 2m_{\bar{\chi}}^4/(t - m_{\bar{\chi}}^2) + 2m_{\bar{\chi}}^2m_{\bar{g}}^2/(t - m_{\bar{g}}^2) \\
&\quad - 2m_{\bar{g}}^4/(t - m_{\bar{g}}^2)) \\
&+ iB_0(s; 0, 0)(t - m_{\bar{q}}^2)g_s^2(C_F - N_C/2)2|\overline{\mathcal{M}^t\mathcal{M}^{t*}}| \\
&\quad (2m_{\bar{g}}^2/(t - m_{\bar{\chi}}^2)/(t - m_{\bar{g}}^2) + 2/(t - m_{\bar{\chi}}^2)) \\
&+ iB_0(m_{\bar{g}}^2; m_{\bar{q}}, 0)(t - m_{\bar{q}}^2)/K(s, m_{\bar{\chi}}^2, m_{\bar{g}}^2)g_s^2(C_F - N_C/2)2|\overline{\mathcal{M}^t\mathcal{M}^{u*}}| \\
&\quad (-2(t - m_{\bar{g}}^2)m_{\bar{\chi}}^2/s + 2(t - m_{\bar{g}}^2)m_{\bar{g}}^2/s - 2s - 2(t - m_{\bar{g}}^2) + 2m_{\bar{\chi}}^2 + 2m_{\bar{g}}^2) \\
&+ iB_0(m_{\bar{g}}^2; m_{\bar{q}}, 0)(t - m_{\bar{q}}^2)/K(s, m_{\bar{\chi}}^2, m_{\bar{g}}^2)g_s^2(C_F - N_C/2)2|\overline{\mathcal{M}^t\mathcal{M}^{t*}}| \\
&\quad (-4sm_{\bar{g}}^4/(t - m_{\bar{\chi}}^2)/(t - m_{\bar{g}}^2) - 2sm_{\bar{\chi}}^2/(t - m_{\bar{\chi}}^2) - 4sm_{\bar{g}}^2/(t - m_{\bar{\chi}}^2) \\
&\quad + 4sm_{\bar{g}}^2/(t - m_{\bar{g}}^2) - 2m_{\bar{\chi}}^2m_{\bar{g}}^2/(t - m_{\bar{\chi}}^2) + 2m_{\bar{\chi}}^4/(t - m_{\bar{\chi}}^2)) \\
&+ iB_0(m_{\bar{\chi}}^2; m_{\bar{q}}, 0)(t - m_{\bar{q}}^2)/K(s, m_{\bar{\chi}}^2, m_{\bar{g}}^2)g_s^2(C_F - N_C/2)2|\overline{\mathcal{M}^t\mathcal{M}^{u*}}| \\
&\quad (2(t - m_{\bar{g}}^2)m_{\bar{\chi}}^2/s - 2(t - m_{\bar{g}}^2)/sm_{\bar{g}}^2 - 2(t - m_{\bar{g}}^2) - 4m_{\bar{g}}^2) \\
&+ iB_0(m_{\bar{\chi}}^2; m_{\bar{q}}, 0)(t - m_{\bar{q}}^2)/K(s, m_{\bar{\chi}}^2, m_{\bar{g}}^2)g_s^2(C_F - N_C/2)2|\overline{\mathcal{M}^t\mathcal{M}^{t*}}| \\
&\quad (-4s/(t - m_{\bar{\chi}}^2)/(t - m_{\bar{g}}^2)m_{\bar{g}}^4 - 4s/(t - m_{\bar{\chi}}^2)m_{\bar{g}}^2 + 2s/(t - m_{\bar{g}}^2)m_{\bar{g}}^2 \\
&\quad - 2/(t - m_{\bar{g}}^2)m_{\bar{\chi}}^2m_{\bar{g}}^2 + 2/(t - m_{\bar{g}}^2)m_{\bar{g}}^4) \\
&- iB_0(m_{\bar{\chi}}^2; m_{\bar{q}}, 0)(t - m_{\bar{q}}^2)g_s^2(C_F - N_C/2)4|\overline{\mathcal{M}^t\mathcal{M}^{u*}}|/s \\
&+ iC_0(m_{\bar{g}}^2, m_{\bar{\chi}}^2, s; 0, m_{\bar{q}}, 0)(t - m_{\bar{q}}^2)/K(s, m_{\bar{\chi}}^2, m_{\bar{g}}^2)g_s^2(C_F - N_C/2)2|\overline{\mathcal{M}^t\mathcal{M}^{u*}}| \\
&\quad (2m_{\bar{q}}^2s + 4m_{\bar{q}}^2(t - m_{\bar{g}}^2) - 2m_{\bar{q}}^2m_{\bar{\chi}}^2 + 2m_{\bar{q}}^2m_{\bar{g}}^2 + 2s(t - m_{\bar{g}}^2) + 2sm_{\bar{g}}^2 \\
&\quad - 2(t - m_{\bar{g}}^2)m_{\bar{\chi}}^2 - 2(t - m_{\bar{g}}^2)m_{\bar{g}}^2 + 2m_{\bar{\chi}}^2m_{\bar{g}}^2 - 2m_{\bar{g}}^4)
\end{aligned}$$

$$\begin{aligned}
& + iC_0(m_{\tilde{g}}^2, m_{\tilde{\chi}}^2, s; 0, m_{\tilde{q}}, 0)(t - m_{\tilde{q}}^2)/K(s, m_{\tilde{\chi}}^2, m_{\tilde{g}}^2)g_s^2(C_F - N_C/2)2|\overline{\mathcal{M}^t \mathcal{M}^{t*}}| \\
& \quad (8m_{\tilde{q}}^2 s/(t - m_{\tilde{\chi}}^2)/(t - m_{\tilde{g}}^2)m_{\tilde{g}}^4 + 2m_{\tilde{q}}^2 s/(t - m_{\tilde{\chi}}^2)m_{\tilde{\chi}}^2 + 8m_{\tilde{q}}^2 s/(t - m_{\tilde{\chi}}^2)m_{\tilde{g}}^2 \\
& \quad - 6m_{\tilde{q}}^2 s/(t - m_{\tilde{g}}^2)m_{\tilde{g}}^2 + 2m_{\tilde{q}}^2/(t - m_{\tilde{\chi}}^2)m_{\tilde{\chi}}^2 m_{\tilde{g}}^2 - 2m_{\tilde{q}}^2/(t - m_{\tilde{\chi}}^2)m_{\tilde{\chi}}^4 \\
& \quad + 2m_{\tilde{q}}^2/(t - m_{\tilde{g}}^2)m_{\tilde{\chi}}^2 m_{\tilde{g}}^2 - 2m_{\tilde{q}}^2/(t - m_{\tilde{g}}^2)m_{\tilde{g}}^4 + 8s/(t - m_{\tilde{\chi}}^2)/(t - m_{\tilde{g}}^2)m_{\tilde{g}}^6 \\
& \quad + 6s/(t - m_{\tilde{\chi}}^2)m_{\tilde{\chi}}^2 m_{\tilde{g}}^2 + 8s/(t - m_{\tilde{\chi}}^2)m_{\tilde{g}}^4 - 2s/(t - m_{\tilde{g}}^2)m_{\tilde{\chi}}^2 m_{\tilde{g}}^2 - 8s/(t - m_{\tilde{g}}^2)m_{\tilde{g}}^4 \\
& \quad + 2/(t - m_{\tilde{\chi}}^2)m_{\tilde{\chi}}^2 m_{\tilde{g}}^4 - 2/(t - m_{\tilde{\chi}}^2)m_{\tilde{\chi}}^4 m_{\tilde{g}}^2 - 2/(t - m_{\tilde{g}}^2)m_{\tilde{\chi}}^2 m_{\tilde{g}}^4 + 2/(t - m_{\tilde{g}}^2)m_{\tilde{\chi}}^4 m_{\tilde{g}}^2) \\
& + iC_0(m_{\tilde{g}}^2, m_{\tilde{\chi}}^2, s; 0, m_{\tilde{q}}, 0)(t - m_{\tilde{q}}^2)g_s^2(C_F - N_C/2)8|\overline{\mathcal{M}^t \mathcal{M}^{u*}}| \\
& + iC_0(m_{\tilde{g}}^2, m_{\tilde{\chi}}^2, s; 0, m_{\tilde{q}}, 0)(t - m_{\tilde{q}}^2)g_s^2(C_F - N_C/2)2|\overline{\mathcal{M}^t \mathcal{M}^{t*}}| \\
& \quad (-m_{\tilde{q}}^2 s/(t - m_{\tilde{\chi}}^2)/(t - m_{\tilde{g}}^2) + 2m_{\tilde{q}}^2/(t - m_{\tilde{\chi}}^2)/(t - m_{\tilde{g}}^2)m_{\tilde{g}}^2 + m_{\tilde{q}}^2/(t - m_{\tilde{\chi}}^2) \\
& \quad - m_{\tilde{q}}^2/(t - m_{\tilde{g}}^2) + s/(t - m_{\tilde{\chi}}^2)/(t - m_{\tilde{g}}^2)m_{\tilde{g}}^2 - s/(t - m_{\tilde{g}}^2) \\
& \quad + 2/(t - m_{\tilde{\chi}}^2)/(t - m_{\tilde{g}}^2)m_{\tilde{g}}^4 + 3/(t - m_{\tilde{\chi}}^2)m_{\tilde{g}}^2 + m_{\tilde{\chi}}^2/(t - m_{\tilde{g}}^2) - 2/(t - m_{\tilde{g}}^2)m_{\tilde{g}}^2) \\
& - iC_0(m_{\tilde{g}}^2, 0, t; m_{\tilde{q}}, 0, 0)(t - m_{\tilde{q}}^2)g_s^2(C_F - N_C/2)4|\overline{\mathcal{M}^t \mathcal{M}^{u*}}| \\
& + iC_0(m_{\tilde{g}}^2, 0, t; m_{\tilde{q}}, 0, 0)(t - m_{\tilde{q}}^2)g_s^2(C_F - N_C/2)2|\overline{\mathcal{M}^t \mathcal{M}^{t*}}| \\
& \quad (-1 + m_{\tilde{q}}^2/(t - m_{\tilde{g}}^2) - m_{\tilde{\chi}}^2/(t - m_{\tilde{g}}^2)) \\
& - iC_0(m_{\tilde{\chi}}^2, 0, t; m_{\tilde{q}}, 0, 0)(t - m_{\tilde{q}}^2)g_s^2(C_F - N_C/2)4|\overline{\mathcal{M}^t \mathcal{M}^{u*}}| \\
& + iC_0(m_{\tilde{\chi}}^2, 0, t; m_{\tilde{q}}, 0, 0)(t - m_{\tilde{q}}^2)g_s^2(C_F - N_C/2)2|\overline{\mathcal{M}^t \mathcal{M}^{t*}}| \\
& \quad (-1 + m_{\tilde{q}}^2/(t - m_{\tilde{\chi}}^2) - m_{\tilde{g}}^2/(t - m_{\tilde{\chi}}^2)) \\
& + iC_0(0, 0, s; 0, 0, 0)(t - m_{\tilde{q}}^2)g_s^2(C_F - N_C/2)2|\overline{\mathcal{M}^t \mathcal{M}^{t*}}| \\
& \quad (m_{\tilde{q}}^2 s/(t - m_{\tilde{\chi}}^2)/(t - m_{\tilde{g}}^2) - s/(t - m_{\tilde{\chi}}^2)/(t - m_{\tilde{g}}^2)m_{\tilde{g}}^2 + s/(t - m_{\tilde{g}}^2)) \\
& + iD_0(m_{\tilde{\chi}}^2, m_{\tilde{g}}^2, 0, 0; 0, m_{\tilde{q}}, 0, 0)(t - m_{\tilde{q}}^2)g_s^2(C_F - N_C/2)4|\overline{\mathcal{M}^t \mathcal{M}^{u*}}|s \\
& + iD_0(m_{\tilde{\chi}}^2, m_{\tilde{g}}^2, 0, 0; 0, m_{\tilde{q}}, 0, 0)(t - m_{\tilde{q}}^2)g_s^2(C_F - N_C/2)4|\overline{\mathcal{M}^t \mathcal{M}^{t*}}|s \\
& + iD_0(m_{\tilde{\chi}}^2, m_{\tilde{g}}^2, 0, 0; 0, m_{\tilde{q}}, 0, 0)(t - m_{\tilde{q}}^2)^2 g_s^2(C_F - N_C/2)2|\overline{\mathcal{M}^t \mathcal{M}^{t*}}| \\
& \quad (-s/(t - m_{\tilde{\chi}}^2) - s/(t - m_{\tilde{g}}^2)) \\
& + iD_0(m_{\tilde{\chi}}^2, m_{\tilde{g}}^2, 0, 0; 0, m_{\tilde{q}}, 0, 0)(t - m_{\tilde{q}}^2)^3 g_s^2(C_F - N_C/2)2|\overline{\mathcal{M}^t \mathcal{M}^{t*}}| \\
& \quad (s/(t - m_{\tilde{\chi}}^2)/(t - m_{\tilde{g}}^2)).
\end{aligned} \tag{A12}$$

Function $K(s, m_{\tilde{\chi}}^2, m_{\tilde{g}}^2) = s^2 - 2s(m_{\tilde{\chi}}^2 + m_{\tilde{g}}^2) + (m_{\tilde{\chi}}^2 - m_{\tilde{g}}^2)^2$ is the triangle (Källén) function of the partonic center-of-mass energy and the masses of the produced particles. The corresponding u -channel contribution is obtained by exchanging t and u .

For the second box diagram in Fig. 5 we find

$$\begin{aligned}
|\overline{\mathcal{M}^{\text{Box2}}}|^2 = & iB_0(t; m_{\tilde{g}}, 0)(u - m_{\tilde{q}}^2)g_s^2(C_F - N_C/2)4|\overline{\mathcal{M}^t\mathcal{M}^{u*}}|/s \\
& + iB_0(t; m_{\tilde{g}}, 0)(u - m_{\tilde{q}}^2)g_s^2(C_F - N_C/2)2|\overline{\mathcal{M}^u\mathcal{M}^{u*}}| \\
& \quad (2/(t - m_{\tilde{\chi}}^2)/(u - m_{\tilde{\chi}}^2)m_{\tilde{\chi}}^2 + 2/(t - m_{\tilde{g}}^2)/(u - m_{\tilde{g}}^2)m_{\tilde{g}}^2 \\
& \quad + 2/(u - m_{\tilde{\chi}}^2)/(u - m_{\tilde{g}}^2)m_{\tilde{g}}^2 + 2/(u - m_{\tilde{\chi}}^2)) \\
& + iB_0(s; m_{\tilde{q}}, m_{\tilde{q}})(u - m_{\tilde{q}}^2)/K(s, m_{\tilde{\chi}}^2, m_{\tilde{g}}^2)g_s^2(C_F - N_C/2)2|\overline{\mathcal{M}^t\mathcal{M}^{u*}}| \\
& \quad (-2s - 4(u - m_{\tilde{g}}^2) + 2m_{\tilde{\chi}}^2 - 2m_{\tilde{g}}^2) \\
& + iB_0(s; m_{\tilde{q}}, m_{\tilde{q}})(u - m_{\tilde{q}}^2)/K(s, m_{\tilde{\chi}}^2, m_{\tilde{g}}^2)g_s^2(C_F - N_C/2)2|\overline{\mathcal{M}^u\mathcal{M}^{u*}}| \\
& \quad (-8s/(u - m_{\tilde{\chi}}^2)/(u - m_{\tilde{g}}^2)m_{\tilde{g}}^4 - 2s/(u - m_{\tilde{\chi}}^2)m_{\tilde{\chi}}^2 - 8s/(u - m_{\tilde{\chi}}^2)m_{\tilde{g}}^2 \\
& \quad + 6s/(u - m_{\tilde{g}}^2)m_{\tilde{g}}^2 - 2/(u - m_{\tilde{\chi}}^2)m_{\tilde{\chi}}^2m_{\tilde{g}}^2 + 2/(u - m_{\tilde{\chi}}^2)m_{\tilde{\chi}}^4 - 2/(u - m_{\tilde{g}}^2)m_{\tilde{\chi}}^2m_{\tilde{g}}^2 \\
& \quad + 2/(u - m_{\tilde{g}}^2)m_{\tilde{g}}^4) \\
& + iB_0(s; m_{\tilde{q}}, m_{\tilde{q}})(u - m_{\tilde{q}}^2)g_s^2(C_F - N_C/2)2|\overline{\mathcal{M}^u\mathcal{M}^{u*}}| \\
& \quad (-2/(u - m_{\tilde{\chi}}^2)/(u - m_{\tilde{g}}^2)m_{\tilde{g}}^2 - 2/(u - m_{\tilde{\chi}}^2)) \\
& + iB_0(m_{\tilde{g}}^2; m_{\tilde{q}}, 0)(u - m_{\tilde{q}}^2)/K(s, m_{\tilde{\chi}}^2, m_{\tilde{g}}^2)g_s^2(C_F - N_C/2)2|\overline{\mathcal{M}^t\mathcal{M}^{u*}}| \\
& \quad (2(u - m_{\tilde{g}}^2)m_{\tilde{\chi}}^2/s - 2(u - m_{\tilde{g}}^2)/sm_{\tilde{g}}^2 + 2s + 2(u - m_{\tilde{g}}^2) - 2m_{\tilde{\chi}}^2 - 2m_{\tilde{g}}^2) \\
& + iB_0(m_{\tilde{g}}^2; m_{\tilde{q}}, 0)(u - m_{\tilde{q}}^2)/K(s, m_{\tilde{\chi}}^2, m_{\tilde{g}}^2)g_s^2(C_F - N_C/2)2|\overline{\mathcal{M}^u\mathcal{M}^{u*}}| \\
& \quad (4s/(u - m_{\tilde{\chi}}^2)/(u - m_{\tilde{g}}^2)m_{\tilde{g}}^4 + 2s/(u - m_{\tilde{\chi}}^2)m_{\tilde{\chi}}^2 + 4s/(u - m_{\tilde{\chi}}^2)m_{\tilde{g}}^2 \\
& \quad - 4s/(u - m_{\tilde{g}}^2)m_{\tilde{g}}^2 + 2/(u - m_{\tilde{\chi}}^2)m_{\tilde{\chi}}^2m_{\tilde{g}}^2 - 2/(u - m_{\tilde{\chi}}^2)m_{\tilde{\chi}}^4) \\
& - iB_0(m_{\tilde{g}}^2; m_{\tilde{q}}, 0)(u - m_{\tilde{q}}^2)g_s^2(C_F - N_C/2)4|\overline{\mathcal{M}^t\mathcal{M}^{u*}}|/s \\
& + iB_0(m_{\tilde{g}}^2; m_{\tilde{q}}, 0)(u - m_{\tilde{q}}^2)g_s^2(C_F - N_C/2)2|\overline{\mathcal{M}^u\mathcal{M}^{u*}}| \\
& \quad (-2/(t - m_{\tilde{\chi}}^2)/(u - m_{\tilde{\chi}}^2)m_{\tilde{\chi}}^2)
\end{aligned}$$

$$\begin{aligned}
& + iB_0(m_{\tilde{\chi}}^2; m_{\tilde{q}}, 0)(u - m_{\tilde{q}}^2)/K(s, m_{\tilde{\chi}}^2, m_{\tilde{g}}^2)g_s^2(C_F - N_C/2)2|\overline{\mathcal{M}^t \mathcal{M}^{u*}}| \\
& \quad (-2(u - m_{\tilde{g}}^2)m_{\tilde{\chi}}^2/s + 2(u - m_{\tilde{g}}^2)/sm_{\tilde{g}}^2 + 2(u - m_{\tilde{g}}^2) + 4m_{\tilde{g}}^2) \\
& + iB_0(m_{\tilde{\chi}}^2; m_{\tilde{q}}, 0)(u - m_{\tilde{q}}^2)/K(s, m_{\tilde{\chi}}^2, m_{\tilde{g}}^2)g_s^2(C_F - N_C/2)2|\overline{\mathcal{M}^u \mathcal{M}^{u*}}| \\
& \quad (4s/(u - m_{\tilde{\chi}}^2)/(u - m_{\tilde{g}}^2)m_{\tilde{g}}^4 + 4s/(u - m_{\tilde{\chi}}^2)m_{\tilde{g}}^2 - 2s/(u - m_{\tilde{g}}^2)m_{\tilde{g}}^2 \\
& \quad + 2/(u - m_{\tilde{g}}^2)m_{\tilde{\chi}}^2m_{\tilde{g}}^2 - 2/(u - m_{\tilde{g}}^2)m_{\tilde{g}}^4) \\
& + iB_0(m_{\tilde{\chi}}^2; m_{\tilde{q}}, 0)(u - m_{\tilde{q}}^2)g_s^2(C_F - N_C/2)2|\overline{\mathcal{M}^u \mathcal{M}^{u*}}| \\
& \quad (-2/(t - m_{\tilde{g}}^2)/(u - m_{\tilde{g}}^2)m_{\tilde{g}}^2) \\
& + iC_0(m_{\tilde{g}}^2, m_{\tilde{\chi}}^2, s; m_{\tilde{q}}, 0, m_{\tilde{q}})(u - m_{\tilde{q}}^2)/K(s, m_{\tilde{\chi}}^2, m_{\tilde{g}}^2)g_s^2(C_F - N_C/2)2|\overline{\mathcal{M}^t \mathcal{M}^{u*}}| \\
& \quad (2m_{\tilde{q}}^2s + 4m_{\tilde{q}}^2(u - m_{\tilde{g}}^2) - 2m_{\tilde{q}}^2m_{\tilde{\chi}}^2 + 2m_{\tilde{q}}^2m_{\tilde{g}}^2 - 2s(u - m_{\tilde{g}}^2) - 2sm_{\tilde{g}}^2 \\
& \quad + 2(u - m_{\tilde{g}}^2)m_{\tilde{\chi}}^2 + 2(u - m_{\tilde{g}}^2)m_{\tilde{g}}^2 - 2m_{\tilde{\chi}}^2m_{\tilde{g}}^2 + 2m_{\tilde{g}}^4) \\
& + iC_0(m_{\tilde{g}}^2, m_{\tilde{\chi}}^2, s; m_{\tilde{q}}, 0, m_{\tilde{q}})(u - m_{\tilde{q}}^2)/K(s, m_{\tilde{\chi}}^2, m_{\tilde{g}}^2)g_s^2(C_F - N_C/2)2|\overline{\mathcal{M}^u \mathcal{M}^{u*}}| \\
& \quad (8m_{\tilde{q}}^2s/(u - m_{\tilde{\chi}}^2)/(u - m_{\tilde{g}}^2)m_{\tilde{g}}^4 + 2m_{\tilde{q}}^2s/(u - m_{\tilde{\chi}}^2)m_{\tilde{\chi}}^2 + 8m_{\tilde{q}}^2s/(u - m_{\tilde{\chi}}^2)m_{\tilde{g}}^2 \\
& \quad - 6m_{\tilde{q}}^2s/(u - m_{\tilde{g}}^2)m_{\tilde{g}}^2 + 2m_{\tilde{q}}^2/(u - m_{\tilde{\chi}}^2)m_{\tilde{\chi}}^2m_{\tilde{g}}^2 - 2m_{\tilde{q}}^2/(u - m_{\tilde{\chi}}^2)m_{\tilde{g}}^4 \\
& \quad + 2m_{\tilde{q}}^2/(u - m_{\tilde{g}}^2)m_{\tilde{\chi}}^2m_{\tilde{g}}^2 - 2m_{\tilde{q}}^2/(u - m_{\tilde{g}}^2)m_{\tilde{g}}^4 - 8s/(u - m_{\tilde{\chi}}^2)/(u - m_{\tilde{g}}^2)m_{\tilde{g}}^6 \\
& \quad - 6s/(u - m_{\tilde{\chi}}^2)m_{\tilde{\chi}}^2m_{\tilde{g}}^2 - 8s/(u - m_{\tilde{\chi}}^2)m_{\tilde{g}}^4 + 2s/(u - m_{\tilde{g}}^2)m_{\tilde{\chi}}^2m_{\tilde{g}}^2 + 8s/(u - m_{\tilde{g}}^2)m_{\tilde{g}}^4 \\
& \quad - 2/(u - m_{\tilde{\chi}}^2)m_{\tilde{\chi}}^2m_{\tilde{g}}^4 + 2/(u - m_{\tilde{\chi}}^2)m_{\tilde{\chi}}^4m_{\tilde{g}}^2 + 2/(u - m_{\tilde{g}}^2)m_{\tilde{\chi}}^2m_{\tilde{g}}^4 - 2/(u - m_{\tilde{g}}^2)m_{\tilde{\chi}}^4m_{\tilde{g}}^2) \\
& + iC_0(m_{\tilde{g}}^2, m_{\tilde{\chi}}^2, s; m_{\tilde{q}}, 0, m_{\tilde{q}})(u - m_{\tilde{q}}^2)g_s^2(C_F - N_C/2)2|\overline{\mathcal{M}^t \mathcal{M}^{u*}}| \\
& \quad (1 - 2m_{\tilde{q}}^2/s + 2(u - m_{\tilde{g}}^2)/s - m_{\tilde{\chi}}^2/s + 3m_{\tilde{g}}^2/s) \\
& + iC_0(m_{\tilde{g}}^2, m_{\tilde{\chi}}^2, s; m_{\tilde{q}}, 0, m_{\tilde{q}})(u - m_{\tilde{q}}^2)g_s^2(C_F - N_C/2)2|\overline{\mathcal{M}^u \mathcal{M}^{u*}}| \\
& \quad (-2m_{\tilde{q}}^2s/(u - m_{\tilde{\chi}}^2)/(u - m_{\tilde{g}}^2) + 4m_{\tilde{q}}^2/(u - m_{\tilde{\chi}}^2)/(u - m_{\tilde{g}}^2)m_{\tilde{g}}^2 + 2m_{\tilde{q}}^2/(u - m_{\tilde{\chi}}^2) \\
& \quad - 2m_{\tilde{q}}^2/(u - m_{\tilde{g}}^2) - s/(u - m_{\tilde{\chi}}^2)/(u - m_{\tilde{g}}^2)m_{\tilde{g}}^2 - s/(u - m_{\tilde{\chi}}^2) + s/(u - m_{\tilde{g}}^2) \\
& \quad + s^2/(u - m_{\tilde{\chi}}^2)/(u - m_{\tilde{g}}^2) - 4/(u - m_{\tilde{\chi}}^2)/(u - m_{\tilde{g}}^2)m_{\tilde{g}}^4 - 3/(u - m_{\tilde{\chi}}^2)m_{\tilde{g}}^2 \\
& \quad + 3/(u - m_{\tilde{g}}^2)m_{\tilde{g}}^2) \\
& + iC_0(m_{\tilde{g}}^2, 0, t; 0, m_{\tilde{q}}, m_{\tilde{g}})(u - m_{\tilde{q}}^2)g_s^2(C_F - N_C/2)2|\overline{\mathcal{M}^t \mathcal{M}^{u*}}| \\
& \quad (-1 + 2m_{\tilde{q}}^2/s - (u - m_{\tilde{g}}^2)/s - 2m_{\tilde{g}}^2/s)
\end{aligned}$$

$$\begin{aligned}
& + iC_0(m_{\tilde{g}}^2, 0, t; 0, m_{\tilde{q}}, m_{\tilde{g}})(u - m_{\tilde{q}}^2)g_s^2(C_F - N_C/2)2|\overline{\mathcal{M}^u\mathcal{M}^{u*}}| \\
& \quad (2m_{\tilde{q}}^2s/(u - m_{\tilde{\chi}}^2)/(u - m_{\tilde{g}}^2) + 2m_{\tilde{q}}^2/(t - m_{\tilde{\chi}}^2)/(u - m_{\tilde{\chi}}^2)m_{\tilde{\chi}}^2 + 2m_{\tilde{q}}^2/(u - m_{\tilde{\chi}}^2) \\
& \quad - s/(u - m_{\tilde{\chi}}^2)/(u - m_{\tilde{g}}^2)m_{\tilde{g}}^2 - s/(u - m_{\tilde{\chi}}^2) - s^2/(u - m_{\tilde{\chi}}^2)/(u - m_{\tilde{g}}^2) \\
& \quad - 2/(t - m_{\tilde{\chi}}^2)/(u - m_{\tilde{\chi}}^2)m_{\tilde{\chi}}^2m_{\tilde{g}}^2 - m_{\tilde{g}}^2/(u - m_{\tilde{\chi}}^2)) \\
& + iC_0(m_{\tilde{\chi}}^2, 0, t; 0, m_{\tilde{q}}, m_{\tilde{g}})(u - m_{\tilde{q}}^2)g_s^2(C_F - N_C/2)2|\overline{\mathcal{M}^t\mathcal{M}^{u*}}| \\
& \quad (-1 + 2m_{\tilde{q}}^2/s - (u - m_{\tilde{g}}^2)/s + m_{\tilde{\chi}}^2/s - 3m_{\tilde{g}}^2/s) \\
& + iC_0(m_{\tilde{\chi}}^2, 0, t; 0, m_{\tilde{q}}, m_{\tilde{g}})(u - m_{\tilde{q}}^2)g_s^2(C_F - N_C/2)2|\overline{\mathcal{M}^u\mathcal{M}^{u*}}| \\
& \quad (2m_{\tilde{q}}^2s/(u - m_{\tilde{\chi}}^2)/(u - m_{\tilde{g}}^2) + 2m_{\tilde{q}}^2/(t - m_{\tilde{g}}^2)/(u - m_{\tilde{g}}^2)m_{\tilde{g}}^2 + 2m_{\tilde{q}}^2/(u - m_{\tilde{g}}^2) \\
& \quad - s/(u - m_{\tilde{\chi}}^2)/(u - m_{\tilde{g}}^2)m_{\tilde{g}}^2 - s/(u - m_{\tilde{g}}^2) - s^2/(u - m_{\tilde{\chi}}^2)/(u - m_{\tilde{g}}^2) \\
& \quad - 2/(t - m_{\tilde{g}}^2)/(u - m_{\tilde{g}}^2)m_{\tilde{g}}^4 - m_{\tilde{g}}^2/(u - m_{\tilde{g}}^2)) \\
& + iC_0(0, 0, s; m_{\tilde{q}}, m_{\tilde{g}}, m_{\tilde{q}})(u - m_{\tilde{q}}^2)g_s^2(C_F - N_C/2)2|\overline{\mathcal{M}^t\mathcal{M}^{u*}}| \\
& + iC_0(0, 0, s; m_{\tilde{q}}, m_{\tilde{g}}, m_{\tilde{q}})(u - m_{\tilde{q}}^2)g_s^2(C_F - N_C/2)2|\overline{\mathcal{M}^u\mathcal{M}^{u*}}| \\
& \quad (-2m_{\tilde{q}}^2s/(u - m_{\tilde{\chi}}^2)/(u - m_{\tilde{g}}^2) + s/(u - m_{\tilde{\chi}}^2)/(u - m_{\tilde{g}}^2)m_{\tilde{g}}^2 + s^2/(u - m_{\tilde{\chi}}^2)/(u - m_{\tilde{g}}^2)) \\
& + iD_0(m_{\tilde{\chi}}^2, m_{\tilde{g}}^2, 0, 0; m_{\tilde{q}}, 0, m_{\tilde{q}}, m_{\tilde{g}})(u - m_{\tilde{q}}^2)g_s^2(C_F - N_C/2)2|\overline{\mathcal{M}^t\mathcal{M}^{u*}}| \\
& \quad (-2m_{\tilde{q}}^2(u - m_{\tilde{g}}^2)/s + m_{\tilde{q}}^2m_{\tilde{\chi}}^2/s - 5m_{\tilde{q}}^2m_{\tilde{g}}^2/s - 2m_{\tilde{q}}^2 + 2m_{\tilde{q}}^4/s + 2(u - m_{\tilde{g}}^2)/sm_{\tilde{g}}^2 \\
& \quad - m_{\tilde{\chi}}^2/sm_{\tilde{g}}^2 + 3/sm_{\tilde{g}}^4 + s + (u - m_{\tilde{g}}^2) - m_{\tilde{\chi}}^2 + 3m_{\tilde{g}}^2) \\
& + iD_0(m_{\tilde{\chi}}^2, m_{\tilde{g}}^2, 0, 0; m_{\tilde{q}}, 0, m_{\tilde{q}}, m_{\tilde{g}})(u - m_{\tilde{q}}^2)g_s^2(C_F - N_C/2)2|\overline{\mathcal{M}^u\mathcal{M}^{u*}}| \\
& \quad (-2m_{\tilde{q}}^2s/(u - m_{\tilde{\chi}}^2)/(u - m_{\tilde{g}}^2)m_{\tilde{g}}^2 - m_{\tilde{q}}^2s/(u - m_{\tilde{\chi}}^2) - 3m_{\tilde{q}}^2s/(u - m_{\tilde{g}}^2) \\
& \quad - 4m_{\tilde{q}}^2s^2/(u - m_{\tilde{\chi}}^2)/(u - m_{\tilde{g}}^2) + 4m_{\tilde{q}}^2/(u - m_{\tilde{\chi}}^2)/(u - m_{\tilde{g}}^2)m_{\tilde{g}}^4 + m_{\tilde{q}}^2/(u - m_{\tilde{\chi}}^2)m_{\tilde{g}}^2 \\
& \quad - 3m_{\tilde{q}}^2/(u - m_{\tilde{g}}^2)m_{\tilde{g}}^2 + 4m_{\tilde{q}}^4s/(u - m_{\tilde{\chi}}^2)/(u - m_{\tilde{g}}^2) - 2m_{\tilde{q}}^4/(u - m_{\tilde{\chi}}^2)/(u - m_{\tilde{g}}^2)m_{\tilde{g}}^2 \\
& \quad + 2m_{\tilde{q}}^4/(u - m_{\tilde{g}}^2) - 2s/(u - m_{\tilde{\chi}}^2)/(u - m_{\tilde{g}}^2)m_{\tilde{g}}^4 - s/(u - m_{\tilde{\chi}}^2)m_{\tilde{g}}^2 + 2s/(u - m_{\tilde{g}}^2)m_{\tilde{g}}^2 \\
& \quad + s^2/(u - m_{\tilde{\chi}}^2)/(u - m_{\tilde{g}}^2)m_{\tilde{g}}^2 + s^2/(u - m_{\tilde{g}}^2) + s^3/(u - m_{\tilde{\chi}}^2)/(u - m_{\tilde{g}}^2) \\
& \quad - 2/(u - m_{\tilde{\chi}}^2)/(u - m_{\tilde{g}}^2)m_{\tilde{g}}^6 - m_{\tilde{g}}^4/(u - m_{\tilde{\chi}}^2) + m_{\tilde{g}}^4/(u - m_{\tilde{g}}^2)). \tag{A13}
\end{aligned}$$

The corresponding u -channel contribution is obtained by exchanging t and u .

For the third box diagram in Fig.5 we find

$$\begin{aligned}
\overline{|\mathcal{M}^{\text{Box3}}|}^2 = & iB_0(t; m_{\bar{q}}, 0)(t - m_{\bar{q}}^2)g_s^2 N_C 2\overline{|\mathcal{M}^t \mathcal{M}^{u*}|}/s \\
& + iB_0(t; m_{\bar{q}}, 0)(t - m_{\bar{q}}^2)g_s^2 N_C 2\overline{|\mathcal{M}^t \mathcal{M}^{t*}|} \\
& \quad (-m_{\bar{g}}^2/((t - m_{\bar{\chi}}^2)(t - m_{\bar{g}}^2)) - 1/(t - m_{\bar{\chi}}^2)) \\
& + iB_0(u; m_{\bar{g}}, 0)(t - m_{\bar{q}}^2)g_s^2 N_C 2\overline{|\mathcal{M}^t \mathcal{M}^{u*}|}/s \\
& + iB_0(u; m_{\bar{g}}, 0)(t - m_{\bar{q}}^2)g_s^2 N_C 2\overline{|\mathcal{M}^t \mathcal{M}^{t*}|} \\
& \quad (m_{\bar{g}}^2/((t - m_{\bar{\chi}}^2)(t - m_{\bar{g}}^2)) + m_{\bar{\chi}}^2/((t - m_{\bar{\chi}}^2)(u - m_{\bar{\chi}}^2)) + 1/(t - m_{\bar{\chi}}^2) \\
& \quad + m_{\bar{g}}^2/((t - m_{\bar{g}}^2)(u - m_{\bar{g}}^2))) \\
& - iB_0(m_{\bar{g}}^2; m_{\bar{q}}, 0)(t - m_{\bar{q}}^2)g_s^2 N_C 2\overline{|\mathcal{M}^t \mathcal{M}^{u*}|}/s \\
& + iB_0(m_{\bar{g}}^2; m_{\bar{q}}, 0)(t - m_{\bar{q}}^2)g_s^2 N_C 2\overline{|\mathcal{M}^t \mathcal{M}^{t*}|} \\
& \quad (-m_{\bar{\chi}}^2/((t - m_{\bar{\chi}}^2)(u - m_{\bar{\chi}}^2))) \\
& - iB_0(m_{\bar{\chi}}^2; m_{\bar{g}}, 0)(t - m_{\bar{q}}^2)g_s^2 N_C 2\overline{|\mathcal{M}^t \mathcal{M}^{u*}|}/s \\
& + iB_0(m_{\bar{\chi}}^2; m_{\bar{g}}, 0)(t - m_{\bar{q}}^2)g_s^2 N_C 2\overline{|\mathcal{M}^t \mathcal{M}^{t*}|}(-m_{\bar{g}}^2/((t - m_{\bar{g}}^2)(u - m_{\bar{g}}^2))) \\
& + iC_0(m_{\bar{g}}^2, 0, t; m_{\bar{q}}, 0, 0)(t - m_{\bar{q}}^2)g_s^2 N_C 2\overline{|\mathcal{M}^t \mathcal{M}^{u*}|} \\
& \quad (-1 - (t - m_{\bar{g}}^2)/(2s) + m_{\bar{\chi}}^2/(2s) - m_{\bar{g}}^2/(2s)) \\
& + iC_0(m_{\bar{g}}^2, 0, t; m_{\bar{q}}, 0, 0)(t - m_{\bar{q}}^2)g_s^2 N_C 2\overline{|\mathcal{M}^t \mathcal{M}^{t*}|} \\
& \quad (-1/2 + m_{\bar{q}}^2/(2(t - m_{\bar{g}}^2)) - m_{\bar{\chi}}^2/(2(t - m_{\bar{g}}^2))) \\
& + iC_0(m_{\bar{g}}^2, 0, u; 0, m_{\bar{q}}, m_{\bar{g}})(t - m_{\bar{q}}^2)g_s^2 N_C 2\overline{|\mathcal{M}^t \mathcal{M}^{u*}|} \\
& \quad (-1/2 + m_{\bar{q}}^2/s - (t - m_{\bar{g}}^2)/(2s) - m_{\bar{g}}^2/s) \\
& + iC_0(m_{\bar{g}}^2, 0, u; 0, m_{\bar{q}}, m_{\bar{g}})(t - m_{\bar{q}}^2)g_s^2 N_C 2\overline{|\mathcal{M}^t \mathcal{M}^{t*}|} \\
& \quad (1/2 + m_{\bar{q}}^2 s/(2(t - m_{\bar{\chi}}^2)(t - m_{\bar{g}}^2)) + m_{\bar{q}}^2 m_{\bar{\chi}}^2/((t - m_{\bar{\chi}}^2)(u - m_{\bar{\chi}}^2)) \\
& \quad + 1/2 m_{\bar{q}}^2/(t - m_{\bar{\chi}}^2) - s m_{\bar{g}}^2/(2(t - m_{\bar{\chi}}^2)(t - m_{\bar{g}}^2)) + s/(2(t - m_{\bar{g}}^2)) \\
& \quad - m_{\bar{\chi}}^2 m_{\bar{g}}^2/((t - m_{\bar{\chi}}^2)(u - m_{\bar{\chi}}^2)) - m_{\bar{g}}^2/(2(t - m_{\bar{\chi}}^2)))
\end{aligned}$$

$$\begin{aligned}
& + iC_0(m_{\tilde{\chi}}^2, 0, u; m_{\tilde{g}}, 0, 0)(t - m_{\tilde{q}}^2)g_s^2 N_C 2|\overline{\mathcal{M}^t \mathcal{M}^{u*}}| \\
& \quad (1/2 + (t - m_{\tilde{g}}^2)/(2s) - m_{\tilde{\chi}}^2/(2s) + m_{\tilde{g}}^2/(2s)) \\
& + iC_0(m_{\tilde{\chi}}^2, 0, u; m_{\tilde{g}}, 0, 0)(t - m_{\tilde{q}}^2)g_s^2 N_C 2|\overline{\mathcal{M}^t \mathcal{M}^{t*}}| \\
& \quad (-1/2 - m_{\tilde{q}}^2 s/(2(t - m_{\tilde{\chi}}^2)(t - m_{\tilde{g}}^2)) - m_{\tilde{q}}^2/(2(t - m_{\tilde{g}}^2)) \\
& \quad + sm_{\tilde{g}}^2/(2(t - m_{\tilde{\chi}}^2)(t - m_{\tilde{g}}^2)) - s/(2(t - m_{\tilde{g}}^2)) + m_{\tilde{\chi}}^2/(2(t - m_{\tilde{g}}^2))) \\
& + iC_0(m_{\tilde{\chi}}^2, 0, t; 0, m_{\tilde{g}}, m_{\tilde{q}})(t - m_{\tilde{q}}^2)g_s^2 N_C 2|\overline{\mathcal{M}^t \mathcal{M}^{u*}}| \\
& \quad (-m_{\tilde{q}}^2/s + (t - m_{\tilde{g}}^2)/(2s) + m_{\tilde{g}}^2/s) \\
& + iC_0(m_{\tilde{\chi}}^2, 0, t; 0, m_{\tilde{g}}, m_{\tilde{q}})(t - m_{\tilde{q}}^2)g_s^2 N_C 2|\overline{\mathcal{M}^t \mathcal{M}^{t*}}| \\
& \quad (-1/2 + m_{\tilde{q}}^2 m_{\tilde{g}}^2/((t - m_{\tilde{\chi}}^2)(t - m_{\tilde{g}}^2)) + m_{\tilde{q}}^2/(2(t - m_{\tilde{\chi}}^2)) - m_{\tilde{g}}^4/((t - m_{\tilde{\chi}}^2)(t - m_{\tilde{g}}^2)) \\
& \quad - m_{\tilde{g}}^2/(2(t - m_{\tilde{\chi}}^2))) \\
& + iD_0(m_{\tilde{\chi}}^2, 0, m_{\tilde{g}}^2, 0; 0, m_{\tilde{g}}, m_{\tilde{q}}, 0)(t - m_{\tilde{q}}^2)g_s^2 N_C 2|\overline{\mathcal{M}^t \mathcal{M}^{u*}}| \\
& \quad (-s - (t - m_{\tilde{g}}^2) + m_{\tilde{\chi}}^2 - m_{\tilde{g}}^2) \\
& + iD_0(m_{\tilde{\chi}}^2, 0, m_{\tilde{g}}^2, 0; 0, m_{\tilde{g}}, m_{\tilde{q}}, 0)(t - m_{\tilde{q}}^2)g_s^2 N_C 2|\overline{\mathcal{M}^t \mathcal{M}^{t*}}| \\
& \quad (-s - (t - m_{\tilde{g}}^2) + m_{\tilde{\chi}}^2 - m_{\tilde{g}}^2) \\
& + iD_0(m_{\tilde{\chi}}^2, 0, m_{\tilde{g}}^2, 0; 0, m_{\tilde{g}}, m_{\tilde{q}}, 0)(t - m_{\tilde{q}}^2)^2 g_s^2 N_C 2|\overline{\mathcal{M}^t \mathcal{M}^{u*}}| \\
& \quad (-1/2 - (t - m_{\tilde{g}}^2)/(2s) + m_{\tilde{\chi}}^2/(2s) - m_{\tilde{g}}^2/(2s)) \\
& + iD_0(m_{\tilde{\chi}}^2, 0, m_{\tilde{g}}^2, 0; 0, m_{\tilde{g}}, m_{\tilde{q}}, 0)(t - m_{\tilde{q}}^2)^2 g_s^2 N_C 2|\overline{\mathcal{M}^t \mathcal{M}^{t*}}| \\
& \quad (1 + s/(2(t - m_{\tilde{\chi}}^2)) + s/(2(t - m_{\tilde{g}}^2)) - m_{\tilde{\chi}}^2/(2(t - m_{\tilde{g}}^2)) + m_{\tilde{g}}^2/(2(t - m_{\tilde{g}}^2))) \\
& + iD_0(m_{\tilde{\chi}}^2, 0, m_{\tilde{g}}^2, 0; 0, m_{\tilde{g}}, m_{\tilde{q}}, 0)(t - m_{\tilde{q}}^2)^3 g_s^2 N_C 2|\overline{\mathcal{M}^t \mathcal{M}^{t*}}| \\
& \quad (-s/(2(t - m_{\tilde{\chi}}^2)(t - m_{\tilde{g}}^2)) - 1/(2(t - m_{\tilde{g}}^2))). \tag{A14}
\end{aligned}$$

The corresponding u -channel contribution is obtained by exchanging t and u .

The coefficients of the infrared singularities in the gluon exchange box diagrams can be simplified considerably. The gluino-exchange box diagram is infrared finite. For the first box diagram in Fig. 5 in the t -channel we find

$$\begin{aligned} |\overline{\mathcal{M}}_{\text{IR}}^{\text{Box1}}|^2 = & -C_\epsilon \left[\frac{1}{\epsilon^2} - \frac{1}{\epsilon} \log \left(\frac{(t - m_{\tilde{q}}^2)^2 s}{(m_{\tilde{g}}^2 - m_{\tilde{q}}^2)(m_{\tilde{\chi}}^2 - m_{\tilde{q}}^2) Q^2} \right) + \frac{1}{\epsilon} \log \left(\frac{m_{\tilde{q}}^2 - t}{m_{\tilde{q}}^2 - m_{\tilde{g}}^2} \right) \frac{t - m_{\tilde{q}}^2}{t - m_{\tilde{g}}^2} \right. \\ & \left. + \frac{1}{\epsilon} \log \left(\frac{m_{\tilde{q}}^2 - t}{m_{\tilde{q}}^2 - m_{\tilde{\chi}}^2} \right) \frac{t - m_{\tilde{q}}^2}{t - m_{\tilde{\chi}}^2} \right] 4 \left(C_F - \frac{N_C}{2} \right) g_s^2 [|\overline{\mathcal{M}}^t \mathcal{M}^{t*}| + |\overline{\mathcal{M}}^t \mathcal{M}^{u*}|], \quad (\text{A15}) \end{aligned}$$

and the u -channel contribution can be obtained by exchanging t and u . The result is completely symmetric under the exchange $m_{\tilde{g}} \leftrightarrow m_{\tilde{\chi}}$.

The infrared singular pieces of the third t -channel box diagram in Fig. 5 are

$$\begin{aligned} |\overline{\mathcal{M}}_{\text{IR}}^{\text{Box3}}|^2 = & -C_\epsilon \left[\frac{1}{2\epsilon^2} + \frac{1}{2\epsilon} \log \left(\frac{Q^2}{m_{\tilde{g}}^2} \right) - \frac{1}{\epsilon} \log \left(\frac{m_{\tilde{q}}^2 - t}{m_{\tilde{q}}^2 - m_{\tilde{\chi}}^2} \right) \frac{m_{\tilde{q}}^2 - m_{\tilde{\chi}}^2}{t - m_{\tilde{\chi}}^2} - \frac{1}{\epsilon} \log \left(\frac{m_{\tilde{g}}^2 - u}{m_{\tilde{g}}^2} \right) \right] \\ & \times 4 \frac{N_C}{2} g_s^2 [|\overline{\mathcal{M}}^t \mathcal{M}^{t*}| + |\overline{\mathcal{M}}^t \mathcal{M}^{u*}|]. \quad (\text{A16}) \end{aligned}$$

For the u -channel result t and u have to be exchanged.

Finally we sum the infrared singularities encountered in the virtual corrections and separate them into C_F and N_C color classes:

$$\begin{aligned} |\overline{\mathcal{M}}_{\text{IR}}^V|^2 = & -C_\epsilon \left[\frac{1}{\epsilon^2} + \frac{3}{2\epsilon} + \frac{1}{\epsilon} \log \left(\frac{Q^2}{s} \right) \right] 4C_F g_s^2 |\overline{\mathcal{M}}^B|^2 \\ & + C_\epsilon \left[-\frac{1}{\epsilon} + \frac{1}{\epsilon} \log \left(\frac{(t - m_{\tilde{g}}^2)(u - m_{\tilde{g}}^2)}{s m_{\tilde{g}}^2} \right) \right] 4 \frac{N_C}{2} g_s^2 |\overline{\mathcal{M}}^B|^2. \quad (\text{A17}) \end{aligned}$$

APPENDIX B: SCALAR INTEGRALS

The tensor integrals that occur in virtual loop diagrams can be reduced to one-, two-, three-, and four-point integrals that are scalar functions of the loop momentum q [31]. The general scalar one-point integral is defined as

$$A_0(m) = Q^{2\epsilon} \int \frac{d^n q}{(2\pi)^n} \frac{1}{q^2 - m^2}. \quad (\text{B1})$$

The general scalar two-point integral is

$$B_0(p^2; m_1, m_2) = Q^{2\epsilon} \int \frac{d^n q}{(2\pi)^n} \frac{1}{[q^2 - m_1^2][(q + p)^2 - m_2^2]}, \quad (\text{B2})$$

and its derivative is

$$B'_0(p^2; m_1, m_2) = \left. \frac{\partial}{\partial q^2} B_0(q^2; m_1, m_2) \right|_{q^2=p^2}. \quad (\text{B3})$$

The general scalar three-point integral is

$$C_0(p_1^2, p_2^2, (p_1 + p_2)^2; m_1, m_2, m_3) = Q^{2\epsilon} \times \int \frac{d^n q}{(2\pi)^n} \frac{1}{[q^2 - m_1^2][(q + p_1)^2 - m_2^2][(q + p_1 + p_2)^2 - m_3^2]}, \quad (\text{B4})$$

and the general scalar four-point integral is

$$D_0(p_1^2, p_2^2, p_3^2, (p_1 + p_2 + p_3)^2, (p_1 + p_2)^2, (p_2 + p_3)^2; m_1, m_2, m_3, m_4) = Q^{2\epsilon} \times \int \frac{d^n q}{(2\pi)^n} \frac{1}{[q^2 - m_1^2][(q + p_1)^2 - m_2^2][(q + p_1 + p_2)^2 - m_3^2][(q + p_1 + p_2 + p_3)^2 - m_4^2]}. \quad (\text{B5})$$

The $p_i, i = 1 \dots 4$, are the four-momenta of the external particles, and the $m_i, i = 1 \dots 4$, are the masses of the adjacent internal particles.

The scalar two- and three-point integrals relevant for the associated production of gluinos and gauginos were calculated previously in a different physical context [42]. We recalculated them and checked that the results in Ref. [42] are correct. The divergent four-point integrals that contribute to the gluon exchange box diagrams in Fig. 5 were unknown, and they are presented here for the first time. We calculate the absorptive parts with Cutkosky cutting rules and the real parts with dispersion techniques.

The exchange of a massless gluon between the initial state quark and antiquark in the first box diagram of Fig. 5 leads to the following divergent four-point integral:

$$\begin{aligned}
D_0(0, 0, m_{\tilde{g}}^2, m_{\tilde{\chi}}^2, s, t; 0, 0, 0, m_{\tilde{q}}) = & iC_\epsilon \frac{1}{s(t - m_{\tilde{q}}^2)} \left[\frac{1}{\epsilon^2} - \frac{1}{\epsilon} \ln \frac{s(t - m_{\tilde{q}}^2)^2}{(m_{\tilde{q}}^2 - m_{\tilde{g}}^2)(m_{\tilde{q}}^2 - m_{\tilde{\chi}}^2)Q^2} \right. \\
& - 2\text{Li}_2 \left(1 + \frac{m_{\tilde{q}}^2 - m_{\tilde{g}}^2}{t - m_{\tilde{q}}^2} \right) - 2\text{Li}_2 \left(1 + \frac{m_{\tilde{q}}^2 - m_{\tilde{\chi}}^2}{t - m_{\tilde{q}}^2} \right) - \text{Li}_2 \left(1 + \frac{(m_{\tilde{q}}^2 - m_{\tilde{g}}^2)(m_{\tilde{q}}^2 - m_{\tilde{\chi}}^2)}{sm_{\tilde{q}}^2} \right) \\
& - \frac{\pi^2}{4} + \frac{1}{2} \ln^2 \left(\frac{s}{Q^2} \right) - \frac{1}{2} \ln^2 \left(\frac{s}{m_{\tilde{q}}^2} \right) + 2 \ln \left(\frac{s}{Q^2} \right) \ln \left(\frac{t - m_{\tilde{q}}^2}{m_{\tilde{q}}^2} \right) \\
& \left. - \ln \left(\frac{m_{\tilde{q}}^2 - m_{\tilde{g}}^2}{Q^2} \right) \ln \left(\frac{m_{\tilde{q}}^2 - m_{\tilde{g}}^2}{m_{\tilde{q}}^2} \right) - \ln \left(\frac{m_{\tilde{q}}^2 - m_{\tilde{\chi}}^2}{Q^2} \right) \ln \left(\frac{m_{\tilde{q}}^2 - m_{\tilde{\chi}}^2}{m_{\tilde{q}}^2} \right) \right]. \quad (\text{B6})
\end{aligned}$$

This integral also contributes to the pair production of gauginos of unequal mass [10]. In the limit of two final state particles of equal mass our result agrees with Ref. [42].

In the third box diagram of Fig. 5, the exchange of a massless gluon between the the final state gluino and the initial state antiquark gives rise to a second divergent four-point integral:

$$\begin{aligned}
D_0(0, m_{\tilde{g}}^2, 0, m_{\tilde{\chi}}^2, t, u; m_{\tilde{q}}, m_{\tilde{g}}, 0, 0) = & iC_\epsilon \frac{1}{(t - m_{\tilde{q}}^2)(u - m_{\tilde{g}}^2)} \left[\frac{1}{2\epsilon^2} - \frac{1}{\epsilon} \left(\ln \left(\frac{-t + m_{\tilde{q}}^2}{m_{\tilde{q}}^2 - m_{\tilde{\chi}}^2} \right) \right. \right. \\
& + \ln \left(\frac{-u + m_{\tilde{g}}^2}{m_{\tilde{g}}Q} \right) \left. \right) - \frac{\pi^2}{8} + \ln^2 \left(\frac{-u + m_{\tilde{g}}^2}{m_{\tilde{g}}Q} \right) + 2 \ln \left(\frac{-u + m_{\tilde{g}}^2}{m_{\tilde{g}}Q} \right) \ln \left(\frac{-t + m_{\tilde{q}}^2}{m_{\tilde{q}}^2 - m_{\tilde{\chi}}^2} \right) \\
& + \text{Li}_2 \left(1 + \frac{u - m_{\tilde{g}}^2}{m_{\tilde{q}}^2 - m_{\tilde{\chi}}^2} \right) + \text{Li}_2 \left(1 + \frac{m_{\tilde{q}}^2(u - m_{\tilde{g}}^2)}{m_{\tilde{g}}^2(m_{\tilde{q}}^2 - m_{\tilde{\chi}}^2)} \right) - 2\text{Li}_2 \left(1 + \frac{m_{\tilde{q}}^2 - m_{\tilde{\chi}}^2}{t - m_{\tilde{q}}^2} \right) \left. \right]. \quad (\text{B7})
\end{aligned}$$

Again, our result agrees with Ref. [42] for the case of two final state particles of equal mass.

The supersymmetric counterpart of the first box diagram is the second box diagram in Fig. 5. Since supersymmetry is broken and the gluino propagator and the two squark propagators are massive, this diagram does not have infrared divergences. The corresponding four-point integral can be expressed in terms of 16 dilogarithms [43].

APPENDIX C: SOFT GLUON EMISSION CONTRIBUTION

In this Appendix, we collect the expressions for the finite pieces of the soft gluon emission contribution. The finite pieces remain after mass-factorization and cancellation of soft poles between soft gluon emission and virtual contributions, as described in the text. We begin with the C_F color class,

$$\begin{aligned} \frac{d^2 \hat{\sigma}^S}{dt_2 du_2} &= \frac{d^2 \hat{\sigma}^B}{dt_2 du_2} \left(\frac{C_F \alpha_S}{\pi} \right) \left\{ \text{Li}_2 \left(\frac{u_2 t_2 - s m_2^2}{(s + t_2)(s + u_2)} \right) \right. \\ &\quad + \frac{1}{2} \log^2 \left(\frac{\mu^2}{m_1^2 \delta^2} \right) + \log \left(\frac{(s + t_2)(s + u_2)}{s m_1^2} \right) \log \left(\frac{\mu^2}{m_1^2 \delta^2} \right) \\ &\quad \left. + \frac{1}{2} \log^2 \left(\frac{(s + t_2)(s + u_2)}{s m_1^2} \right) \right\}, \end{aligned} \quad (\text{C1})$$

where $\delta = \Delta/m_1^2$ is the cut-off between hard and soft emission mentioned in the text. Its appearance in these terms is the explicit cut-off dependence that matches the implicit logarithmic behavior of the hard real emission contributions.

The soft terms associated with the N_C color class are

$$\begin{aligned} \frac{d^2 \hat{\sigma}^S}{dt_2 du_2} &= -\frac{d^2 \hat{\sigma}^B}{dt_2 du_2} \left(\frac{N_C \alpha_S}{2\pi} \right) \left\{ -2 + \text{Li}_2 \left(\frac{u_2 t_2 - s m_2^2}{(s + t_2)(s + u_2)} \right) \right. \\ &\quad + \frac{1}{2} \log^2 \left(\frac{\mu^2}{m_1^2 \delta^2} \right) \\ &\quad \left. + \left[\log \left(\frac{(s + t_2)(s + u_2)}{s m_1^2} \right) - 1 \right] \log \left(\frac{(s + t_2)(s + u_2)}{s m_1^2} \right) \right\}. \end{aligned} \quad (\text{C2})$$

Again logarithmic dependence on the hard/soft cut-off δ is apparent.

APPENDIX D: HARD GLUON EMISSION CONTRIBUTION

In this Appendix, we collect explicit expressions for the thirty-six matrix elements that contribute to the real emission of a gluon in the 2-to-3 partonic subprocess $q \bar{q} \rightarrow g \tilde{g} \tilde{\chi}$.

The hard gluon emission cross section (in four dimensions) is

$$\frac{d^3 \hat{\sigma}^h}{ds_4 dt_2 du_2} = \frac{d^3 \hat{\sigma}_1^g}{ds_4 dt_2 du_2} + \frac{\alpha_S \hat{\alpha}_S}{16 \pi^2} \frac{s_4 \delta(s + t_2 + u_1 - s_4)}{36 s^2 (s_4 + m_1^2)} \sum_{i=1..8} \sum_{j=i..8} \hat{M}_{ij}^g, \quad (\text{D1})$$

where i and j label the diagrams in Fig. 6. The remainder of the factorization process is

$$\begin{aligned} \frac{d^3 \hat{\sigma}_1^g}{ds_4 dt_2 du_2} &= \frac{C_F \alpha_S \hat{\alpha}_S \delta(s + t_2 + u_1 - s_4)}{36 \pi s^2} \log \left(\frac{\mu^2 (s_4 + m_1^2)}{s_4^2} \right) \\ &\times \left\{ \left(\frac{s_4^2 - 2 s_4 (s + u_2) + 2 (s + u_2)^2}{s_4 (s + u_2)} \right) \left(\frac{X_t t_2}{(t - m_{\tilde{q}_t}^2)^2} \right) \right. \\ &+ \frac{2 X_{tu} s m_1 m_2}{(t - m_{\tilde{q}_t}^2) [(\Delta_u - s - t_2)(s + u_2) + s s_4]} + \frac{X_u u_2 [s_4 u_2 - u_1 (s + u_2)]}{[(\Delta_u - s - t_2)(s + u_2) + s s_4]^2} \Big) \\ &+ \left(\frac{s_4^2 - 2 s_4 (s + t_2) + 2 (s + t_2)^2}{s_4 (s + t_2)} \right) \left(\frac{X_t t_2 [s_4 t_2 - t_1 (s + t_2)]}{[(\Delta_t - s - u_2)(s + t_2) + s s_4]^2} \right. \\ &\left. \left. + \frac{2 X_{tu} s m_1 m_2}{(u - m_{\tilde{q}_u}^2) [(\Delta_t - s - u_2)(s + t_2) + s s_4]} + \frac{X_u u_2}{(u - m_{\tilde{q}_u}^2)^2} \right) \right\}. \end{aligned} \quad (\text{D2})$$

The elements \hat{M}_{ij}^g are

$$\begin{aligned} \hat{M}_{11}^g &= \frac{-16 C_F \pi X_t t_2 (s_4 + m_1^2)}{(t - m_{\tilde{q}_t}^2)^2 (s + u_2)}, \\ \hat{M}_{12}^g &= \left(\frac{8 (C_F - N_C/2) X_t}{(t - m_{\tilde{q}_t}^2) (\Delta_t - s - u_2)} \right) \\ &\times \left\{ s [-2 t_2 (s + u_2) + s_4 (s + t_2 + u_2)] \hat{I} \left(\frac{1}{t' u'} \right) + [s - t_2] \hat{I} \left(\frac{u'}{t'} \right) \right. \\ &+ [\Delta_t s (\Delta_t + t_1) + t_2 (s (m_2^2 - m_1^2) + \Delta_t (t_2 + u_2 - \Delta_t) - u_2 t_2)] \hat{I} \left(\frac{1}{t' u_{7\Delta}} \right) \\ &\left. + [\Delta_t (s + u_2 - t_2) + t_2 (\Delta_t - s - u_2)] \hat{I} \left(\frac{1}{u_{7\Delta}} \right) + [s - t_2] \hat{I} \left(\frac{u_{7\Delta}}{t'} \right) \right\}, \end{aligned} \quad (\text{D3})$$

$$\hat{M}_{13}^g = \frac{8 N_C X_t t_2 (s + u_2 - m_1^2)}{s_4 (t - m_{q_t}^2)^2} \hat{I}(1),$$

$$\begin{aligned} \hat{M}_{14}^g = & \left(\frac{4 (C_F - N_C/2) X_t t_2}{(t - m_{q_t}^2)^2} \right) \left\{ [4 t_1 (s + u_2)] \hat{I} \left(\frac{1}{u' u_{7\Delta}} \right) \right. \\ & \left. + [2 (2 t_2 + 2 m_2^2 - s - u_2)] \hat{I} \left(\frac{1}{u_{7\Delta}} \right) - 2 \hat{I} \left(\frac{u'}{u_{7\Delta}} \right) \right\}, \end{aligned}$$

$$\hat{M}_{15}^g = \frac{-16 (C_F - N_C/2) X_{tu} s^2 m_1 m_2}{(t - m_{q_t}^2) (u - m_{q_u}^2)} \hat{I} \left(\frac{1}{t' u'} \right),$$

$$\begin{aligned} \hat{M}_{16}^g = & \left(\frac{-16 C_F X_{tu} m_1 m_2}{(t - m_{q_t}^2)} \right) \left\{ [\Delta_u - s - t_2] \hat{I} \left(\frac{1}{u' u_{6\Delta}} \right) \right. \\ & \left. - \frac{2 \pi (s_4 + m_1^2) (\Delta_u - s - t_2)}{s_4 [(\Delta_u - s - t_2)(s + u_2) + s s_4]} + \frac{2 \pi (s_4 + m_1^2)}{s_4 (s + u_2)} \right\}, \end{aligned}$$

$$\hat{M}_{17}^g = \left(\frac{4 N_C X_{tu} m_1 m_2}{s_4 (t - m_{q_t}^2) (u - m_{q_u}^2)} \right) \left\{ [s + u_2] \hat{I} \left(\frac{t'}{u'} \right) + [s - t_2] \hat{I}(1) \right\},$$

$$\begin{aligned} \hat{M}_{18}^g = & \left(\frac{-4 C_F X_{tu} m_1 m_2}{(t - m_{q_t}^2) (u - m_{q_u}^2)} \right) \left\{ 2 [s (\Delta_u + m_2^2 - m_1^2) - u_2 (\Delta_u - t_2)] \hat{I} \left(\frac{1}{u' u_{6\Delta}} \right) \right. \\ & \left. + [2 t_2] \hat{I} \left(\frac{1}{u_{6\Delta}} \right) \right\}, \end{aligned}$$

$$\begin{aligned} \hat{M}_{22}^g = & (8 C_F X_t) \left\{ [\Delta_t (\Delta_t + t_1)] \hat{I} \left(\frac{1}{t' u_{7\Delta}^2} \right) - [2 \Delta_t + t_1] \hat{I} \left(\frac{1}{t' u_{7\Delta}} \right) + \Delta_t \hat{I} \left(\frac{1}{u_{7\Delta}^2} \right) \right. \\ & - \hat{I} \left(\frac{1}{u_{7\Delta}} \right) - \left(\frac{2 \pi (s_4 + m_1^2)}{s_4} \right) \left(\frac{(s + t_2) \Delta_t (\Delta_t + t_1)}{[(\Delta_u - s - t_2)(s + u_2) + s s_4]^2} \right. \\ & \left. \left. - \frac{2 \Delta_t + t_1}{[(\Delta_u - s - t_2)(s + u_2) + s s_4]} + \frac{1}{(s + t_2)} \right) \right\}, \end{aligned}$$

$$\begin{aligned}\hat{M}_{23}^g &= \left(\frac{-4 N_C X_t}{s_4 (t - m_{\tilde{q}_t}^2)} \right) \times \\ &\left\{ [\Delta_t((s + t_2)(\Delta_t + m_2^2 - m_1^2) + s_4 t_2) + t_2(ss_4 - s^2 - st_2 - su_2 - t_2 u_2)] \hat{I}\left(\frac{1}{t' u_{7\Delta}}\right) \right. \\ &+ [s + t_2] \hat{I}\left(\frac{u_{7\Delta}}{t'}\right) + [\Delta_t(m_1^2 + m_2^2 + s_4) - t_2(s + u_2 - \Delta_t)] \hat{I}\left(\frac{1}{u_{7\Delta}}\right) \\ &\left. - [t + m_1^2 + s_4] \hat{I}(1) \right\},\end{aligned}$$

$$\begin{aligned}\hat{M}_{24}^g &= \left(\frac{-4 C_F X_t}{(t - m_{\tilde{q}_t}^2)} \right) \left\{ [4 t_2 \Delta_t (\Delta_t + m_2^2 - m_1^2)] \hat{I}\left(\frac{1}{t' u_{7\Delta}^2}\right) + [2 \Delta_t (t_2 + 2 m_2^2)] \hat{I}\left(\frac{1}{u_{7\Delta}^2}\right) \right. \\ &\left. - [4 t_2 (2 \Delta_t + m_2^2 - m_1^2)] \hat{I}\left(\frac{1}{t' u_{7\Delta}}\right) - 2 [t_2 + 2 m_2^2] \hat{I}\left(\frac{1}{u_{7\Delta}}\right) \right\},\end{aligned}$$

$$\begin{aligned}\hat{M}_{25}^g &= \left(\frac{-16 C_F X_{tu} m_1 m_2}{(u - m_{\tilde{q}_u}^2)} \right) \left\{ [\Delta_t - s - u_2] \hat{I}\left(\frac{1}{t' u_{7\Delta}}\right) \right. \\ &\left. - \frac{2 \pi (\Delta_t - s - u_2)(s_4 + m_1^2)}{s_4 [(\Delta_t - s - u_2)(s + t_2) + s s_4]} + \frac{2 \pi (s_4 + m_1^2)}{s_4 (s + t_2)} \right\},\end{aligned}$$

$$\begin{aligned}\hat{M}_{26}^g &= \left(\frac{-16 (C_F - N_C/2) X_{tu} s m_1 m_2}{(\Delta_t - s - u_2)(\Delta_u - s - t_2)} \right) \left\{ [s] \hat{I}\left(\frac{1}{t' u'}\right) + [\Delta_t - u_2] \hat{I}\left(\frac{1}{t' u_{7\Delta}}\right) \right. \\ &\left. + [\Delta_u - t_2] \hat{I}\left(\frac{1}{u' u_{6\Delta}}\right) + [\Delta_u + \Delta_t - s - t_2 - u_2] \hat{I}\left(\frac{1}{u_{6\Delta} u_{7\Delta}}\right) \right\},\end{aligned}$$

$$\begin{aligned}\hat{M}_{27}^g &= \left(\frac{4 N_C X_{tu} m_1 m_2}{s_4 (u - m_{\tilde{q}_u}^2)} \right) \left\{ [\Delta_t s + s^2 - s s_4 + \Delta_t t_2 + s t_2 - s u_2 - t_2 u_2] \hat{I}\left(\frac{1}{t' u_{7\Delta}}\right) \right. \\ &\left. + [s + u_2 - 2 \Delta_t] \hat{I}\left(\frac{1}{u_{7\Delta}}\right) + 2 \hat{I}(1) \right\},\end{aligned}$$

$$\begin{aligned}\hat{M}_{28}^g &= \left(\frac{4 (C_F - N_C/2) X_{tu} m_1 m_2}{(u - m_{\tilde{q}_u}^2)(\Delta_u - s - t_2)} \right) \left\{ 2 [s u_1 - (s + t_2)(\Delta_t - u_2)] \hat{I}\left(\frac{1}{t' u_{7\Delta}}\right) \right. \\ &\left. + 2 [s + t_2] \hat{I}\left(\frac{1}{u_{6\Delta}}\right) + [-2 \Delta_t (s + t_2) + 2 \Delta_u u_2 + 2 s u_1] \hat{I}\left(\frac{1}{u_{6\Delta} u_{7\Delta}}\right) \right\},\end{aligned}$$

$$\hat{M}_{33}^g = \left(\frac{8 N_C X_t t_2}{s_4^2 (t - m_{\tilde{q}_t}^2)^2} \right) \left\{ 2 m_1^2 (s + u_2) \hat{I}(1) + s_4 \hat{I}(u') \right\},$$

$$\begin{aligned}\hat{M}_{34}^g &= \left(\frac{-4 N_C X_t t_2}{s_4 (t - m_{\tilde{q}_t}^2)^2} \right) \left\{ [\Delta_t (s_4 - 2 t) - 2 m_1^2 (u_2 + 2 s)] \hat{I}\left(\frac{1}{u_{7\Delta}}\right) \right. \\ &\left. + [m_2^2 + m_1^2 - s + t_2 - u_2] \hat{I}(1) \right\},\end{aligned}$$

$$\hat{M}_{35}^g = \left(\frac{4 N_C X_{tu} m_1 m_2}{s_4 (t - m_{\tilde{q}_t}^2)(u - m_{\tilde{q}_u}^2)} \right) \left\{ [s + t_2] \hat{I} \left(\frac{u'}{t'} \right) + [s - u_2] \hat{I}(1) \right\},$$

$$\begin{aligned} \hat{M}_{36}^g = & \left(\frac{4 N_C X_{tu} m_1 m_2}{s_4 (t - m_{\tilde{q}_t}^2)} \right) \left\{ [\Delta_u(s + u_2) + s^2 - s s_4 - s t_2 + s u_2 - t_2 u_2] \hat{I} \left(\frac{1}{u' u_{6\Delta}} \right) \right. \\ & \left. + [s + t_2 - 2\Delta_u] \hat{I} \left(\frac{1}{u_{6\Delta}} \right) + 2 \hat{I}(1) \right\}, \end{aligned}$$

$$\hat{M}_{37}^g = \frac{16 N_C X_{tu} s m_1 m_2 (s_4 + 2 m_1^2)}{s_4^2 (t - m_{\tilde{q}_t}^2)(u - m_{\tilde{q}_u}^2)} \hat{I}(1),$$

$$\begin{aligned} \hat{M}_{38}^g = & \left(\frac{-4 N_C X_{tu} m_1 m_2}{s_4 (t - m_{\tilde{q}_t}^2)(u - m_{\tilde{q}_u}^2)} \right) \left\{ [u_2 (t_2 - \Delta_u) + s(\Delta_u - s_4 - m_2^2 - 3m_1^2)] \hat{I} \left(\frac{1}{u_{6\Delta}} \right) \right. \\ & \left. + [s + t_2] \hat{I} \left(\frac{u'}{u_{6\Delta}} \right) + [u_2 - s] \hat{I}(1) \right\}, \end{aligned}$$

$$\hat{M}_{44}^g = \left(\frac{-8 C_F X_t t_2}{(t - m_{\tilde{q}_t}^2)^2} \right) \left\{ [\Delta_t(\Delta_t - t - m_1^2)] \hat{I} \left(\frac{1}{u_{7\Delta}^2} \right) + [t + m_1^2 - 2\Delta_t] \hat{I} \left(\frac{1}{u_{7\Delta}} \right) + \hat{I}(1) \right\},$$

$$\hat{M}_{45}^g = \left(\frac{-8 C_F X_{tu} m_1 m_2}{(t - m_{\tilde{q}_t}^2)(u - m_{\tilde{q}_u}^2)} \right) \left\{ [t_2(u_2 - \Delta_t) + s(\Delta_t + m_2^2 - m_1^2)] \hat{I} \left(\frac{1}{t' u_{7\Delta}} \right) + u_2 \hat{I} \left(\frac{1}{u_{7\Delta}} \right) \right\},$$

$$\begin{aligned} \hat{M}_{46}^g = & \left(\frac{4 (C_F - N_C/2) X_{tu} m_1 m_2}{(t - m_{\tilde{q}_t}^2)(\Delta_t - s - u_2)} \right) \left\{ 2 [(t_2 - \Delta_u)(s + u_2) + s t_1] \hat{I} \left(\frac{1}{u' u_{6\Delta}} \right) \right. \\ & \left. + 2 [s + u_2] \hat{I} \left(\frac{1}{u_{7\Delta}} \right) + [-2 \Delta_u (s + u_2) + 2 s t_1 + 2 \Delta_t t_2] \hat{I} \left(\frac{1}{u_{6\Delta} u_{7\Delta}} \right) \right\}, \end{aligned}$$

$$\begin{aligned} \hat{M}_{47}^g = & \left(\frac{-4 N_C X_{tu} m_1 m_2}{s_4 (t - m_{\tilde{q}_t}^2)(u - m_{\tilde{q}_u}^2)} \right) \left\{ [t_2 (u_2 - \Delta_t) + \Delta_t s - s (s_4 + m_2^2 + 3m_1^2)] \hat{I} \left(\frac{1}{u_{7\Delta}} \right) \right. \\ & \left. + [s + u_2] \hat{I} \left(\frac{t'}{u_{7\Delta}} \right) + [t_2 - s] \hat{I}(1) \right\}, \end{aligned}$$

$$\begin{aligned} \hat{M}_{48}^g = & \left(\frac{-8 (C_F - N_C/2) X_{tu} s m_1 m_2}{(t - m_{\tilde{q}_t}^2)(u - m_{\tilde{q}_u}^2)} \right) \left\{ [2 s + 2 m_1^2 - \Delta_t - \Delta_u + t + u] \hat{I} \left(\frac{1}{u_{6\Delta} u_{7\Delta}} \right) \right. \\ & \left. + \hat{I} \left(\frac{1}{u_{6\Delta}} \right) + \hat{I} \left(\frac{1}{u_{7\Delta}} \right) \right\}, \end{aligned}$$

$$\hat{M}_{55}^g = \frac{-16 C_F \pi X_u u_2 (s_4 + m_1^2)}{(u - m_{\tilde{q}_u}^2)^2 (s + t_2)},$$

$$\begin{aligned}
\hat{M}_{56}^g &= \left(\frac{8 (C_F - N_C/2) X_u}{(u - m_{\tilde{q}_u}^2) (\Delta_u - s - t_2)} \right) \\
&\times \left\{ [\Delta_u^2 (s - u_2) + \Delta_u (s u_1 + u_2 (t_2 + u_2)) + s u_2 (m_2^2 - m_1^2) - t_2 u_2^2] \hat{I} \left(\frac{1}{u' u_{6\Delta}} \right) \right. \\
&+ [s - u_2] \hat{I} \left(\frac{u_{6\Delta}}{u'} \right) + [\Delta_u (s + t_2) - u_2 (s + t_2)] \hat{I} \left(\frac{1}{u_{6\Delta}} \right) \\
&+ s [(s + t_2)(s + t_1) + u_2 u_1] \hat{I} \left(\frac{1}{u' t'} \right) + [s - u_2] \hat{I} \left(\frac{t'}{u'} \right) \left. \right\}, \\
\hat{M}_{57}^g &= \left(\frac{8 N_C X_u u_2 [s + t_2 - m_1^2]}{s_4 (u - m_{\tilde{q}_u}^2)^2} \right) \hat{I}(1), \\
\hat{M}_{58}^g &= \left(\frac{4 (C_F - N_C/2) X_u u_2}{(u - m_{\tilde{q}_u}^2)^2} \right) \left\{ 4 u_1 [s + t_2] \hat{I} \left(\frac{1}{t' u_{6\Delta}} \right) + 2 [3 u_1 + 2 m_1^2 - s_4] \hat{I} \left(\frac{1}{u_{6\Delta}} \right) \right. \\
&\left. - 2 \hat{I} \left(\frac{t'}{u_{6\Delta}} \right) \right\}, \\
\hat{M}_{66}^g &= (8 C_F X_u) \left\{ \Delta_u [\Delta_u + u_1] \hat{I} \left(\frac{1}{u' u_{6\Delta}^2} \right) - [2 \Delta_u + u_1] \hat{I} \left(\frac{1}{u' u_{6\Delta}} \right) \right. \\
&+ \Delta_u \hat{I} \left(\frac{1}{u_{6\Delta}^2} \right) - \hat{I} \left(\frac{1}{u_{6\Delta}} \right) \\
&- \left(\frac{2 \pi (s_4 + m_1^2)}{s_4} \right) \left(\frac{\Delta_u (\Delta_u + u_1) (s + u_2)}{[(\Delta_u - s - t_2)(s + u_2) + s s_4]^2} \right. \\
&\left. \left. - \frac{2 \Delta_u + u_1}{[(\Delta_u - s - t_2)(s + u_2) + s s_4]} + \frac{1}{s + u_2} \right) \right\}, \\
\hat{M}_{67}^g &= \left(\frac{-4 N_C X_u}{s_4 (u - m_{\tilde{q}_u}^2)} \right) \left\{ [s + u_2] \hat{I} \left(\frac{u_{6\Delta}}{u'} \right) - [s_4 + m_1^2 + u] \hat{I}(1) \right. \\
&+ [\Delta_u^2 (s + u_2) + \Delta_u (s (m_2^2 - m_1^2) \\
&+ u_2 (m_2^2 - m_1^2)) - t_2 u_2] \hat{I} \left(\frac{1}{u' u_{6\Delta}} \right) \\
&\left. + [\Delta_u (s + t + u) + u_2 (\Delta_u - s - t_2)] \hat{I} \left(\frac{1}{u_{6\Delta}} \right) \right\}, \\
\hat{M}_{68}^g &= \left(\frac{-4 C_F X_u}{(u - m_{\tilde{q}_u}^2)} \right) \left\{ 4 \Delta_u u_2 [\Delta_u + m_2^2 - m_1^2] \hat{I} \left(\frac{1}{u' u_{6\Delta}^2} \right) + 2 \Delta_u [u_2 + 2 m_2^2] \hat{I} \left(\frac{1}{u_{6\Delta}^2} \right) \right. \\
&\left. + 4 u_2 [-2 \Delta_u - m_2^2 + m_1^2] \hat{I} \left(\frac{1}{u' u_{6\Delta}} \right) - 2 [u_2 + 2 m_2^2] \hat{I} \left(\frac{1}{u_{6\Delta}} \right) \right\},
\end{aligned}$$

$$\hat{M}_{77}^g = \left(\frac{4 N_C X_u u_2}{s_4^2 (u - m_{\tilde{q}_u}^2)^2} \right) \left\{ 4m_1^2 [s + t_2] \hat{I}(1) + 2 s_4 \hat{I}(t') \right\},$$

$$\begin{aligned} \hat{M}_{78}^g = & \left(\frac{-2 N_C X_u u_2}{s_4^2 (u - m_{\tilde{q}_u}^2)^2} \right) \left\{ 2 [m_2^2 + m_1^2 - s - t_2 + u_2] \hat{I}(1) \right. \\ & + [s_4(s + t_2) + \Delta_u(\Delta_u - 3m_2^2 - 5m_1^2 - 3u_2) \\ & + (\Delta_u - s - t_2)(-\Delta_u + m_2^2 + 3m_1^2 + s + t_2 + u_2)] \hat{I}\left(\frac{1}{u_{6\Delta}}\right) \left. \right\}, \end{aligned}$$

$$\begin{aligned} \hat{M}_{88}^g = & \left(\frac{-4 C_F X_u u_2}{(u - m_{\tilde{q}_u}^2)^2} \right) \left\{ -2 \Delta_u [-\Delta_u + m_2^2 + m_1^2 + u_2] \hat{I}\left(\frac{1}{u_{6\Delta}^2}\right) \right. \\ & + 2 [u_2 + m_2^2 + m_1^2 - 2 \Delta_u] \hat{I}\left(\frac{1}{u_{6\Delta}}\right) + 2 \hat{I}(1) \left. \right\}. \end{aligned}$$

APPENDIX E: (ANTI-) QUARK EMISSION CONTRIBUTIONS

In this Appendix we present the matrix elements for the contributions from emission of an additional light quark or anti-quark in the final state. These matrix elements may be obtained from those for gluon emission upon crossing one of the initial state partons and the final state gluon. However, we compute them *ab initio* in order to provide a check on the validity of the results. In all cases, the result of the crossing agrees with the explicit computation. We limit our presentation to the quark emission contributions since the anti-quark emission contributions may be obtained from these expressions by replacements of $t \leftrightarrow u$, $t' \leftrightarrow u'$, and $u_6 \leftrightarrow u_7$ everywhere.

The quark emission contribution has two parts, consisting of the remainder of terms that are collinear singular, and thus have the angular integrations done analytically, as well as a large class of terms which are collinear finite and for which the angular integrations are done numerically. The matrix elements with collinear singularities may be written in a form very similar to the gluon emission cross section, with

$$\frac{d^3 \hat{\sigma}^h}{ds_4 dt_2 du_2} = \frac{d^3 \hat{\sigma}_1^q}{ds_4 dt_2 du_2} + \frac{\alpha_S \hat{\alpha}_S}{16 \pi^2} \frac{s_4 \delta(s + t_2 + u_1 - s_4)}{96 s^2 (s_4 + m_1^2)} \sum_{i=1..2} \sum_{j=i..8} \hat{M}_{ij}^q. \quad (\text{E1})$$

The remainder of the factorization is

$$\begin{aligned} \frac{d^3 \hat{\sigma}_1^q}{ds_4 dt_2 du_2} = & \frac{\alpha_S \hat{\alpha}_S C_F}{48 \pi s^2} \left(1 + \log \left[\frac{\mu^2 (s_4 + m_1^2)}{s_4^2} \right] \right) \frac{1}{2} \left(\frac{2s_4^2 - 2s_4(s + u_2) + (s + u_2)^2}{(s + u_2)^2} \right) \\ & \left\{ \frac{X_t t_2}{(t - m_{q_t}^2)^2} + \frac{2 X_{tu} s m_1 m_2}{(t - m_{q_t}^2)[(s + u_2)(\Delta_u - s - t_2) + s s_4]} \right. \\ & \left. + \frac{X_u u_2 (u_2 s_4 - u_1 (s + u_2))}{[(s + u_2)(\Delta_u - s - t_2) + s s_4]^2} \right\}. \end{aligned} \quad (\text{E2})$$

After partial-fractionation, the collinearly-divergent pieces of the hard matrix elements are

$$\begin{aligned} \hat{M}_{11}^q = & (-8 C_F X_u u_2) \left\{ -\Delta_u \hat{I} \left(\frac{1}{u' u_{6\Delta}^2} \right) + \hat{I} \left(\frac{1}{u' u_{6\Delta}} \right) + \frac{\Delta_u 2\pi (s_4 + m_1^2) (s + u_2)}{s_4 [(s + u_2)(\Delta_u - s - t_2) + s s_4]^2} \right. \\ & \left. - \frac{2\pi (s_4 + m_1^2)}{s_4 [(s + u_2)(\Delta_u - s - t_2) + s s_4]} \right\}, \\ \hat{M}_{12}^q = & \left(\frac{16 C_F X_{tu} s m_1 m_2}{(t - m_{q_t}^2)} \right) \left\{ \hat{I} \left(\frac{1}{u' u_{6\Delta}} \right) - \frac{2\pi (s_4 + m_1^2)}{s_4 [(s + u_2)(\Delta_u - s - t_2) + s s_4]} \right\}, \end{aligned} \quad (\text{E3})$$

$$\begin{aligned}\hat{M}_{13}^q = & \left(\frac{4(C_F - N_C/2)X_{tu}m_1m_2s_{4\Delta}}{(s_{4\Delta}^2 + m_{\hat{q}t}^2\Gamma^2)(t - m_{\hat{q}t}^2)} \right) \left\{ [-2\Delta_um_2^2 + 2\Delta_um_1^2 + sm_2^2 - sm_1^2 \right. \\ & - ss - 2\Delta_us_4 + ss_4 - 2\Delta_ut_2 + 2m_2^2t_2 - 2m_1^2t_2 + st_2 + 2s_4t_2 + 2t_2t_2 - su_2] \hat{I}\left(\frac{1}{u'u_{6\Delta}}\right) \\ & \left. - [2\Delta_u] \hat{I}\left(\frac{1}{u_{6\Delta}}\right) + 2\hat{I}(1) \right\},\end{aligned}$$

$$\begin{aligned}\hat{M}_{14}^q = & \left(\frac{4C_F X_u}{u_2^2} \right) \left\{ [4(u_2 - \Delta_u)(-\Delta_u - m_2^2 + m_1^2)(-\Delta_u - m_2^2 + m_1^2 + u_2)] \hat{I}\left(\frac{1}{u's_{3\Delta}}\right) \right. \\ & + 2[-6\Delta_u + 4m_1^2 - 4m_2^2 + 4u_2] \hat{I}\left(\frac{s_{3\Delta}}{u'}\right) + 4\hat{I}\left(\frac{s_{3\Delta}^2}{u'}\right) \\ & + [2(-\Delta_u + m_1^2 - 3m_2^2)(-\Delta_u + u_2) \\ & + (-\Delta_u + m_1^2 - m_2^2 + u_2)(-2\Delta_u + m_1^2 - m_2^2 + s - s_4 + t_2 + u_2) \\ & + (-\Delta_u + m_1^2 - m_2^2)(-2\Delta_u + m_1^2 - m_2^2 + s - s_4 + t_2 + 3u_2)] \hat{I}\left(\frac{1}{s_{3\Delta}}\right) \\ & + 2[-6\Delta_u + 4m_1^2 - 6m_2^2 + s - s_4 + t_2 + 4u_2] \hat{I}(1) + 6\hat{I}(s_{3\Delta}) \\ & \left. + 2[-\Delta_u + m_1^2 - 3m_2^2] \hat{I}\left(\frac{u'}{s_{3\Delta}}\right) + 2\hat{I}(u') \right\} \\ & + \left(\frac{-4C_F X_u}{u_2} \right) \left\{ -\Delta_u[(\Delta_u - m_1^2 + m_2^2)(2\Delta_u - m_1^2 + m_2^2 - s + s_4 - t_2 + u_2) \right. \\ & + (-\Delta_u + m_1^2 - m_2^2 - u_2)(-2\Delta_u + m_1^2 - m_2^2 + s - s_4 + t_2 + u_2)] \hat{I}\left(\frac{1}{u'u_{6\Delta}^2}\right) \\ & + [(\Delta_u - m_1^2 + m_2^2)(2\Delta_u - m_1^2 + m_2^2 - s + s_4 - t_2 + u_2) \\ & + 2\Delta_u(4\Delta_u - 3m_1^2 + 3m_2^2 - s + s_4 - t_2 + u_2) \\ & + (-\Delta_u + m_1^2 - m_2^2 - u_2)(-2\Delta_u + m_1^2 - m_2^2 + s - s_4 + t_2 + u_2)] \hat{I}\left(\frac{1}{u'u_{6\Delta}}\right) \\ & + 4\hat{I}\left(\frac{u_{6\Delta}}{u'}\right) + 2\Delta_u[-3\Delta_u + 2m_1^2 + s - s_4 + t_2] \hat{I}\left(\frac{1}{u_{6\Delta}^2}\right) \\ & \left. + 2[6\Delta_u - 2m_1^2 - s + s_4 - t_2] \hat{I}\left(\frac{1}{u_{6\Delta}}\right) - 6\hat{I}(1) - 2\Delta_u \hat{I}\left(\frac{u'}{u_{6\Delta}^2}\right) + 2\hat{I}\left(\frac{u'}{u_{6\Delta}}\right) \right\}\end{aligned}$$

$$\begin{aligned}
& + \left(\frac{-4C_F X_u}{u_2^2} \right) \left\{ -\Delta_u [(\Delta_u - m_1^2 + m_2^2)(2\Delta_u - m_1^2 + m_2^2 - s + s_4 - t_2 + u_2) \right. \\
& \quad + (-\Delta_u + m_1^2 - m_2^2 - u_2)(-2\Delta_u + m_1^2 - m_2^2 + s - s_4 + t_2 + u_2)] \hat{I} \left(\frac{1}{u' u_{6\Delta}} \right) \\
& \quad + 2[-6\Delta_u + 3m_1^2 - 3m_2^2 + s - s_4 + t_2 - u_2] \hat{I} \left(\frac{u_{6\Delta}}{u'} \right) + 4 \hat{I} \left(\frac{u_{6\Delta}^2}{u'} \right) \\
& \quad + 2\Delta_u [-3\Delta_u + 2m_1^2 + s - s_4 + t_2] \hat{I} \left(\frac{1}{u_{6\Delta}} \right) + 2[6\Delta_u - 2m_1^2 - s + s_4 - t_2] \hat{I}(1) \\
& \quad \left. - 6\hat{I}(u_{6\Delta}) - 2\Delta_u \hat{I} \left(\frac{u'}{u_{6\Delta}} \right) + 2\hat{I}(u') \right\}, \\
\hat{M}_{15}^q & = \left(\frac{16(C_F - N_C/2)X_{tu}m_1m_2s_{4\Delta}}{s(s_{4\Delta}^2 + m_{\tilde{q}_t}^2\Gamma^2)} \right) \left\{ [(-\Delta_u + t_2)(-\Delta_u + s + t_2)] \hat{I} \left(\frac{1}{u' u_{6\Delta}} \right) \right. \\
& \quad \left. + [\Delta_u - s - t_2] \hat{I} \left(\frac{1}{u_{6\Delta}} \right) - \hat{I}(1) + \hat{I} \left(\frac{u_{6\Delta}}{u'} \right) \right\}, \\
\hat{M}_{16}^q & = \left(\frac{8(C_F - N_C/2)X_u}{su_2} \right) \left\{ [(-\Delta_u + m_1^2 - m_2^2)ss_4 + (\Delta_u - m_1^2 + m_2^2)s(-\Delta_u + u_2) \right. \\
& \quad + 2(-\Delta_u + m_1^2 - m_2^2)(-\Delta_u + u_2)(-\Delta_u + s + t_2 + u_2) + u_2(-\Delta_u + u_2)(-\Delta_u + s + t_2 + u_2) \\
& \quad + (\Delta_u - m_1^2 + m_2^2)(s + u_2)(-\Delta_u + s + t_2 + u_2)] \hat{I} \left(\frac{1}{u' s_{3\Delta}} \right) \\
& \quad + 2[-3\Delta_u + m_1^2 - m_2^2 + t_2 + 2u_2] \hat{I} \left(\frac{s_{3\Delta}}{u'} \right) + 2 \hat{I} \left(\frac{s_{3\Delta}^2}{u'} \right) \\
& \quad + [2\Delta_u\Delta_u - 2\Delta_um_1^2 + 2\Delta_um_2^2 + \Delta_us - m_1^2s + m_2^2s - 2\Delta_ut_2 + m_1^2t_2 - m_2^2t_2 - 3\Delta_uu_2 \\
& \quad + m_1^2u_2 - m_2^2u_2 + su_2 + 2t_2u_2 + 2u_2u_2] \hat{I} \left(\frac{1}{s_{3\Delta}} \right) \\
& \quad \left. + [-4\Delta_u + 2m_1^2 - 2m_2^2 - s + 2t_2 + 3u_2] \hat{I}(1) + 2\hat{I}(s_{3\Delta}) + [t_2 + u_2] \hat{I} \left(\frac{u'}{s_{3\Delta}} \right) \right\} \\
& + \left(\frac{-8(C_F - N_C/2)X_u}{su_2} \right) \left\{ [ss_4(-\Delta_u + m_1^2 - m_2^2 - u_2) + \Delta_uu_2(\Delta_u - s - t_2) \right. \\
& \quad - \Delta_us(\Delta_u - m_1^2 + m_2^2 + u_2) + 2\Delta_u(-\Delta_u + s + t_2)(\Delta_u - m_1^2 + m_2^2 + u_2) \\
& \quad + (s + u_2)(-\Delta_u + s + t_2)(\Delta_u + u_1)] \hat{I} \left(\frac{1}{u' u_{6\Delta}} \right) + 2[-3\Delta_u + m_1^2 - m_2^2 + t_2 - u_2] \hat{I} \left(\frac{u_{6\Delta}}{u'} \right) \\
& \quad + 2 \hat{I} \left(\frac{u_{6\Delta}^2}{u'} \right) + [-4\Delta_u\Delta_u - 2\Delta_um_2^2 + \Delta_us + 2\Delta_um_1^2 - m_1^2s + m_2^2s + s^2 \\
& \quad - ss_4 + 2\Delta_ut_2 - m_1^2t_2 + m_2^2t_2 + st_2 - 3\Delta_uu_2 + 2su_2 + 2t_2u_2] \hat{I} \left(\frac{1}{u_{6\Delta}} \right) \\
& \quad + [8\Delta_u - 2m_1^2 + 2m_2^2 - s - 2t_2 + 3u_2] \hat{I}(1) - 4\hat{I}(u_{6\Delta}) \\
& \quad \left. + [-2\Delta_u + s + t_2] \hat{I} \left(\frac{u'}{u_{6\Delta}} \right) + 2\hat{I}(u') \right\},
\end{aligned}$$

$$\begin{aligned}
\hat{M}_{17}^q = & \left(\frac{-4N_C X_u}{u_2(s+u_2)} \right) \left\{ [(\Delta_u - m_1^2 + m_2^2)ss_4 + s_4u_2(\Delta_u - u_2) + 2(\Delta_u - m_1^2 + m_2^2)s_4(-\Delta_u + u_2) \right. \\
& + (-\Delta_u + m_1^2 - m_2^2)(-\Delta_u + u_2)(s + u_2) \\
& + (-\Delta_u + m_1^2 - m_2^2)(s + u_2)(-\Delta_u + s + t_2 + u_2)] \hat{I} \left(\frac{1}{u's_{3\Delta}} \right) \\
& + 2[s + u_2 - s_4] \hat{I} \left(\frac{s_{3\Delta}}{u'} \right) + [2\Delta_u m_2^2 - 3\Delta_u s + 3m_1^2 s - 3m_2^2 s + 2\Delta_u s_4 - 2m_1^2 s_4 \\
& + 2m_2^2 s_4 + m_1^2 t_2 - m_2^2 t_2 - \Delta_u u_2 + 2m_1^2 u_2 - 4m_2^2 u_2 - s_4 u_2 - t_2 u_2 - u_2 u_2] \hat{I} \left(\frac{1}{s_{3\Delta}} \right) \\
& + [-2m_2^2 + 3s - 2s_4 + u_2] \hat{I}(1) + [-2m_2^2 - t_2 - u_2] \hat{I} \left(\frac{u'}{s_{3\Delta}} \right) \Big\} \\
& + \left(\frac{4N_C X_u}{u_2(s+u_2)} \right) \left\{ [2s_4 \Delta_u (-\Delta_u + m_1^2 - m_2^2 - u_2) + \Delta_u s_4 u_2 + ss_4(\Delta_u - m_1^2 + m_2^2 + u_2) \right. \\
& + \Delta_u(\Delta_u + u_1)(s + u_2) + (\Delta_u - s - t_2)(\Delta_u + u_1)(s + u_2)] \hat{I} \left(\frac{1}{u'u_{6\Delta}} \right) \\
& + 2[s + u_2 - s_4] \hat{I} \left(\frac{u_{6\Delta}}{u'} \right) + [2\Delta_u m_2^2 + \Delta_u s + m_1^2 s - m_2^2 s - ss - 2\Delta_u s_4 + ss_4 \\
& + m_1^2 t_2 - m_2^2 t_2 - st_2 + 3\Delta_u u_2 - 2su_2 - 2t_2 u_2] \hat{I} \left(\frac{1}{u_{6\Delta}} \right) \\
& + [-2m_2^2 - s + 2s_4 - 3u_2] \hat{I}(1) - [s + t_2] \hat{I} \left(\frac{u'}{u_{6\Delta}} \right) \Big\},
\end{aligned}$$

$$\begin{aligned}
\hat{M}_{18}^q = & \left(\frac{-4N_C X_{tu} m_1 m_2}{(t - m_{q_t}^2)(s + u_2)} \right) \times \\
& \left\{ [-\Delta_u s + ss + 2\Delta_u s_4 - ss_4 + st_2 - 2s_4 t_2 - \Delta_u u_2 + su_2 + t_2 u_2] \hat{I} \left(\frac{1}{u'u_{6\Delta}} \right) \right. \\
& \left. + [2\Delta_u + s - t_2] \hat{I} \left(\frac{1}{u_{6\Delta}} \right) - 2\hat{I}(1) \right\},
\end{aligned}$$

$$\hat{M}_{22}^q = \left(\frac{8C_F X_t t_2}{(t - m_{q_t}^2)(t - m_{q_t}^2)} \right) \left\{ \hat{I}(1) - \frac{2\pi(s_4 + m_1^2)}{s_4} \right\},$$

$$\hat{M}_{23}^q = \left(\frac{4(C_F - N_C/2) X_t t_2 s_{4\Delta}}{(t - m_{q_t}^2)(t - m_{q_t}^2)(s_{4\Delta}^2 + m_{q_t}^2 \Gamma^2)} \right) \left\{ -2[m_1^2 + m_2^2 + s + t_2 + u_2] \hat{I}(1) \right\},$$

$$\begin{aligned}
\hat{M}_{24}^q = & \left(\frac{4C_F X_{tu} m_1 m_2}{u_2(t - m_{\tilde{q}t}^2)} \right) \left\{ 4\hat{I}\left(\frac{s_{3\Delta}}{u'}\right) + 6\hat{I}(1) + 2\hat{I}\left(\frac{u'}{s_{3\Delta}}\right) \right. \\
& + 2[-3\Delta_u + m_1^2 - m_2^2 + 2s - s_4 + 3t_2 + 3u_2] \hat{I}\left(\frac{1}{s_{3\Delta}}\right) \\
& + [4\Delta_u^2 - 2\Delta_u m_1^2 + 2\Delta_u m_2^2 - 4\Delta_u s + m_1^2 s - m_2^2 s + s^2 + 2\Delta_u s_4 - s s_4 - 6\Delta_u t_2 + 2m_1^2 t_2 \\
& - 2m_2^2 t_2 + 3s t_2 - 2s_4 t_2 + 2t_2^2 - 8\Delta_u u_2 + 2m_1^2 u_2 + 4u_2^2 - 2m_2^2 u_2 + 5s u_2 \\
& \left. - 2s_4 u_2 + 6t_2 u_2] \hat{I}\left(\frac{1}{u' s_{3\Delta}}\right) \right\} \\
& + \left(\frac{-4C_F X_{tu} m_1 m_2}{u_2(t - m_{\tilde{q}t}^2)} \right) \left\{ 2\Delta_u \hat{I}\left(\frac{1}{u_{6\Delta}}\right) - 2\hat{I}(1) + 4\hat{I}\left(\frac{u_{6\Delta}}{u'}\right) \right. \\
& + [4\Delta_u^2 - 2\Delta_u m_1^2 + 2\Delta_u m_2^2 - 4\Delta_u s + m_1^2 s - m_2^2 s + s^2 + 2\Delta_u s_4 - s s_4 - 6\Delta_u t_2 \\
& \left. + 2m_1^2 t_2 - 2m_2^2 t_2 + 3s t_2 - 2s_4 t_2 + 2t_2^2 + s u_2] \hat{I}\left(\frac{1}{u' u_{6\Delta}}\right) \right\},
\end{aligned}$$

$$\begin{aligned}
\hat{M}_{25}^q = & \left(\frac{8(C_F - N_C/2) X_{ts_4\Delta}}{s(s_{4\Delta}^2 + m_{\tilde{q}t}^2 \Gamma^2)(t - m_{\tilde{q}t}^2)} \right) \left\{ [-(s + t_2)(s_4 + t_2)] \hat{I}(1) \right. \\
& \left. + [-s s_4 + s t_2 - 2s_4 t_2 - s_4 u_2 + t_2 u_2] \hat{I}\left(\frac{t'}{u'}\right) \right\},
\end{aligned}$$

$$\begin{aligned}
\hat{M}_{26}^q = & \left(\frac{16(C_F - N_C/2) X_{tu} m_1 m_2}{s(t - m_{\tilde{q}t}^2)} \right) \left\{ [(-\Delta_u + t_2 + u_2)(-\Delta_u + s + t_2 + u_2)] \hat{I}\left(\frac{1}{u' s_{3\Delta}}\right) \right. \\
& \left. + \hat{I}(1) + [-\Delta_u + t_2 + u_2] \hat{I}\left(\frac{1}{s_{3\Delta}}\right) + \hat{I}\left(\frac{s_{3\Delta}}{u'}\right) \right\},
\end{aligned}$$

$$\begin{aligned}
\hat{M}_{27}^q = & \left(\frac{-4N_C X_{tu} m_1 m_2}{(s + u_2)(t - m_{\tilde{q}t}^2)} \right) \left\{ [2s - 2s_4 + t_2 + u_2] \hat{I}\left(\frac{1}{s_{3\Delta}}\right) \right. \\
& \left. + [s s_4 - 2s_4(-\Delta_u + s + t_2 + u_2) + (s + u_2)(-\Delta_u + s + t_2 + u_2)] \hat{I}\left(\frac{1}{u' s_{3\Delta}}\right) \right\},
\end{aligned}$$

$$\hat{M}_{28}^q = \left\{ \frac{8N_C X_t t_2}{(t - m_{\tilde{q}t}^2)(t - m_{\tilde{q}t}^2)} \right\} \left(-s_4^2 \hat{I}\left(\frac{1}{u' u_7}\right) + (m_1^2 - s_4) \hat{I}\left(\frac{1}{u_7}\right) - \hat{I}(1) \right).$$

A squark width Γ is included to regularize a possible on-shell squark pole. As discussed in the text, Γ serves only to regulate the divergence of these interference terms, and it is taken to be very small compared to all physical masses and momenta.

The finite pieces of the quark emission terms are evaluated directly from Eq. (28) with the angular integrals integrated numerically. They may be expressed as

$$|\overline{\mathcal{M}^q}|^2 = \left(\frac{\pi^2 \alpha_S \hat{\alpha}_S}{3} \right) \sum_{i=1..8} \sum_{j=i..8} M_{ij}^q, \quad (\text{E4})$$

with

$$M_{11}^q = M_{12}^q = M_{13}^q = M_{15}^q = M_{22}^q = M_{23}^q = M_{25}^q = M_{26}^q = M_{28}^q = 0, \quad (\text{E5})$$

$$\begin{aligned} M_{14}^q &= \left(\frac{-4 C_F X_t u_7 s_{3\Delta}}{t_2^2 (s_{3\Delta}^2 + m_{\tilde{q}t}^2 \Gamma^2) u_{7\Delta}} \right) \{ 2 s_{32}^2 - s s_{32} - 2 s_4 s_{32} + 2 t_2 s_{32} - 2 s_{32} u' - u_6 s_{32} + t' s_5 - t' m_1^2 \\ &\quad - 3 t' m_2^2 + t' u_2 - s_4 t_2 - t_2 u' \} \\ &+ \left(\frac{-4 C_F X_t u_7 s_{3\Delta}}{t_2 (s_{3\Delta}^2 + m_{\tilde{q}t}^2 \Gamma^2) u_{7\Delta}^2} \right) \{ 2 s_{32}^2 - s s_{32} - 2 s_4 s_{32} + 2 t_2 s_{32} - 2 s_{32} u' - u_6 s_{32} + t' s_5 - t' m_1^2 \\ &\quad - 3 t' m_2^2 + t' u_2 - s_4 t_2 - t_2 u' \}, \end{aligned}$$

$$\begin{aligned} M_{16}^q &= \left(\frac{8 (C_F - N_C/2) X_t s_{3\Delta}}{s (s_{3\Delta}^2 + m_{\tilde{q}t}^2 \Gamma^2) u_{7\Delta} t_2} \right) \{ -s s_{32} s_4 + s_{32} u' u_6 + s s_{32} u_7 + s_{32} t' u_7 \\ &\quad + 2 s_{32} u' u_7 + t_2 u' u_7 - t' u_2 u_7 \}, \end{aligned}$$

$$\begin{aligned} M_{17}^q &= \left(\frac{4 N_C X_t s_{3\Delta}}{(s + t_2) (s_{3\Delta}^2 + m_{\tilde{q}t}^2 \Gamma^2) u_{7\Delta} t_2} \right) \{ -s s_{32} s_4 + s_{32} u' u_6 - 2 s_4 s_{32} u_7 - t' u_7 m_2^2 \\ &\quad - m_1^2 t' u_7 - s_{32} t' u_7 + s_5 t' u_7 - s_4 t_2 u_7 - s_{32} u_6 u_7 \} \\ &+ \left(\frac{-4 N_C X_t s_{3\Delta}}{u_6 (s_{3\Delta}^2 + m_{\tilde{q}t}^2 \Gamma^2) u_{7\Delta} (s + t_2)} \right) \{ -s s_{32} s_4 + s_{32} u' u_6 - 2 s_4 s_{32} u_7 - t' u_7 m_2^2 \\ &\quad - m_1^2 t' u_7 - s_{32} t' u_7 + s_5 t' u_7 - s_4 t_2 u_7 - s_{32} u_6 u_7 \} \end{aligned}$$

$$M_{18}^q = \left(\frac{4 N_C X_{tu} m_1 m_2}{u_6 (u - m_{\tilde{q}u}^2) u_{7\Delta} (s + t_2)} \right) \{ -s s_4 - 2 s t' - 2 s_4 u' - 2 t' u' - u' u_6 + t' u_7 \},$$

$$\begin{aligned} M_{24}^q &= \left(\frac{-4 C_F X_{tu} m_1 m_2 s_{3\Delta}}{u_{7\Delta} (s_{3\Delta}^2 + m_{\tilde{q}t}^2 \Gamma^2) (u - m_{\tilde{q}u}^2) t_2} \right) \{ -s s_{32} + s s_4 + 2 s u' - 2 s_{32} u' + 2 s_4 u' - t_2 u' \\ &\quad + 2 u'^2 + t' u_2 + u' u_6 - t' u_7 \}, \end{aligned}$$

$$M_{27}^q = \left(\frac{-4 N_C X_{tu} m_1 m_2 s_{3\Delta}}{u_6 (s_{3\Delta}^2 + m_{\tilde{q}t}^2 \Gamma^2) (u - m_{\tilde{q}u}^2) (s + t_2)} \right) \{ -s s_4 - 2 s_4 u' - u' u_6 + t' u_7 \},$$

$$M_{33}^q = \left(\frac{4 C_F X_u s_4 u_2}{(u - m_{\tilde{q}u}^2)^2 (s_{4\Delta}^2 + m_{\tilde{q}t}^2 \Gamma^2)} \right) \{ 2 m_2^2 + 2 m_1^2 - s_{32} + s_4 - s_5 - u' + u_2 - u_7 \},$$

$$M_{34}^q = \left(\frac{-8 (C_F - N_C/2) X_{tu} s_{4\Delta} s_{3\Delta} m_1 m_2 u'}{(u - m_{\tilde{q}u}^2)^2 (s_{4\Delta}^2 + m_{\tilde{q}t}^2 \Gamma^2) u_{7\Delta} (s_{3\Delta}^2 + m_{\tilde{q}t}^2 \Gamma^2)} \right) \{ s_5 - u' - 2 m_2^2 - 2 m_1^2 \},$$

$$\begin{aligned}
M_{35}^q &= \left(\frac{-4 C_F X_u s_4}{(u - m_{\tilde{q}_u}^2)(s_{4\Delta}^2 + m_{\tilde{q}_t}^2 \Gamma^2) s} \right) \{ 3 m_2^2 s + m_1^2 s - s s_{32} - s s_5 + t_2 u' + t' u_2 \\
&\quad - 2 t_2 u_2 + 2 u' u_2 - 2 u_2^2 + u_2 u_6 + t_2 u_7 + 2 u_2 u_7 \}, \\
M_{36}^q &= \left(\frac{4 C_F X_{tu} s_{4\Delta} s_{3\Delta} m_1 m_2}{(u - m_{\tilde{q}_u}^2)(s_{4\Delta}^2 + m_{\tilde{q}_t}^2 \Gamma^2)(s_{3\Delta}^2 + m_{\tilde{q}_t}^2 \Gamma^2) s} \right) \{ s s_{32} - s s_4 + 2 t' u' - t_2 u' + 2 u'^2 - t' u_2 \\
&\quad - 2 u' u_2 + u' u_6 + t' u_7 + 2 u' u_7 \}, \\
M_{37}^q &= \left(\frac{2 N_C X_{tu} s_{4\Delta} s_{3\Delta} m_1 m_2}{(u - m_{\tilde{q}_u}^2)(s_{4\Delta}^2 + m_{\tilde{q}_t}^2 \Gamma^2)(s_{3\Delta}^2 + m_{\tilde{q}_t}^2 \Gamma^2) u_6} \right) \{ s s_{32} - s s_4 - 2 m_2^2 u' - 6 m_1^2 u' \\
&\quad + 2 s u' - 2 s_4 u' + 2 s_5 u' + t_2 u' - t' u_2 - u' u_6 + t' u_7 + 2 u' u_7 \}, \\
M_{38}^q &= \left(\frac{-2 N_C X_u s_{4\Delta} u_2}{(u - m_{\tilde{q}_u}^2)^2 (s_{4\Delta}^2 + m_{\tilde{q}_t}^2 \Gamma^2) u_6} \right) \{ -2 m_2^2 s_4 - 6 m_1^2 s_4 + s s_4 - 2 s_4^2 + 2 s_4 s_5 \\
&\quad - m_2^2 t' - 3 m_1^2 t' - 2 s_4 t' + s_5 t' + s_4 t_2 - s_{32} u_6 - u' u_6 + 2 s_4 u_7 + t' u_7 \}, \\
M_{44}^q &= \left(\frac{4 C_F X_t s_{32} u_7}{u_{7\Delta}^2 (s_{3\Delta}^2 + m_{\tilde{q}_t}^2 \Gamma^2)} \right) \{ 2 m_2^2 + 2 m_1^2 + s_{32} - s_4 - s_5 - u' - u_2 + u_7 \}, \\
M_{45}^q &= \left(\frac{4 (C_F - N_C/2) X_{tu} s_{4\Delta} s_{3\Delta} m_1 m_2}{u_{7\Delta} (s_{3\Delta}^2 + m_{\tilde{q}_t}^2 \Gamma^2) s (s_{4\Delta}^2 + m_{\tilde{q}_t}^2 \Gamma^2)} \right) \{ -s s_{32} + s s_4 + 2 t' u' + t_2 u' + 2 u'^2 + t' u_2 \\
&\quad + 2 u' u_2 - u' u_6 - t' u_7 - 2 u' u_7 \}, \\
M_{46}^q &= \left(\frac{-4 (C_F - N_C/2) X_t s_{32}}{u_{7\Delta} (s_{3\Delta}^2 + m_{\tilde{q}_t}^2 \Gamma^2) s} \right) \{ s m_2^2 + 3 s m_1^2 - s s_4 - s s_5 + u' u_6 + u_2 u_6 \\
&\quad + t' u_7 + t_2 u_7 + 2 u' u_7 + 2 u_2 u_7 - 2 u_6 u_7 - 2 u_7^2 \}, \\
M_{47}^q &= \left(\frac{2 N_C X_t s_{32}}{u_{7\Delta} (s_{3\Delta}^2 + m_{\tilde{q}_t}^2 \Gamma^2) u_6} \right) \{ s m_2^2 + 3 s m_1^2 - s s_4 - s s_5 + 2 u_7 m_2^2 + u' u_6 + u_2 u_6 \\
&\quad + 6 u_7 m_1^2 + 2 s u_7 - 2 s_4 u_7 - 2 s_5 u_7 - t' u_7 - t_2 u_7 + 2 u_7^2 \}, \\
M_{48}^q &= \left(\frac{-2 N_C X_{tu} s_{3\Delta} m_1 m_2}{u_{7\Delta} (s_{3\Delta}^2 + m_{\tilde{q}_t}^2 \Gamma^2) u_6 (u - m_{\tilde{q}_u}^2)} \right) \{ s s_{32} - s s_4 + 2 u' m_2^2 + 6 u' m_1^2 - 2 s_4 u' \\
&\quad - 2 s_5 u' - 2 t' u' - t_2 u' - t' u_2 + u' u_6 + t' u_7 + 2 u' u_7 \},
\end{aligned}$$

$$M_{55}^q = \left(\frac{-8 C_F X_u s_4 t_2}{s (s_{4\Delta}^2 + m_{\tilde{q}_t}^2 \Gamma^2)} \right),$$

$$M_{56}^q = \left(\frac{16 C_F X_{tu} s_{4\Delta} s_{3\Delta} m_1 m_2 t'}{s (s_{3\Delta}^2 + m_{\tilde{q}_t}^2 \Gamma^2) (s_{4\Delta}^2 + m_{\tilde{q}_t}^2 \Gamma^2)} \right),$$

$$M_{57}^q = \left(\frac{4 N_C X_{tu} s_{4\Delta} s_{3\Delta} m_1 m_2}{s (s_{3\Delta}^2 + m_{\tilde{q}_t}^2 \Gamma^2) u_6 (s_{4\Delta}^2 + m_{\tilde{q}_t}^2 \Gamma^2)} \right) \{-s s_4 + 2 s t' + 2 s u' + u' u_6 + t' u_7 + 2 u' u_7\},$$

$$M_{58}^q = \left(\frac{4 N_C X_u s_{4\Delta}}{s (u - m_{\tilde{q}_u}^2) u_6 (s_{4\Delta}^2 + m_{\tilde{q}_t}^2 \Gamma^2)} \right) \{-s s_4 m_2^2 - s s_4 m_1^2 + s s_4 s_5 - s s_4 u_2 - s_4 u_2 u_6 + u' u_2 u_6 - s_4 t_2 u_7 - 2 s_4 u_2 u_7 - t' u_2 u_7\},$$

$$M_{66}^q = \left(\frac{-8 C_F X_t s_{32} s u_6}{s^2 (s_{3\Delta}^2 + m_{\tilde{q}_t}^2 \Gamma^2)} \right),$$

$$M_{67}^q = \left(\frac{-2 N_C X_t}{s u_6 (s_{3\Delta}^2 + m_{\tilde{q}_t}^2 \Gamma^2)} \right) \{-4 s m_1^2 + 4 s u_6 + 4 s u_7 + 4 u_6 u_7 + 4 u_7^2\},$$

$$M_{68}^q = \left(\frac{2 N_C X_{tu} s_{3\Delta} m_1 m_2}{s u_6 (s_{3\Delta}^2 + m_{\tilde{q}_t}^2 \Gamma^2) (u - m_{\tilde{q}_u}^2)} \right) \{-s s_4 + u' u_6 + t' u_7 + 2 u' u_7\},$$

$$M_{77}^q = \left(\frac{-4 N_C X_t s_{32}}{u_6^2 (s_{3\Delta}^2 + m_{\tilde{q}_t}^2 \Gamma^2)} \right) \{-4 m_1^2 s + 2 s u_6 - 4 m_1^2 u_7\},$$

$$M_{78}^q = \left(\frac{-16 N_C X_{tu} s_{3\Delta} m_1 m_2 u' (2 m_1^2 + u_6)}{u_6^2 (s_{3\Delta}^2 + m_{\tilde{q}_t}^2 \Gamma^2) (u - m_{\tilde{q}_u}^2)} \right),$$

$$M_{88}^q = \left(\frac{4 N_C X_u u_2}{u_6^2 (u - m_{\tilde{q}_u}^2)^2} \right) \{4 m_1^2 s_4 + 4 m_1^2 t' - 2 t' u_6\}.$$

REFERENCES

- [1] J. Wess and B. Zumino, Nucl. Phys. **B 70**, 39 (1974).
- [2] E. Witten, Nucl. Phys. **B 188**, 513 (1981); J. Polchinski and L. Susskind, Phys. Rev. **D 26**, 3661 (1982); R.K. Kaul and P. Majumdar, Nucl. Phys. **B 199**, 36 (1982).
- [3] L.E. Ibañez and G.G. Ross, Phys. Lett. **B 110**, 215 (1982); J. Ellis, D.V. Nanopoulos, and K. Tamvakis, Phys. Lett. **B 121**, 123 (1983).
- [4] L.E. Ibañez and G.G. Ross, Phys. Lett. **B 105**, 439 (1981); S. Dimopoulos, S. Raby, and F. Wilczek, Phys. Rev. **D 24**, 1681 (1981); P. Langacker and M. Luo, Phys. Rev. **D 44**, 817 (1991); U. Amaldi, W. de Boer, and H. Fürstenau, Phys. Lett. **B 260**, 447 (1991).
- [5] Recent reviews include M. Carena, R.L. Culbertson, S. Eno, H.J. Frisch, and S. Mrenna, Rev. Mod. Phys. **71**, 937 (1999) hep-ex/9712022 and hep-ex/9802006.
- [6] H.P. Nilles, Phys. Rep. **110**, 1 (1984); H. Haber and G.L. Kane, Phys. Rep. **117**, 75 (1985). For a recent review, consult S. Dawson, TASI-97 lectures, hep-ph/9712464.
- [7] W. Beenakker, R. Höpker, M. Spira, and P.M. Zerwas, Nucl. Phys. **B 492**, 51 (1997).
- [8] W. Beenakker, M. Krämer, T. Plehn, M. Spira, and P.M. Zerwas, Nucl. Phys. **B 515**, 3 (1998).
- [9] H. Baer, B.W. Harris, and M. Hall Reno, Phys. Rev. **D 57**, 5871 (1998).
- [10] W. Beenakker, M. Klasen, M. Krämer, T. Plehn, M. Spira, and P.M. Zerwas, Phys. Rev. Lett. **83**, 3780 (1999).
- [11] E.L. Berger, M. Klasen, and T. Tait, Phys. Lett. **B 459**, 165 (1999).
- [12] R. Arnowitt and P. Nath, to appear in “Perspectives on Supergravity”, World Scientific, Editor G. Kane, hep-ph/9708254, and references therein; M. Drees and S. P. Martin,

- Report of the DPF Working Group on Electroweak Symmetry Breaking and Beyond the Standard Model, hep-ph/9504324.
- [13] C. Kolda, Nucl. Phys. Proc. Suppl. **62**, 266 (1998) hep-ph/9707450, and original references therein.
 - [14] H. Baer, D.D. Karatas, and X. Tata, Phys. Rev. **D 42**, 2259 (1990).
 - [15] S. Dawson, E. Eichten, and C. Quigg, Phys. Rev. **D 31**, 1581 (1985).
 - [16] J. Ellis, C. Kounnas, and D. V. Nanopoulos, Nucl. Phys. **B 247**, 373 (1984); A.B. Lahanas and D. V. Nanopoulos, Phys. Rep. **145**, 1 (1987).
 - [17] D. E. Kaplan, G. D. Kribs, and M. Schmaltz, hep-ph/9911293; Z. Chacko, M. A. Luty, A. E. Nelson, and E. Ponton, JHEP **0001**, 003 (2000); M. Schmaltz and W. Skiba, hep-ph/0001172; M. Schmaltz and W. Skiba, hep-ph/0004210.
 - [18] D. E. Kaplan and T. M. P. Tait, hep-ph/0004200.
 - [19] L. Randall and R. Sundrum, Nucl. Phys. **B 557**, 79 (1999) hep-ph/9810155; G. F. Giudice, M. A. Luty, H. Murayama, and R. Rattazzi, JHEP **9812**, 027 (1998); T. Gherghetta, G. F. Giudice, and J. D. Wells, Nucl. Phys. **B 559**, 27 (1999) hep-ph/9904378.
 - [20] S. Abel *et al.* [SUGRA Working Group Collaboration], Report of the SUGRA Working group, Fermilab workshop in preparation for Run II at the Fermilab Tevatron, November, 1998, hep-ph/0003154.
 - [21] ALEPH Collaboration, R. Barate *et al.*, Eur. Phys. J. **C 11**, 193 (1999) and G. Ganis *et al.*, ALEPH 2000-012 (CONF 2000-009); DELPHI Collaboration, P. Abreu *et al.*, Phys. Lett. **B466**, 61 (1999); L3 Collaboration, M. Acciarri *et al.*, Phys. Lett. **B459**, 354 (1999); OPAL Collaboration, G. Abbiendi *et al.*, CERN report CERN-EP-99-123 (1999) hep-ex/9909051 and references therein.

- [22] S. Raby, Phys. Rev. **D56**, 2852 (1997); Phys. Lett. B **422**, 158 (1998).
- [23] A. Mafi and S. Raby, hep-ph/9912436.
- [24] Higgsino couplings to down-type quarks may be enhanced for large $\tan\beta$ and can be appreciable for bottom (b) quarks. Thus, associated production modes involving b quarks and Higgsinos, ignored in our calculations, could play an important role in searches for supersymmetry at hadron colliders.
- [25] A. Denner, H. Eck, O. Hahn, and J. Küblbeck, Nucl. Phys. **B 387**, 467 (1992).
- [26] J. F. Gunion and H. Haber, Nucl. Phys. **B 272**, 1 (1986).
- [27] H. Baer, F. E. Paige, S. D. Protopopescu, and X. Tata, Brookhaven report BNL-HET-99-43, hep-ph/0001086.
- [28] Report of the Working group on Gauge Mediation / Low-Scale SUSY Breaking, Fermilab workshop in preparation for Run II at the Fermilab Tevatron, November, 1998.
- [29] J. A. M. Vermaseren, KEK-TH-326 (1992).
- [30] M. Chanowitz, M. Furman, I. Hinchliffe, Nucl. Phys. **B 159**, 225 (1979).
- [31] G. Passarino and M. Veltman, Nucl. Phys. **B 160**, 151 (1979).
- [32] W. A. Bardeen, A. J. Buras, D. W. Duke, T. Muta, Phys. Rev. **D 18**, 3998 (1978).
- [33] S. P. Martin and M. T. Vaughn, Phys. Lett. **B 318**, 331 (1993).
- [34] W. Beenakker, H. Kuijf, and W. L. van Neerven, Phys. Rev. **D 40**, 54 (1989).
- [35] G. Altarelli, R. K. Ellis, and G. Martinelli, Nucl. Phys. **B 157**, 461 (1979).
- [36] G. Altarelli and G. Parisi, Nucl. Phys. **B 126**, 298 (1977).
- [37] P. Nason, S. Dawson, and R. K. Ellis, Nucl. Phys. **B 303**, 607 (1988).
- [38] W. Beenakker, W. L. van Neerven, R. Meng, G. A. Schuler, and J. Smith, Nucl. Phys.

B 351, 507 (1991), and references therein.

- [39] H. L. Lai *et al* [CTEQ Collaboration], Eur. Phys. J. **C12**, 375 (2000).
- [40] H. L. Lai *et al* [CTEQ Collaboration], Phys. Rev. **D 55**, 1280 (1997).
- [41] M. C. Smith and S. Willenbrock, Phys.Rev. **D54**, 6696 (1996).
- [42] R. Höpker, Ph.D. Thesis, University of Hamburg, DESY-T-96-02 (1996).
- [43] A. Denner, U. Nierste, and R. Scharf, Nucl. Phys. **B 367**, 637 (1991).

TABLES

$m_{1/2}$ (GeV)	$m_{\tilde{g}}$ (GeV)	$m_{\tilde{\chi}}$ (GeV)	Tevatron (pb)	LHC (pb)
100	284.9	31.1	0.165	2.82
100	284.9	62.6	0.233	4.50
100	284.9	-211.3	0.00588	0.176
100	284.9	240.9	0.00424	0.364
100	284.9	56.8	0.329	9.61
100	284.9	240.2	0.0100	0.928
200	533.7	77.6	0.00283	0.212
200	533.7	146.6	0.00231	0.354
200	533.7	-358.2	$1.22 \cdot 10^{-5}$	0.00452
200	533.7	380.6	$9.73 \cdot 10^{-6}$	0.0151
200	533.7	145.2	0.00238	0.720
200	533.7	379.5	$1.680 \cdot 10^{-5}$	0.0379
300	775.5	120.3	$5.51 \cdot 10^{-5}$	0.0400
300	775.5	232.3	$2.07 \cdot 10^{-5}$	0.0605
300	775.5	-510.9	$1.46 \cdot 10^{-8}$	0.000385
300	775.5	528.2	$7.71 \cdot 10^{-9}$	0.00144
300	775.5	231.7	$1.58 \cdot 10^{-5}$	0.128
300	775.5	527.2	$1.06 \cdot 10^{-8}$	0.00368
400	1012.4	162.2	$6.58 \cdot 10^{-7}$	0.0110
400	1012.4	317.1	$6.85 \cdot 10^{-8}$	0.0151
400	1012.4	-665.3	$5.23 \cdot 10^{-13}$	$5.53 \cdot 10^{-5}$
400	1012.4	679.2	$9.85 \cdot 10^{-14}$	0.000207
400	1012.4	316.77	$3.52 \cdot 10^{-8}$	0.0327
400	1012.4	678.4	$1.16 \cdot 10^{-13}$	0.000550

TABLE I. Total cross sections in pb at the Tevatron and at the LHC for the parameters of the SUGRA model. Shown in column 1 are four chosen values of the common fermion mass. In column 2 are the derived values of the gluino masses, and in column 3 are the masses of the four neutralinos and the two charginos. See also Figs. 11 and 12.

FIGURES

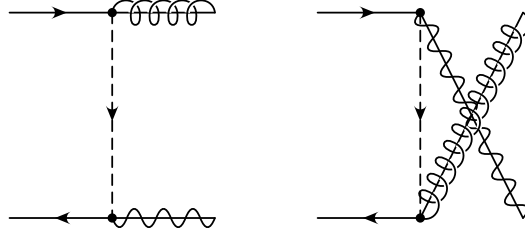


FIG. 1. Leading order Feynman diagrams for $q\bar{q} \rightarrow \tilde{g}\tilde{\chi}$.

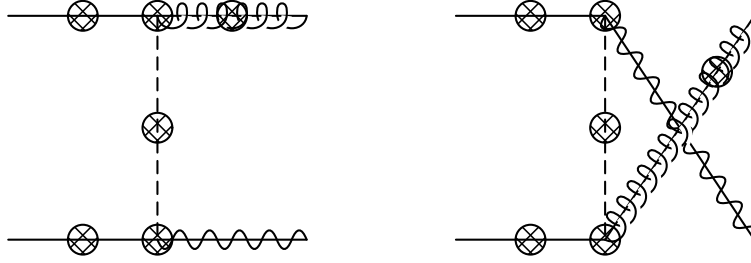


FIG. 2. Generic virtual one-loop diagrams for the associated production of a gluino and a gaugino. The crossed regions denote self-energy and vertex corrections that are present only one at a time at next-to-leading order.

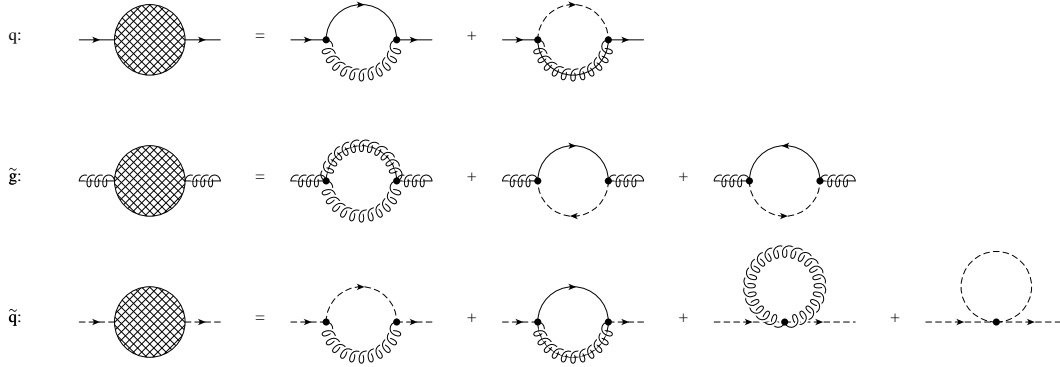


FIG. 3. Self-energy diagrams for external quarks (q) and gluinos (\tilde{g}) and internal squarks (\tilde{q}) including the full supersymmetric QCD particle spectrum. Contributions from the tadpole graphs vanish.

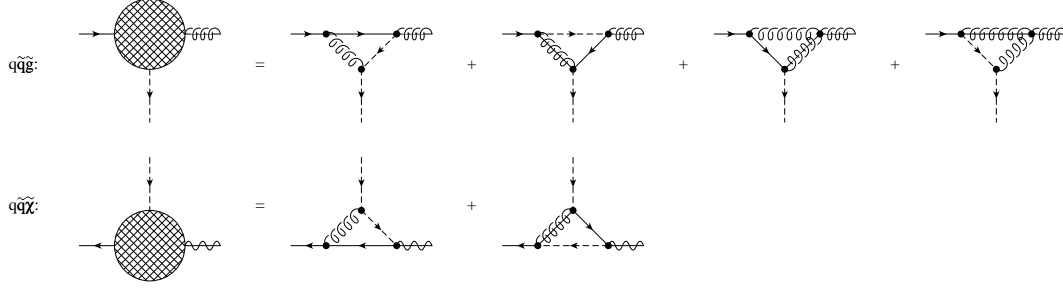


FIG. 4. Vertex corrections for the quark-squark-gluino ($q\tilde{q}\tilde{g}$) and quark-squark-gaugino ($q\tilde{q}\tilde{\chi}$) vertices including the full supersymmetric QCD particle spectrum.

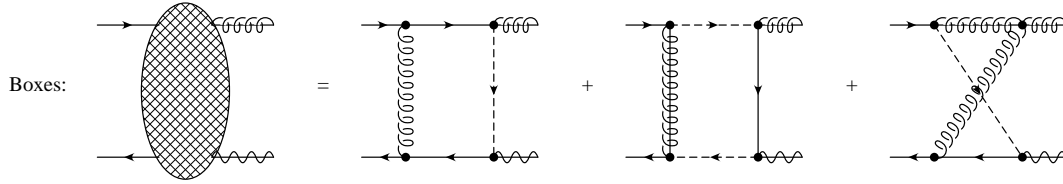


FIG. 5. Box diagrams for associated production of a gluino and a gaugino. There are u -channel box diagrams in addition to the diagrams shown.

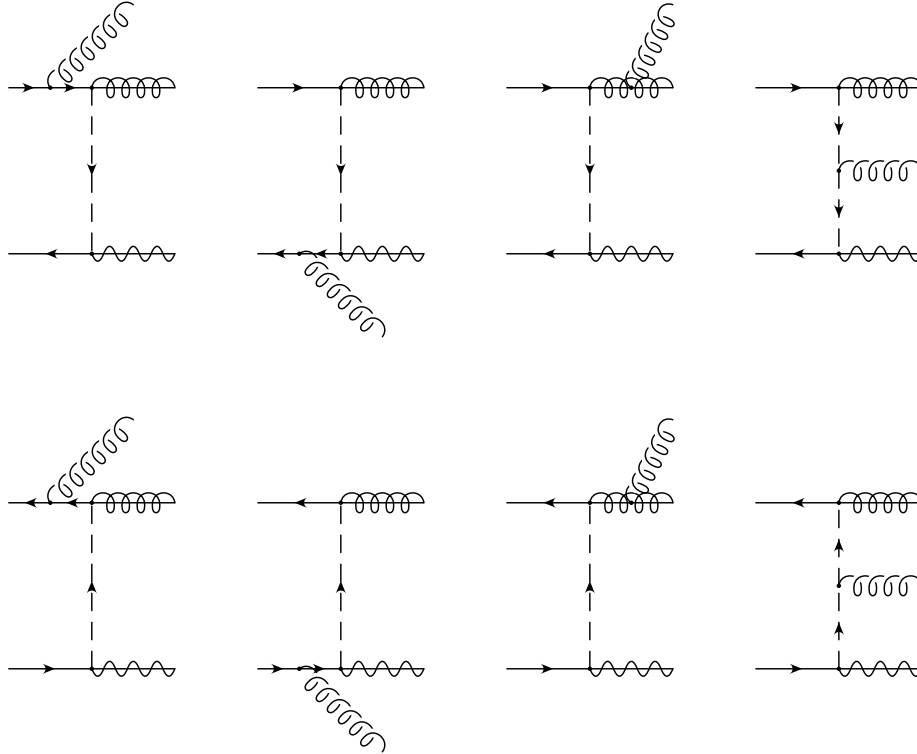


FIG. 6. Feynman diagrams for the gluon emission contribution, $q\bar{q} \rightarrow g\tilde{g}\tilde{\chi}$.

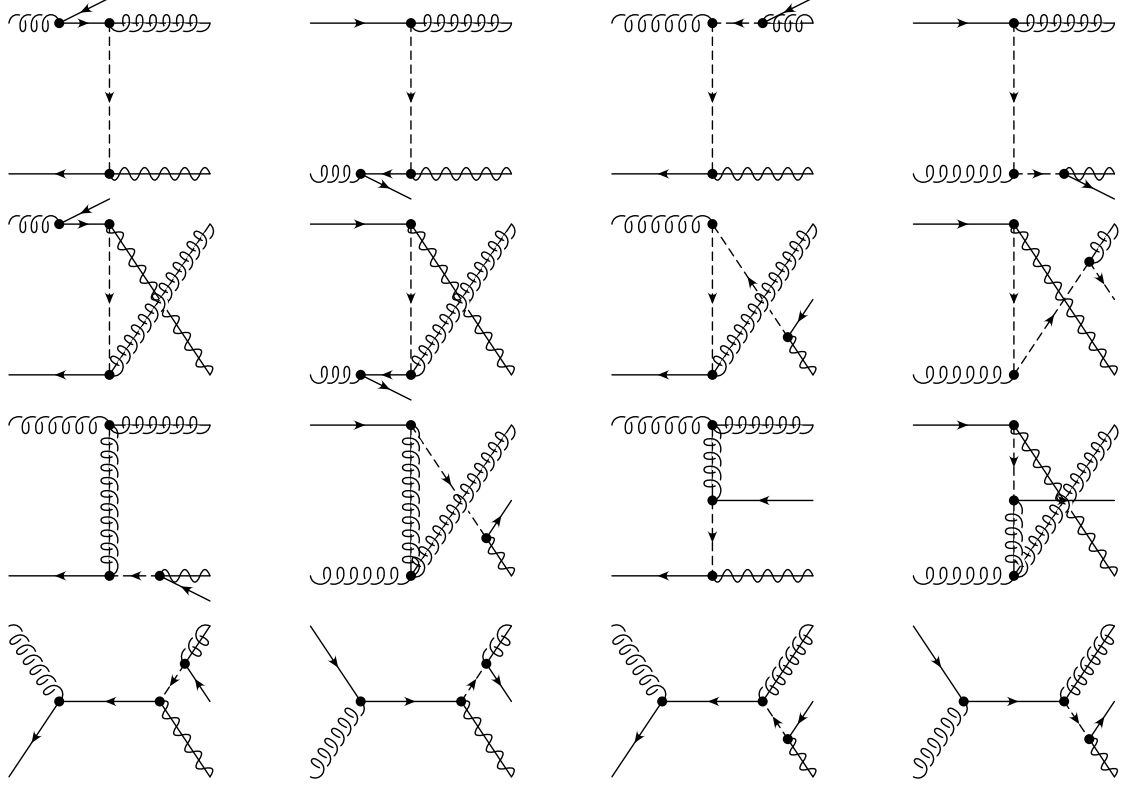


FIG. 7. Feynman diagrams for the emission of a light quark, $q + g \rightarrow q + \tilde{g} + \tilde{\chi}$.

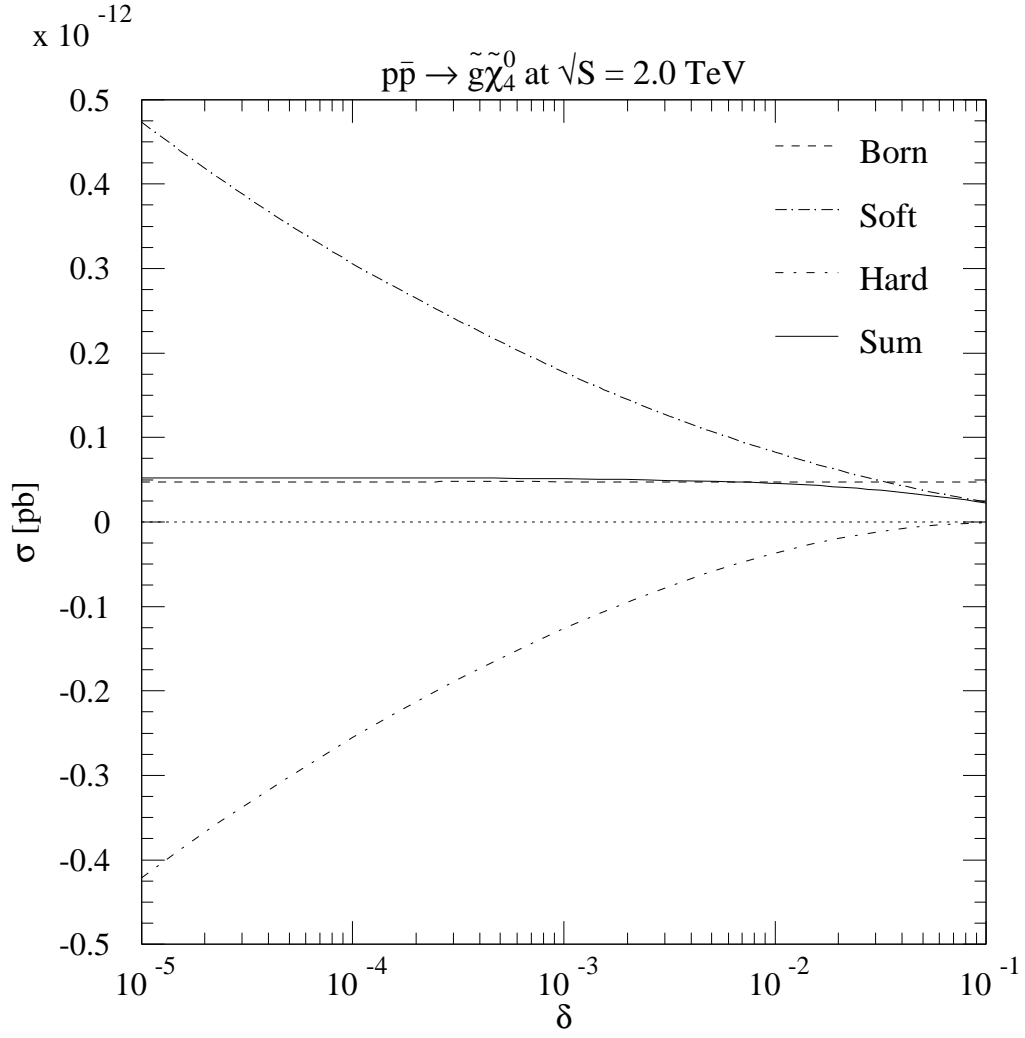


FIG. 8. Dependence of the total hadronic cross section on the cutoff parameter δ for the $\tilde{g}\tilde{\chi}_4^0$ channel in the SUGRA model at the Tevatron, with $m_{\tilde{g}} = 1012$ GeV and $m_{\tilde{\chi}_4^0} = 679$ GeV.

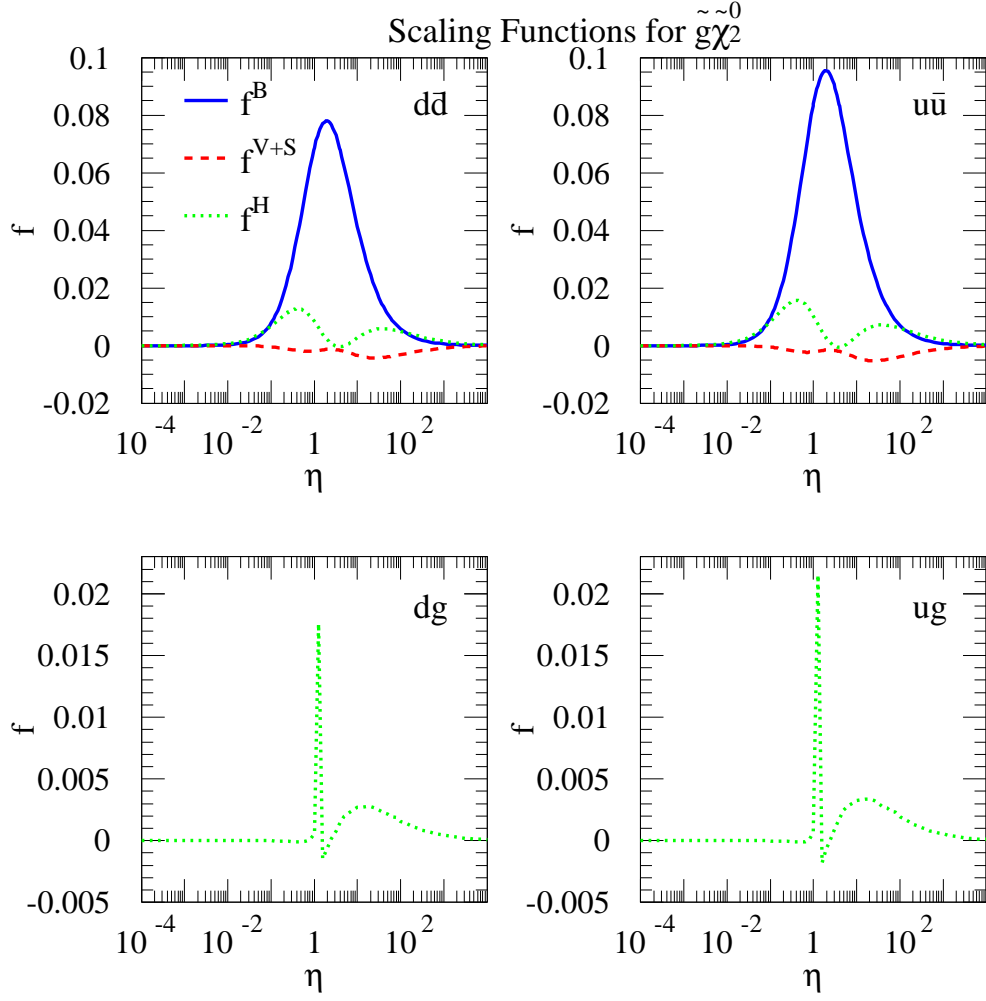


FIG. 9. Scaling functions for the SUGRA $\tilde{g}\tilde{\chi}_2^0$ channel, with $m_{\tilde{g}} = 410$ GeV and $m_{\tilde{\chi}_2^0} = 104$ GeV.

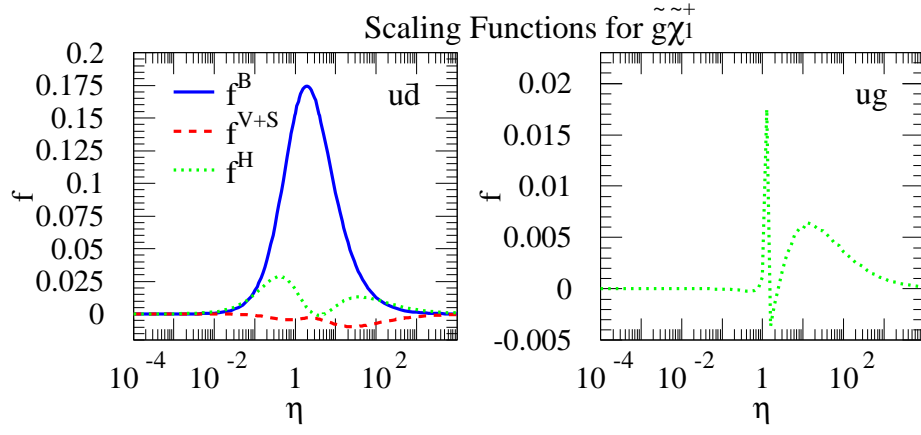


FIG. 10. Scaling functions for the $\tilde{g}\tilde{\chi}_1^+$ channel in the SUGRA model with $m_{\tilde{g}} = 410$ GeV and $m_{\tilde{\chi}_1^+} = 101$ GeV.

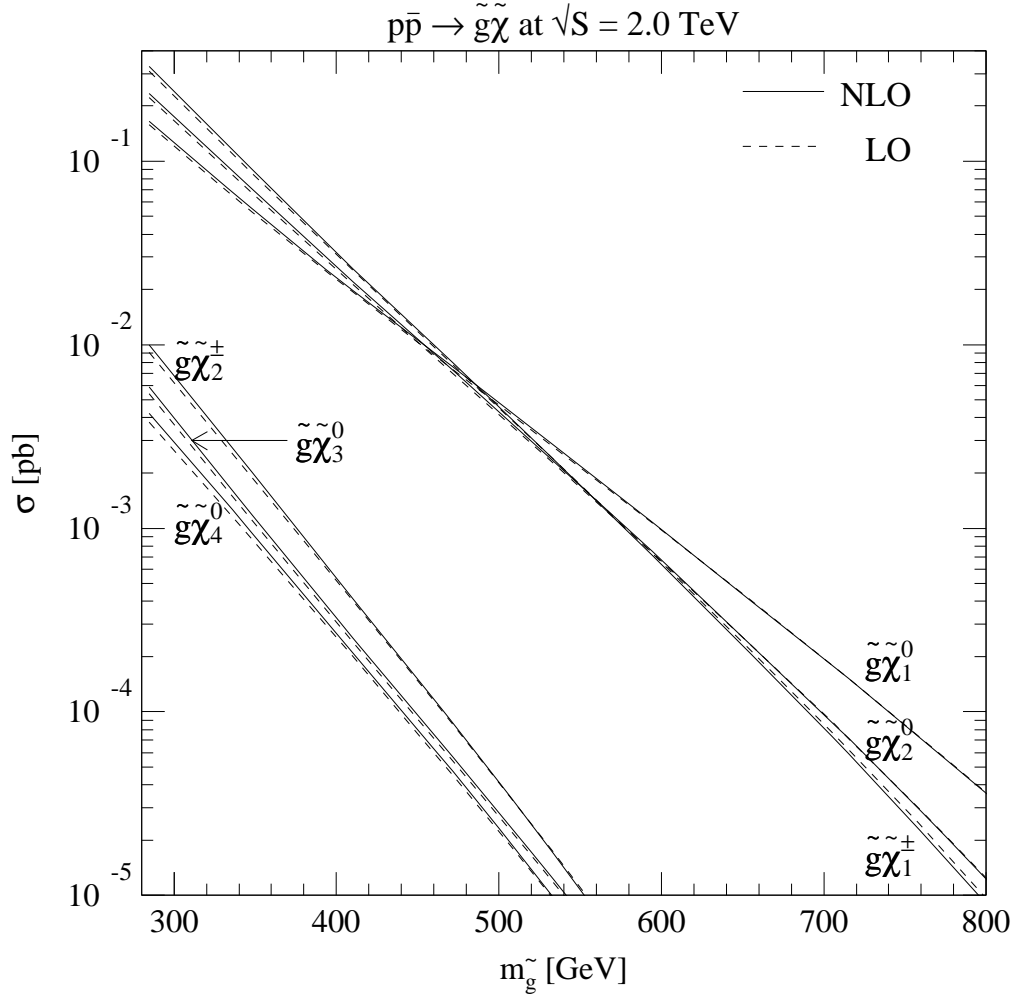


FIG. 11. Predicted total cross sections at the Tevatron for all six $\tilde{g}\tilde{\chi}$ channels in the SUGRA model as functions of the mass of the gluino. See also Table I.

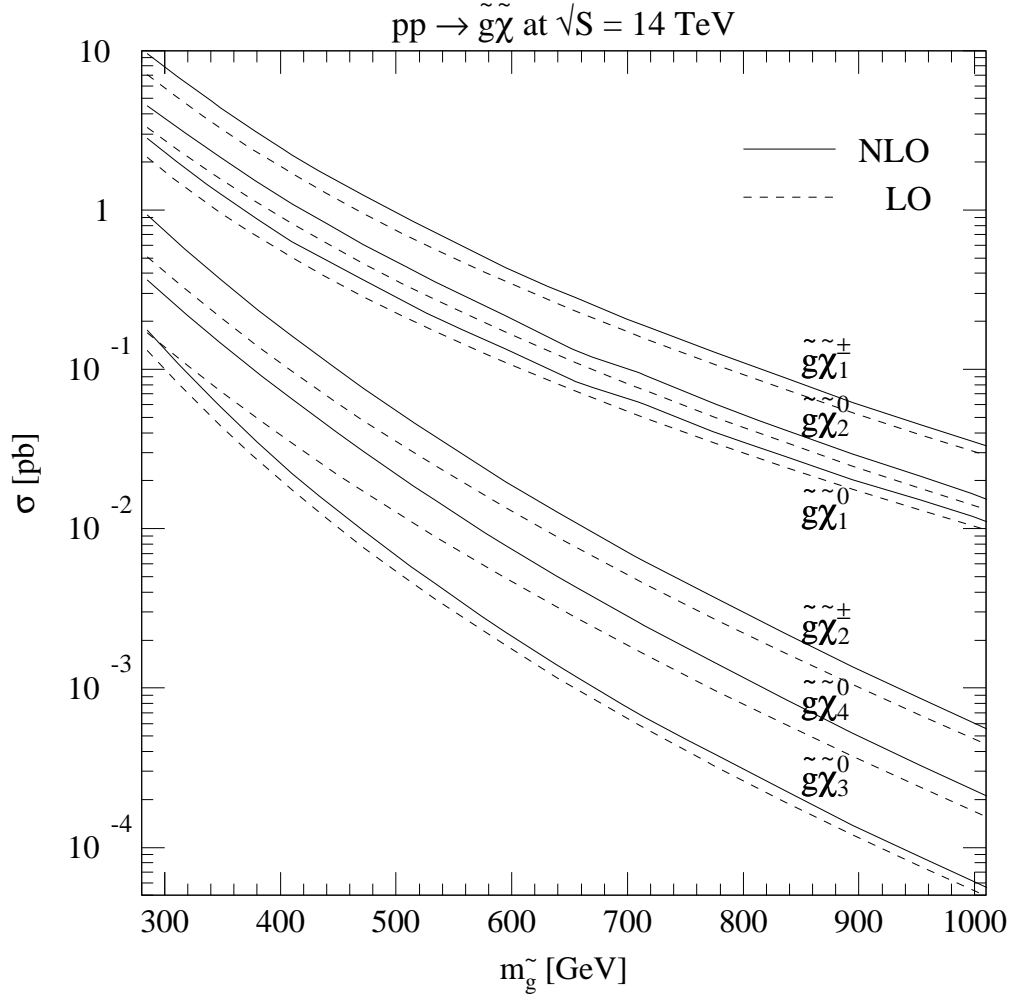


FIG. 12. Predicted total cross sections at LHC energies for all six $\tilde{g}\tilde{\chi}$ channels in the SUGRA model as functions of the mass of the gluino. See also Table I.

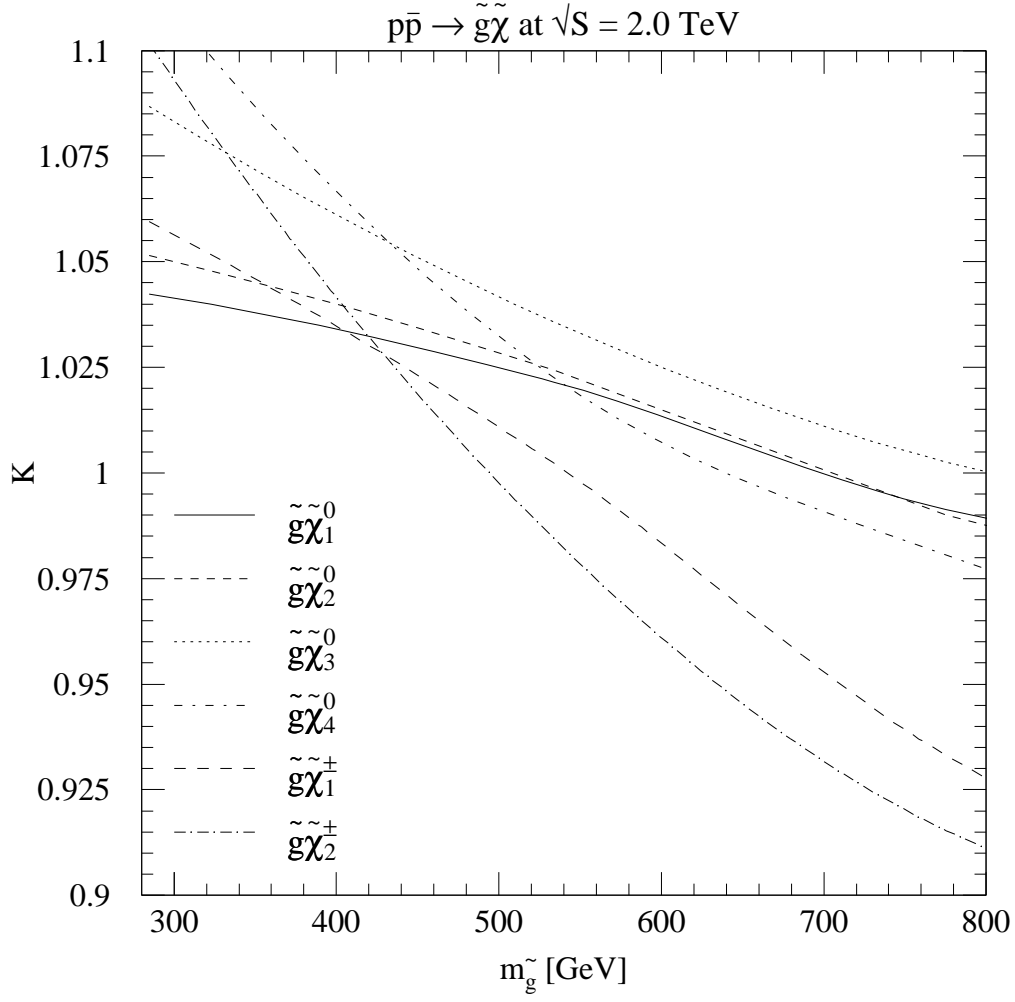


FIG. 13. Calculated enhancements of the cross sections from NLO contributions at the Tevatron for all six SUGRA $\tilde{g}\tilde{\chi}$ channels as functions of the mass of the gluino.

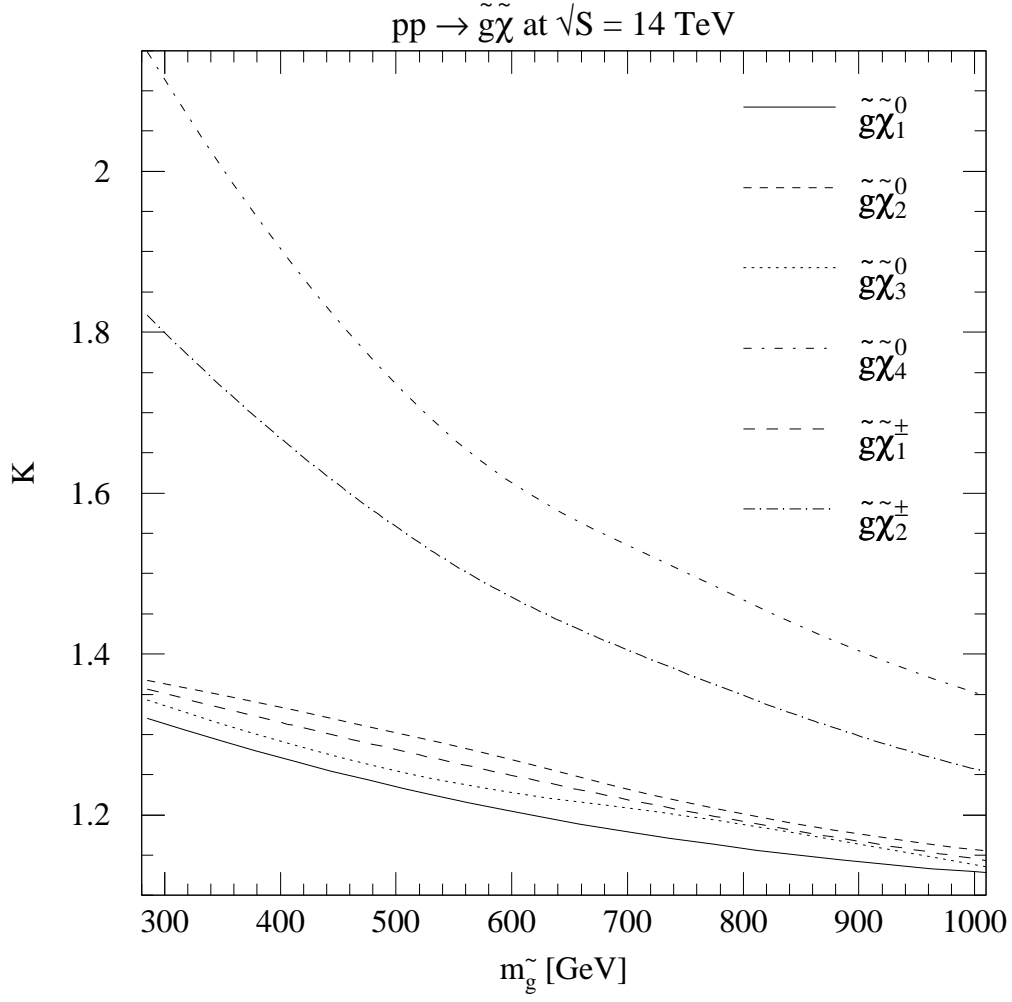


FIG. 14. Calculated enhancements of the cross sections from NLO contributions at the LHC for all six SUGRA $\tilde{g}\tilde{\chi}$ channels as functions of the mass of the gluino.

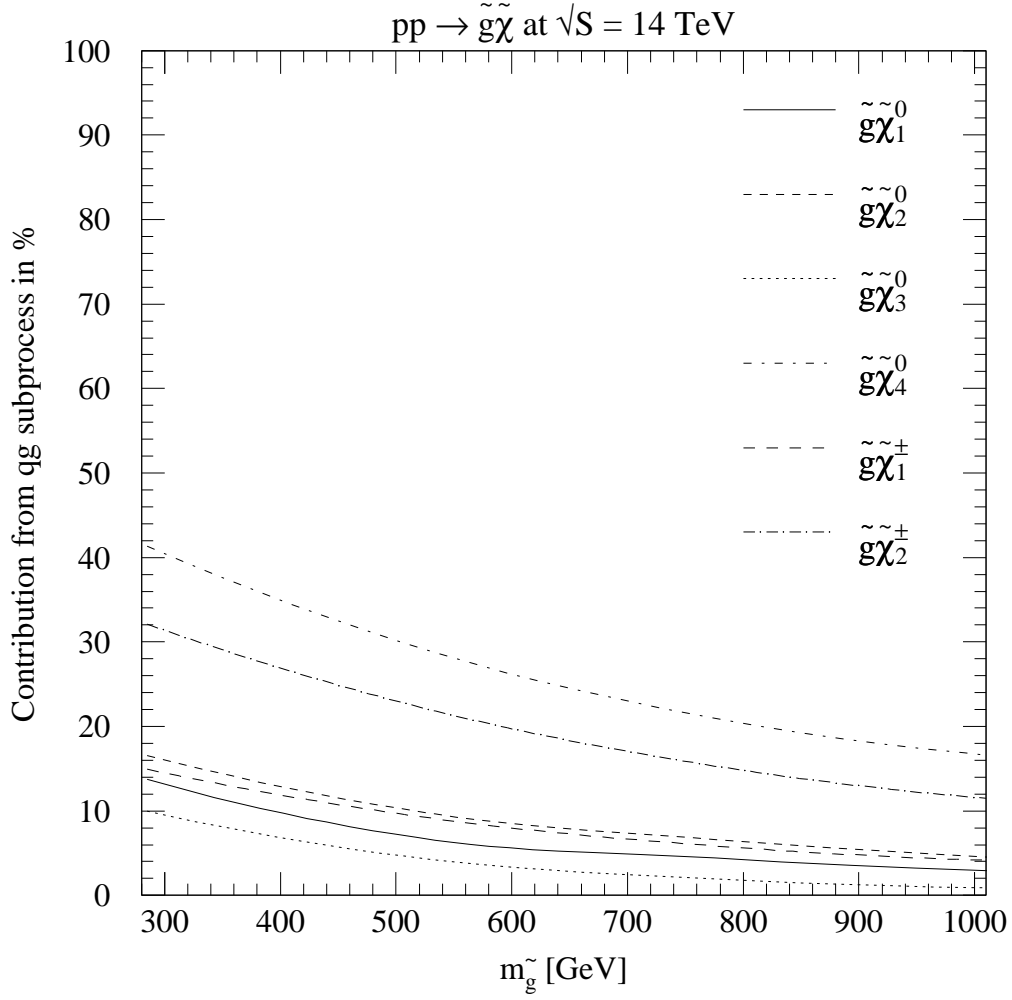


FIG. 15. Fraction of the NLO cross sections at the LHC from the qg initial state for all six SUGRA $\tilde{g}\tilde{\chi}$ channels as functions of the mass of the gluino.

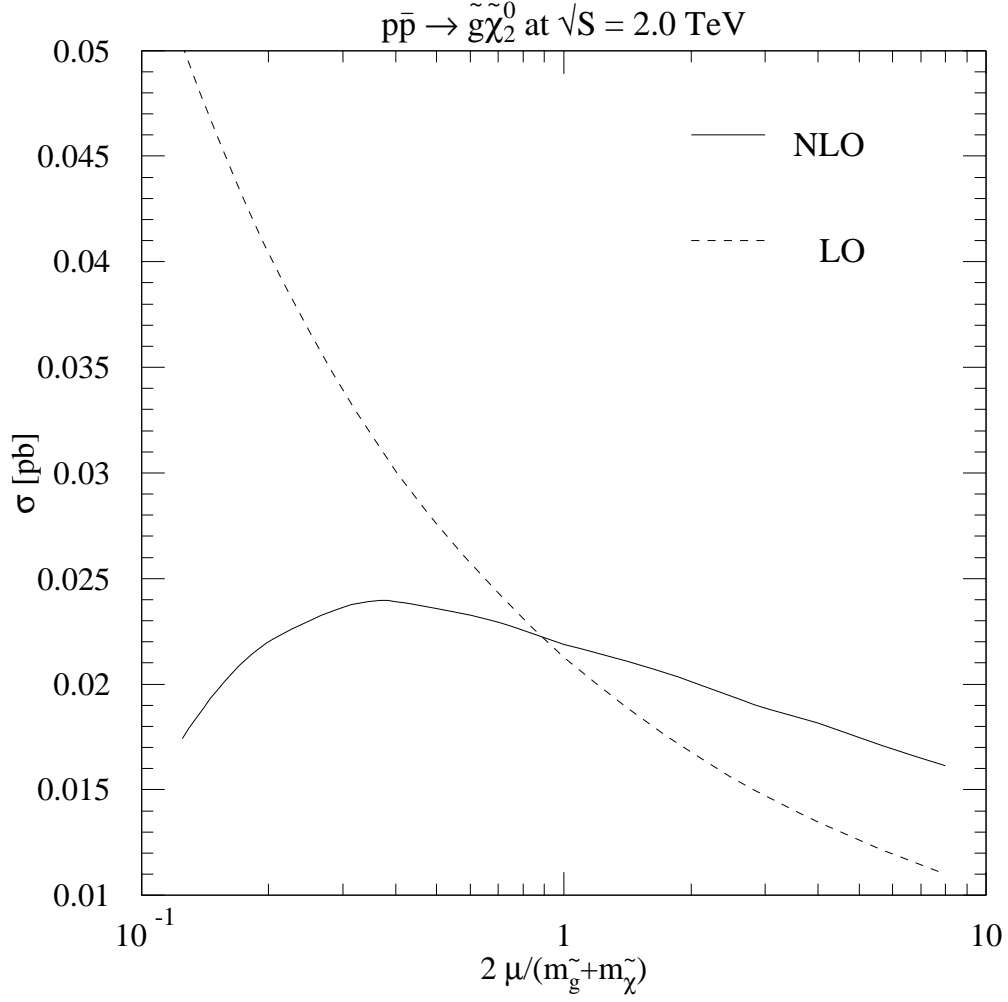


FIG. 16. Dependence of the predicted NLO and LO total cross sections at the Tevatron on the renormalization and factorization scale. We show the case $\tilde{g}\tilde{\chi}_2^0$ production in the SUGRA model, with $m_{\tilde{g}} = 410$ GeV and $m_{\tilde{\chi}_2^0} = 104$ GeV.

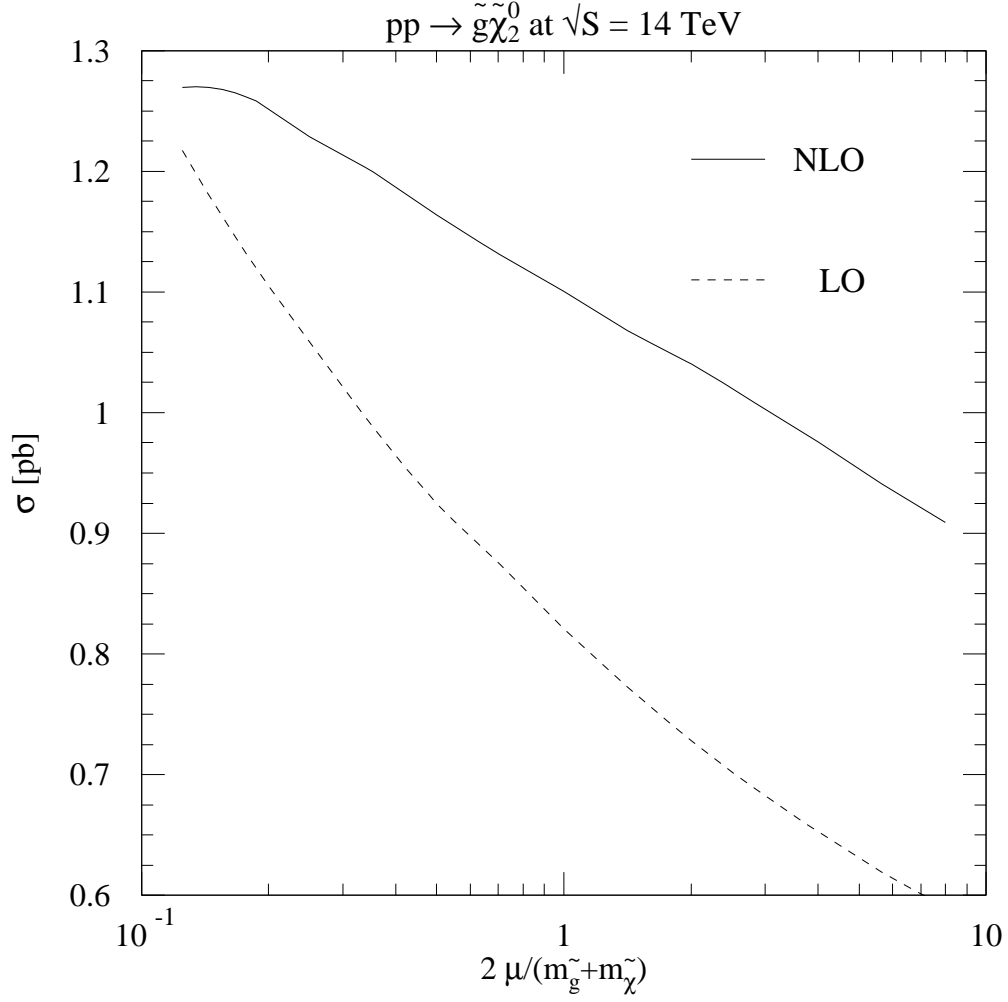


FIG. 17. Dependence of the predicted NLO and LO total cross sections at the LHC on the renormalization and factorization scale. We select $\tilde{g}\tilde{\chi}_2^0$ production in the SUGRA model, with $m_{\tilde{g}} = 410$ GeV and $m_{\tilde{\chi}_2^0} = 104$ GeV.

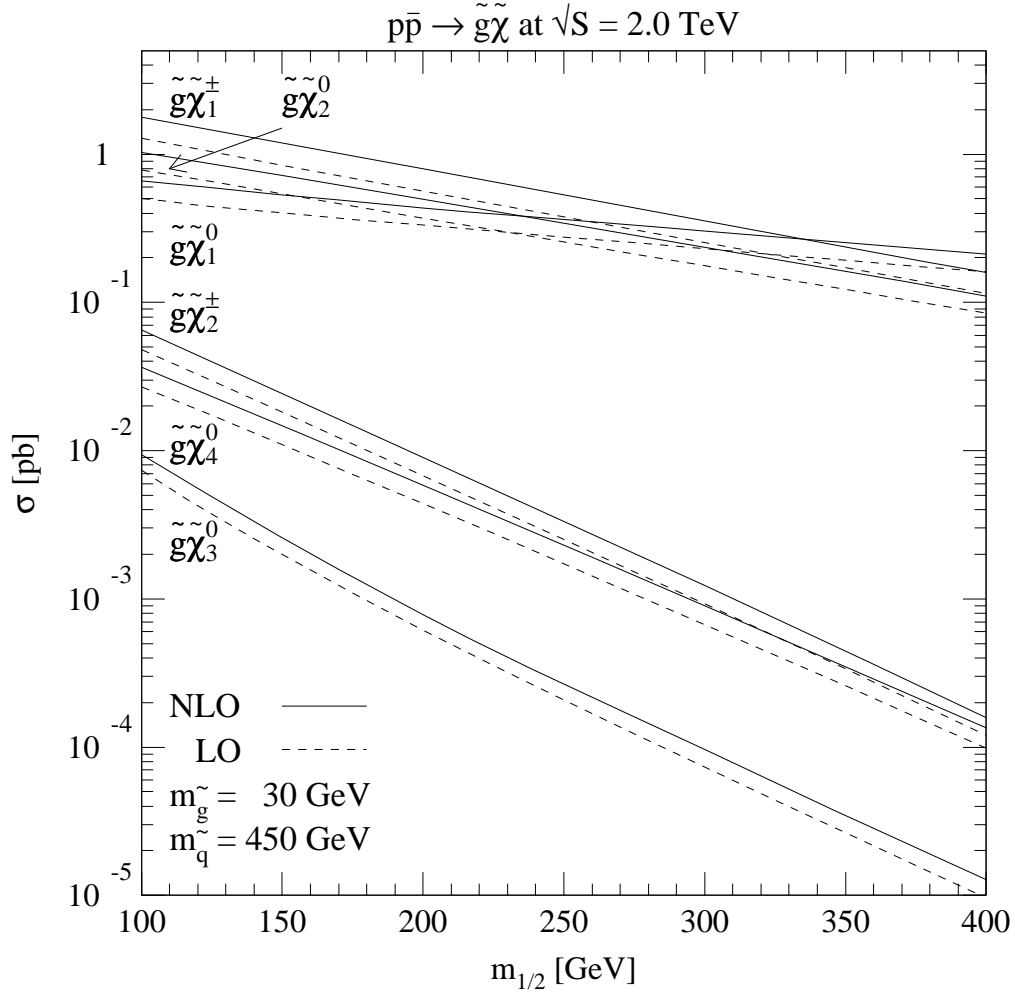


FIG. 18. Predicted total cross sections at the Tevatron for all six $\tilde{g}\tilde{\chi}$ channels for a gluino with mass 30 GeV as functions of $m_{1/2}$.

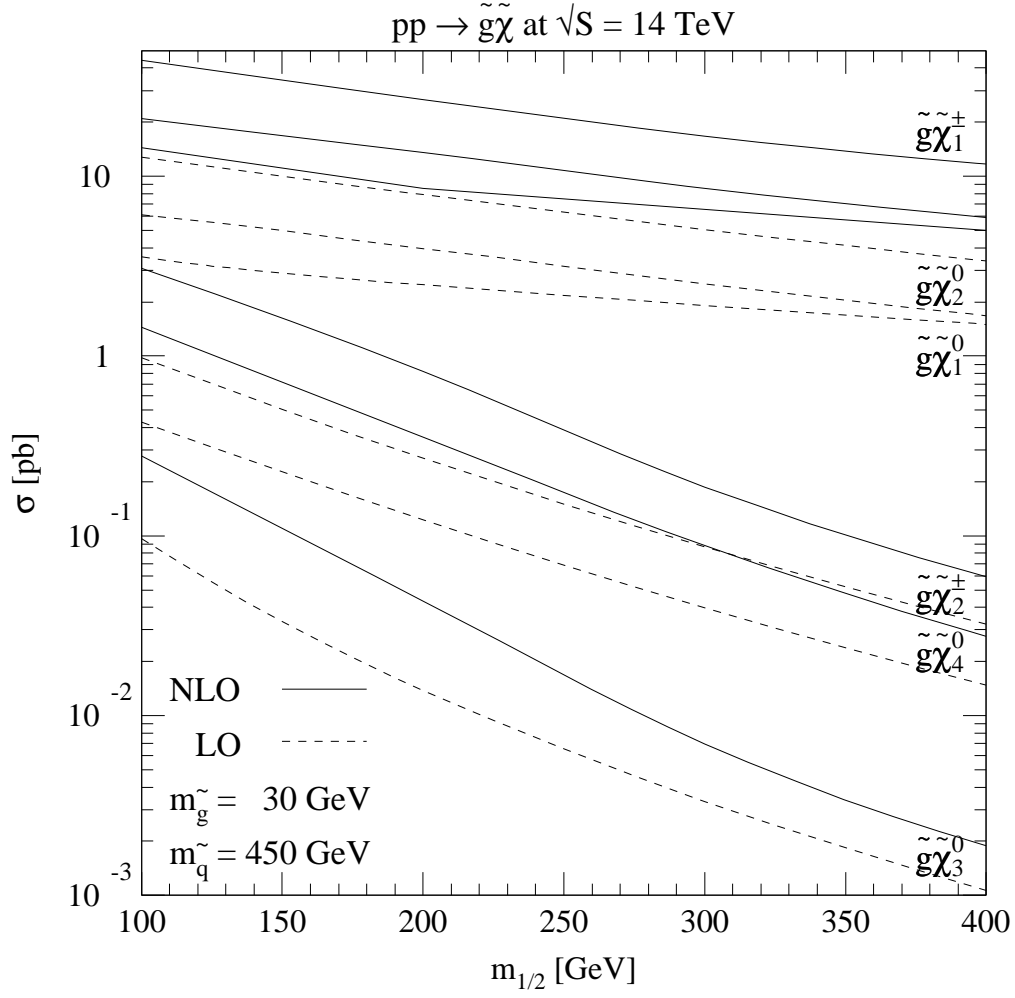


FIG. 19. Predicted total cross sections at LHC energies for all six $\tilde{g}\tilde{\chi}$ channels for a gluino with mass 30 GeV as functions of $m_{1/2}$.

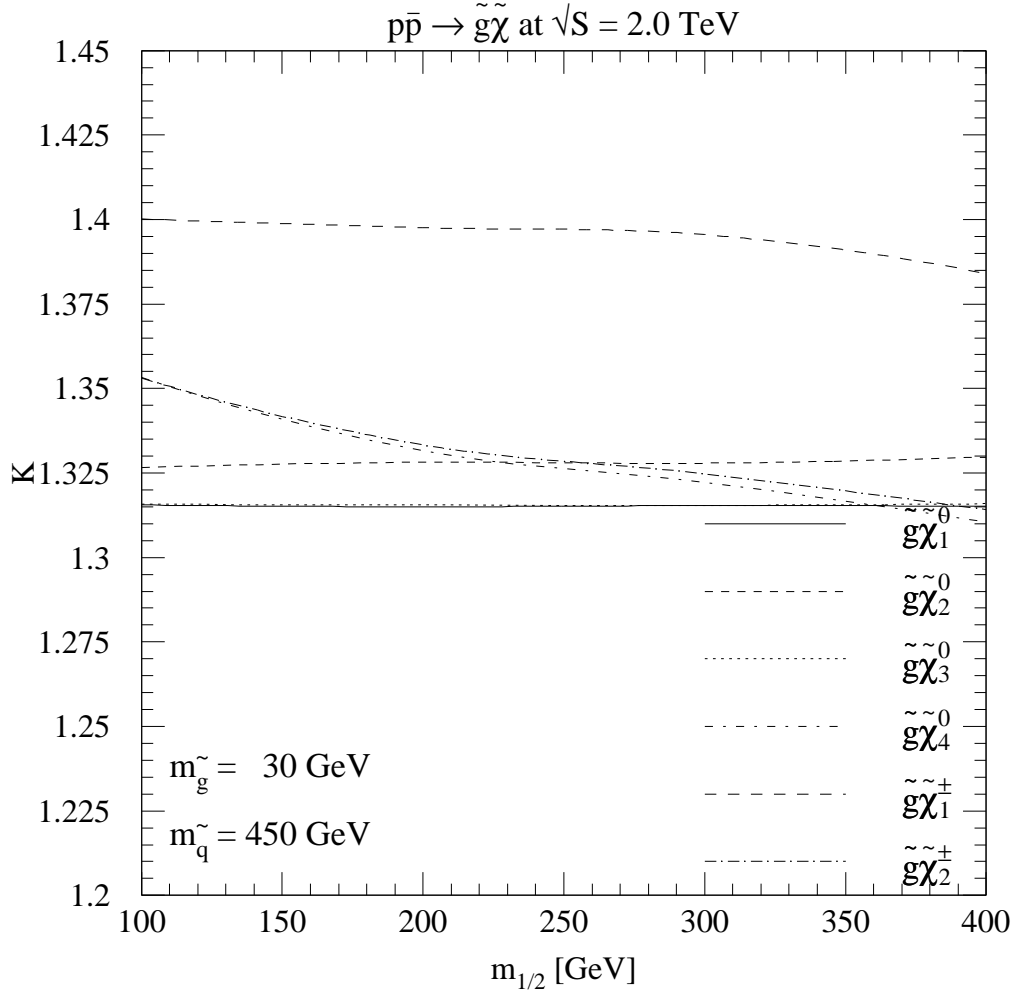


FIG. 20. Calculated enhancements of the cross sections from NLO contributions at the Tevatron for all six $\tilde{g}\tilde{\chi}$ channels with a light gluino of mass 30 GeV as functions of $m_{1/2}$.

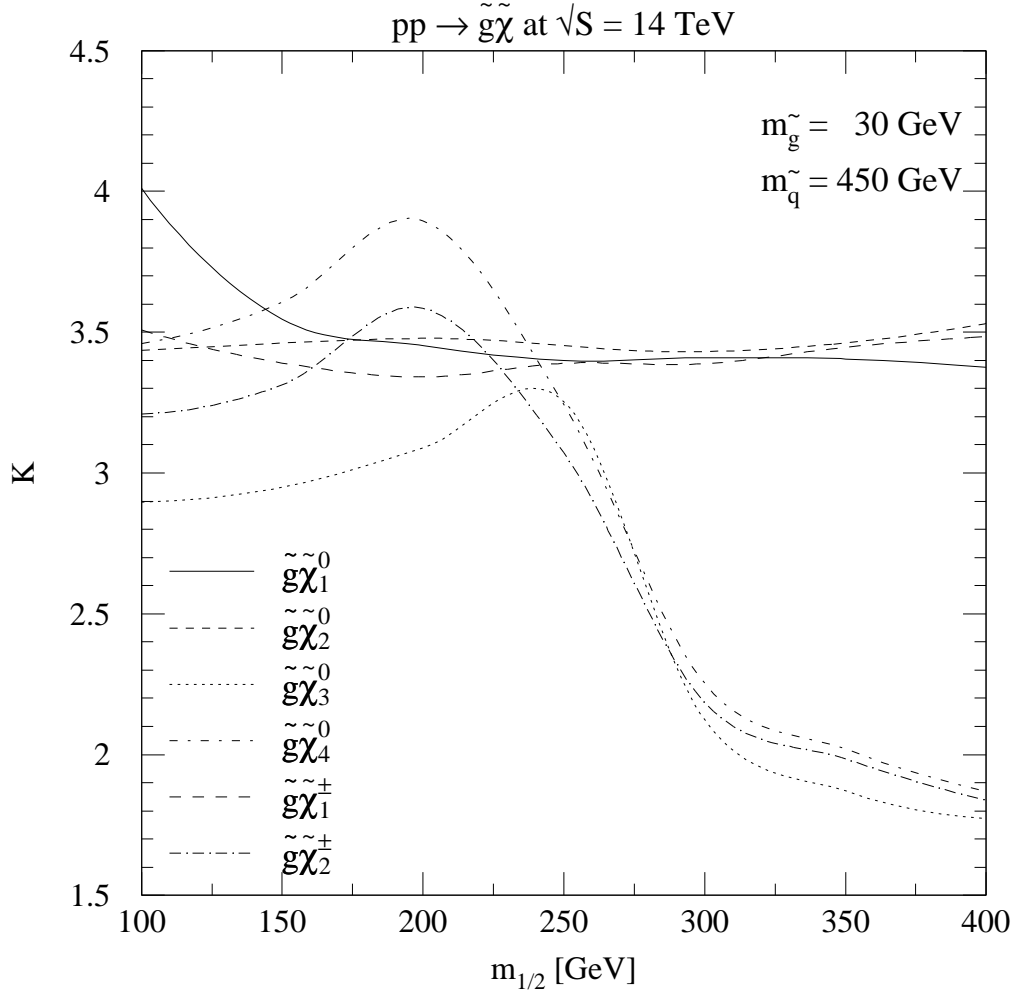


FIG. 21. Calculated enhancements of the cross sections from NLO contributions at the LHC for all six $\tilde{g}\tilde{\chi}$ channels with a light gluino of mass 30 GeV as functions of $m_{1/2}$.

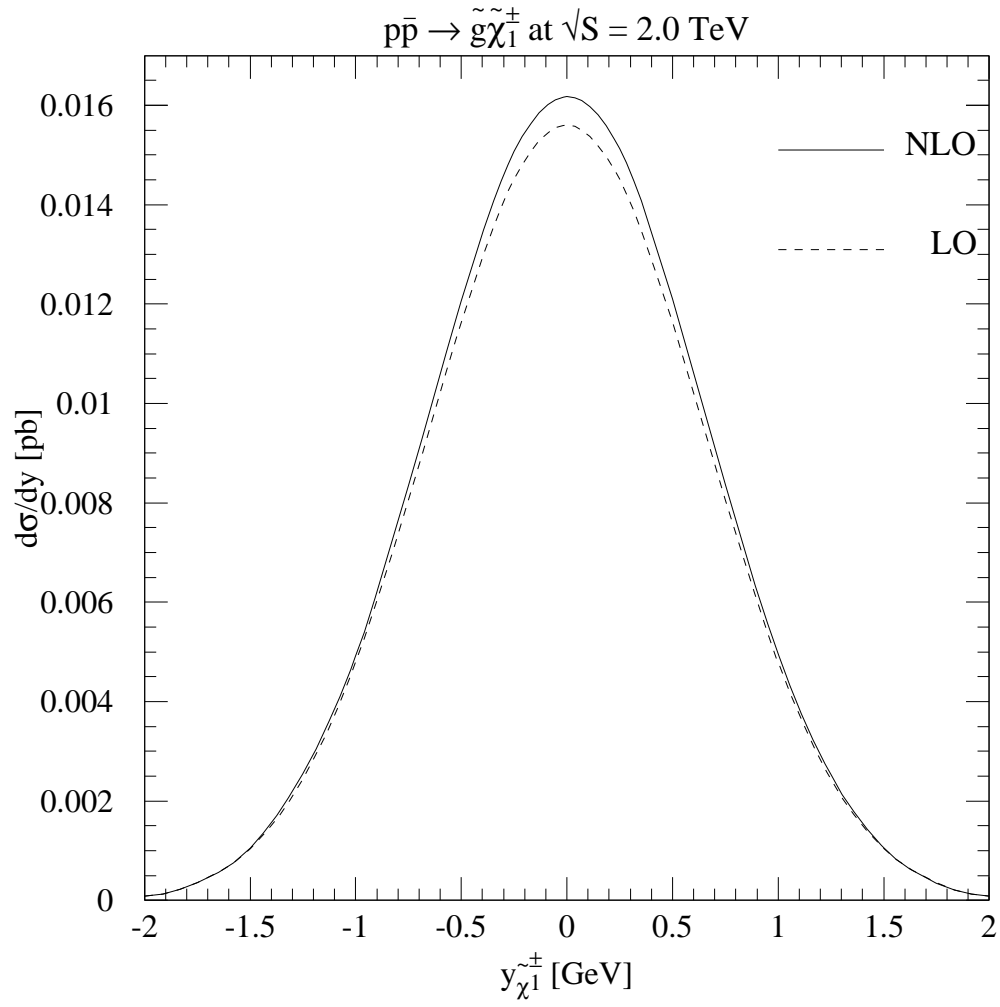


FIG. 22. Differential cross section in rapidity $d\sigma/dy$ for the production of $\tilde{\chi}_1^\pm$ with mass 101 GeV in association with a \tilde{g} of mass 410 GeV at the Tevatron.

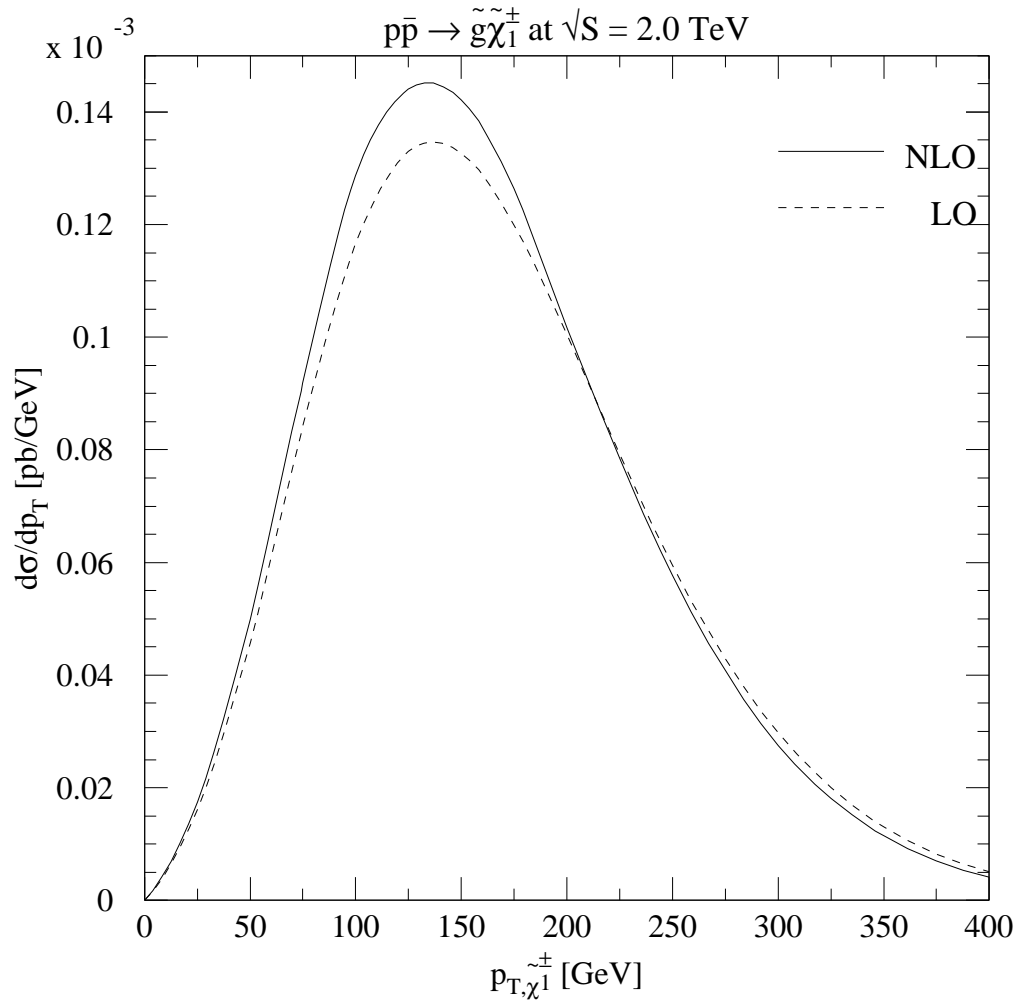


FIG. 23. Differential cross section in transverse momentum $d\sigma/dp_T$ for the production of $\tilde{\chi}_1^\pm$ with mass 101 GeV in association with a \tilde{g} of mass 410 GeV at the Tevatron.

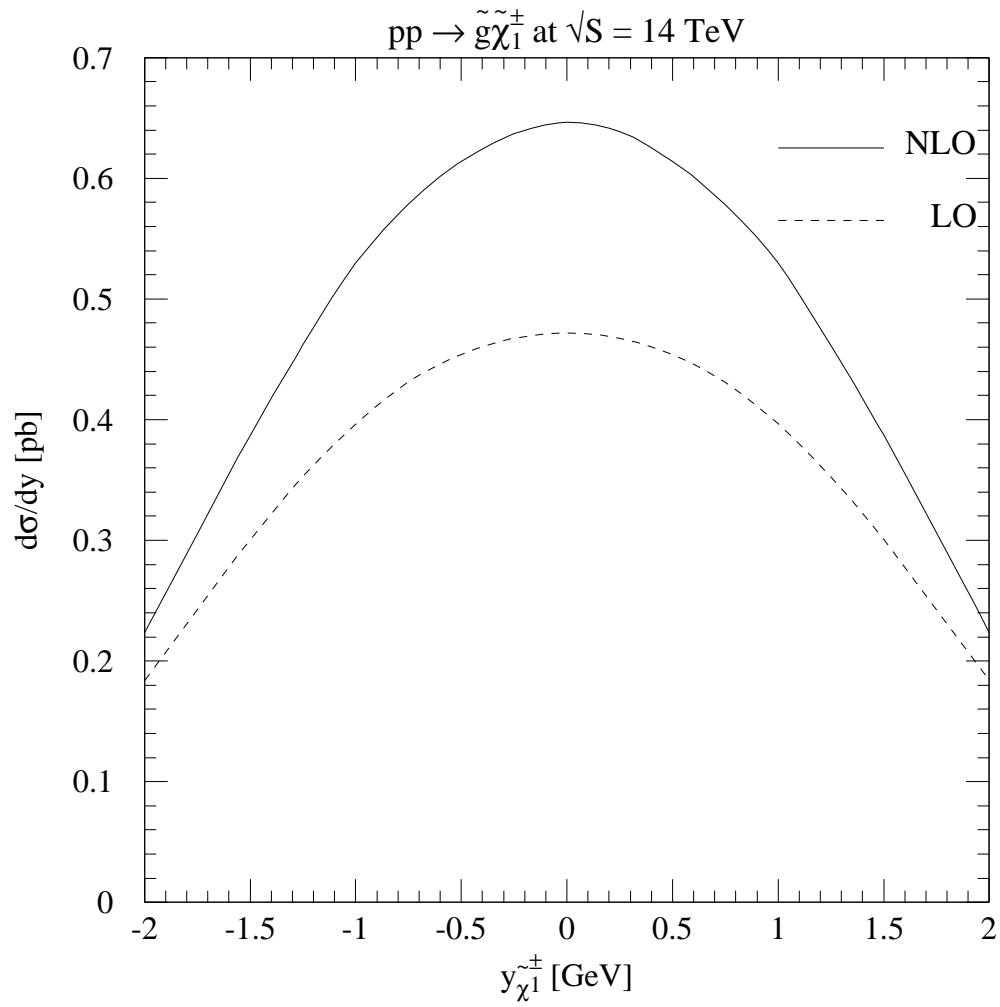


FIG. 24. Differential cross section in rapidity $d\sigma/dy$ for the production of $\tilde{\chi}_1^\pm$ with mass 101 GeV in association with a \tilde{g} of mass 410 at the LHC.

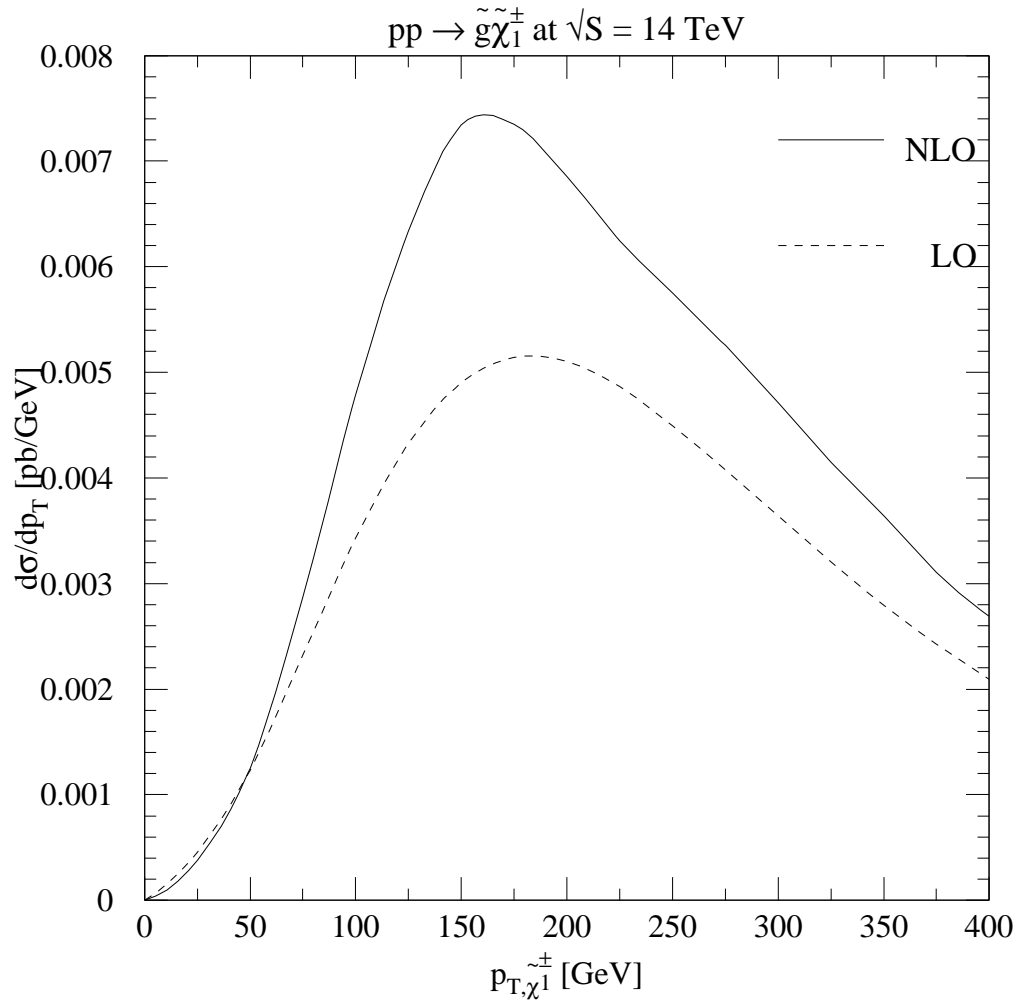


FIG. 25. Differential cross section in transverse momentum $d\sigma/dp_T$ for the production of $\tilde{\chi}_1^\pm$ with mass 101 GeV in association with a \tilde{g} of mass 410 GeV at the LHC.

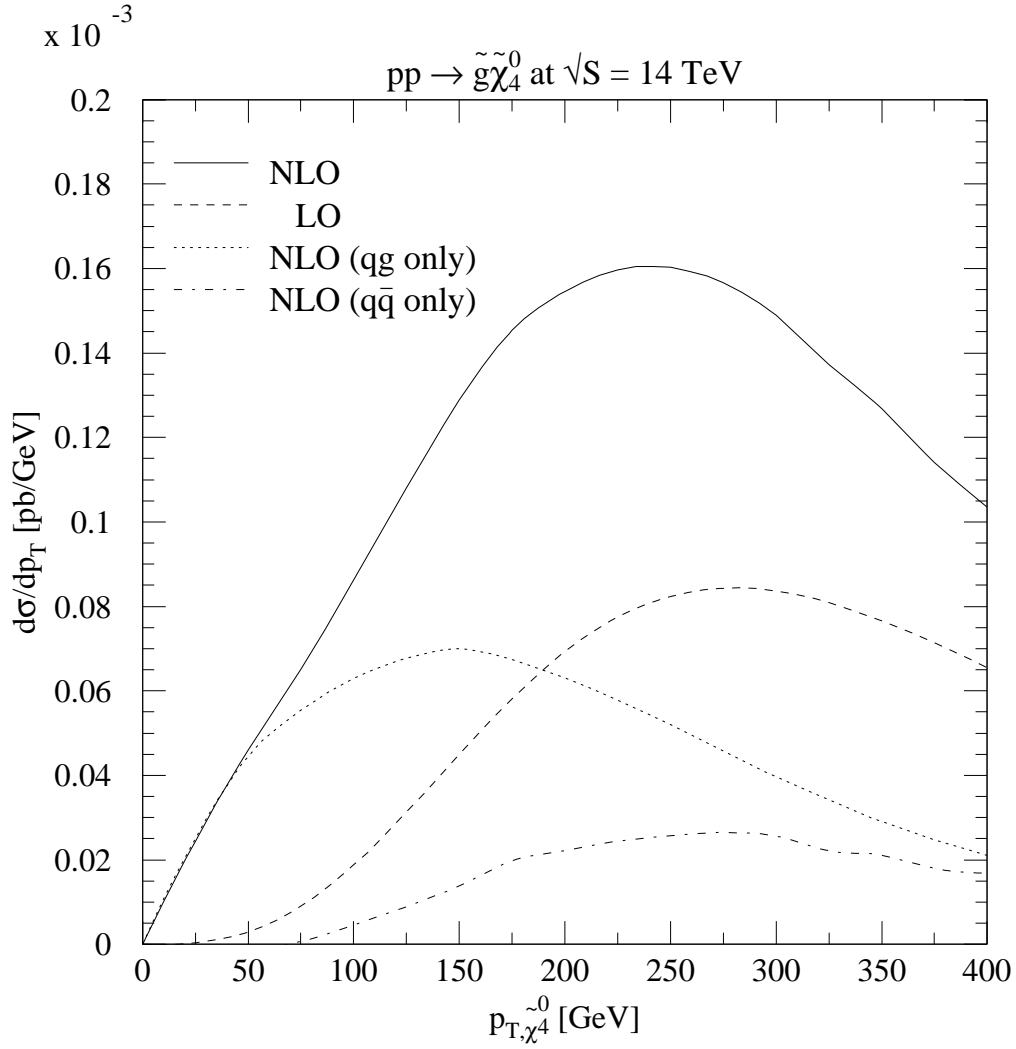


FIG. 26. Differential cross section in transverse momentum $d\sigma/dp_T$ for the production of $\tilde{\chi}_4^0$ with mass 309 GeV in association with a \tilde{g} of mass 410 GeV at the LHC. The solid line is the full NLO cross section. The dashed curve shows the LO Born cross section. The dotted line shows the contribution of the qg initial state subprocess. The dot-dashed curve is the difference between the full NLO result and the sum of the Born and qg contributions.